

國立交通大學

電信工程研究所

博士論文

多載波系統之時域等化

Time Domain Equalization for Multicarrier Systems

研究生：李俊芳

指導教授：吳文榕 博士

中華民國 九十九年 六月

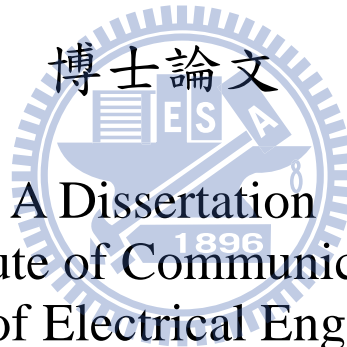
多載波系統之時域等化
Time Domain Equalization
for Multicarrier Systems

研究生：李俊芳
指導教授：吳文榕 博士

Student : Chun-Fang Lee
Advisor : Dr. Wen-Rong Wu

國立交通大學

電信工程研究所



A Dissertation
Submitted to Institute of Communication Engineering
College of Electrical Engineering
National Chiao Tung University
in Partial Fulfillment of the Requirements
for the Degree of Doctor of Philosophy
in
Communication Engineering
Hsinchu, Taiwan

2010 年 6 月

多載波系統之時域等化

研究生：李俊芳

指導教授：吳文榕 博士

國立交通大學

電信工程研究所博士班

摘要

在多載波系統中，循環前置(cyclic prefix)是用以避免符元之間的干擾(intersymbol interference)。然而循環前置需額外的頻寬，其長度通常取決於傳輸效率和系統效能之間的一個權衡。假如通道響應長度超過循環前置的範圍，則會產生符元之間的干擾而導致系統效能降低。一個簡單的補救方法是使用一時域等化器，將通道響應縮短至循環前置之範圍以內。本論文針對兩個眾所周知的多載波系統：離散多頻系統和正交分頻多工系統，發展出新的時域等化器之設計方法。時域等化器是一普遍用於離散多頻系統的裝置。許多方法已經被提出用來以設計容量最大化之時域等化器。在這些已提出的方法中都有一共同的假設即循環迴旋(circular convolution)可被用於雜訊信號及時域等化器。然而這個假設是不成立的，因為在一離散多頻系統中雜訊信號並不含有循環前置。對於等化後殘留之符元之間干擾，現存方法亦有類似的假設。由於這些不正確的假設，導致經過時域等化後之子載波雜訊和殘留之符元之間干擾量並未被正確的計算出，因而現存之最佳解事實上並不是最佳的。在本論文的第一部份，我們嘗試解決此問題。我們首先仔細的分析經時域等化後的雜訊信號和殘留之符元之間干擾信號之統計特性，並推導出計算時域等化後的雜訊和殘留符元之間干擾功率的正確公式。然後我們重新審視通道容量並設計一真正最佳的時域等化器。模擬顯示我們所提出的方法優於現存的方法，且效能非常接近於理論之上限。

一典型的無線通道有多路徑(multipath)響應，這響應通常具有有限脈衝響應(finite impulse response)的特性。因此其所對應的時域等化器會有無限脈衝響應(infinite impulse response)，這將導致傳統的時域等化器設計及其應用會有很高的計算複雜度。另在正交分頻多工系統中時域等化器的設計標的是平均位元錯誤率(bit-error-rate)，而平均位元錯誤率是等化器的一複雜函數，因此要求出最佳的時域等化器是一個非常困難的問題。在本論文的第二部份中，我們發展一些新的方法用以克服上述問題。首先我們提出一具無限脈衝響應之時域等化器來縮短通道的響應。在理論上吾人可以證明無線通道之時域等化器具有低階的無限脈衝響應特性，因此其階數可以遠小於有限脈衝響應之時域等化器。模擬顯示我們所提出的方法可以有效的降低計算複雜度，而其效能幾乎與現存之方法相同。我們接著進一步的提出一具有么正前置編碼(unitary precoding)之正交分頻多工系統。經過前置編碼的正交分頻多工系統不只可以提高子載波的多樣性(diversity)，同時也可以方便時域等化器之設計。我們提出一時域等化器的設計方法稱之為最大訊雜干擾比(maximum signal-to-interference-plus-noise ratio)。我們證明最佳的時域等化器可以將所有子載波的訊雜干擾比最大化，並且其解可以很容易的被導出。另一方面，要能完全的得到通道所提供的多樣性，接收端必須使用最大相似(maximum likelihood)偵測器。然而，用於前置編碼之正交分頻多工系統之最大相似偵測器的計算複雜度相當高，我們因此提出一偵測的方法稱之為混合型球型解碼和連續干擾消除(sphere-decoding-and-successive-interference-cancellation)。由模擬得知，此方法可以逼近最佳之效能，但其計算複雜度低。

Time Domain Equalization for Multicarrier Systems

Student: Chun-Fang Lee

Advisor: Dr. Wen-Rong Wu

Institute of Communication Engineering
National Chiao Tung University

Abstract

In multicarrier systems, cyclic prefix (CP) is introduced to avoid intersymbol interference (ISI). The CP is an overhead and its size is chosen as a compromise between the transmission efficiency and system performance. If the length of the channel response exceeds the CP range, the ISI is induced and the system performance will be degraded. A simple remedy for this problem is to apply a time-domain equalizer (TEQ) such that the channel response can be shortened into the CP range. This dissertation is aimed to develop new TEQ design methods for two well known multicarrier systems: discrete multitone (DMT) and orthogonal frequency division multiplexing (OFDM). The TEQ is a commonly used device in DMT systems. Many methods have been proposed to design the TEQ with a capacity maximization criterion. An implicit assumption used by existing methods is that circular convolution can be conducted for the noise signal and the TEQ. This assumption is not valid because the noise vector, observed in a DMT symbol, does not have a CP. A similar assumption is also made for the residual ISI signal. Due to these invalid assumptions, the TEQ-filtered noise and residual ISI powers in each subcarrier were not properly evaluated. As a result, the existing optimum solutions are actually not optimal. In the first part of the dissertation, we attempt to resolve this problem. We first analyze the statistical properties of the TEQ-filtered noise signal and the residual ISI signal in detail, and derive precise formulae for the calculation of the TEQ-filtered noise and residual ISI powers. Then, we re-formulate the capacity

maximization criterion to design the true optimum TEQ. Simulations show that the proposed method outperforms the existing ones, and its performance closely approaches the theoretical upper bound.

A wireless channel typically has the multi-path response, exhibiting a finite impulse response (FIR) characteristic. Thus, the corresponding TEQ will have an infinite impulse response (IIR). The direct application of conventional TEQ designs results in a filter with high computational complexity. In OFDM systems, the criterion for the TEQ design is the average bit error rate (BER) which is a complicated function of the TEQ, and the optimum TEQ is difficult to obtain. In the second part of the dissertation, we develop new methods to overcome the problems. We propose using an IIR TEQ to shorten the CIR. It can be shown that the ideal TEQ exhibits low-order IIR characteristics, and the order of the IIR TEQ can be much lower than that of the FIR TEQ. Simulations show that while the proposed method can reduce the computational complexity significantly, its performance is almost as good as existing methods. We then further propose an OFDM system with a unitary precoding. The precoded OFDM system not only enhances the diversity of subcarriers, but also facilitates the TEQ design. We propose a TEQ design method called the maximum signal-to-interference-plus-noise ratio (MSINR). It is shown that the optimum TEQ, maximizing the SINR of all subcarriers, can be easily derived. To fully explore the diversity the channel provides, the detector used at the receiver must be the maximum-likelihood (ML). The computational complexity of the ML detector for the precoded OFDM system can be very high. We then propose a detection method, called the sphere-decoding-and-successive-interference-cancellation (SDSIC). The proposed method can have near-optimal performance but the computational complexity is low.

Acknowledgements

I have a long list of people to thank for their sincere support and help. First of all, I express my gratitude to my advisor, Prof. Wen-Rong Wu, for taking a chance on me and guiding me in my doctoral studies. He spends a lot of time in discussing the problems I encounter in my research, providing valuable suggestions, and teaching me how to write technical papers. Under his enthusiastic instruction, I learned not only how to do a research but also learned the optimistic study attitude. I also learned to appreciate and mimic his clarity of expression and attention to detail. Prof. Wu has my deepest respect professionally and personally.

Secondly, I am deeply indebted to my beloved wife, Chin-Jung Wu, for her love, patience and understanding. She took care most family issues during my long studying period and persevered by my side through ups and downs although I know that I was not always the easiest person to deal with. I would like to express my sincere gratitude to my parents Run-Yuan Lee and Bi-Tao Chang, for their selflessly sacrificing and support. Then, I want to thank to my lovely children, Ting-Ying Lee, and Gia-Ann Lee. They are the sources of my power. Also I would like to thank to my brother Ming-Fang Lee, and my sister Hsiu-Ping Lee for their undertaking many family issues without complaint. Without their kindly cares, I will never think about pursuing a doctoral degree.

Moreover, I am grateful to all members in Wideband Transmission & Signal Processing Laboratory for the camaraderie and helpful research suggestions including Fan-Shao Tseng, Chao-Yuan Hsu, Hung-Dow Hsieh, Chun-Tao Lin, Nan-Chiun Lien, and so on. I would like

to thank them for their constructive suggestions and prompt help during the period of the PhD program. Finally, I would like to thank all friends who ever encourage or help me.

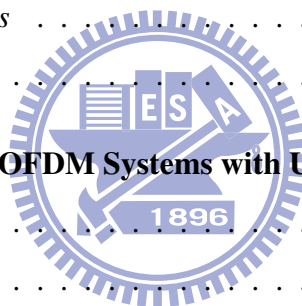


Contents

Acknowledgements	i
Contents	iii
List of Tables	v
List of Figures	vi
1 Introduction	1
1.1 Problem Statement	1
1.2 Review of Previous Works	3
1.3 Contributions and Dissertation Organization	6
2 Conventional Time Domain Equalization for DMT Systems	9
2.1 Signal Model	9
2.2 Minimum Mean Squared Error (MMSE) Method	14
2.3 Maximum Shortened SNR (MSSNR) Method	17
2.4 Maximum Bit Rate (MBR) Method	18
3 Time Domain Equalization for DMT Systems with Enhanced MBR Method	23
3.1 Analysis of Noise/Residual ISI Effect	24
3.1.1 <i>Conventional SINR calculation</i>	24

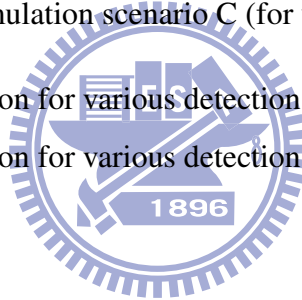


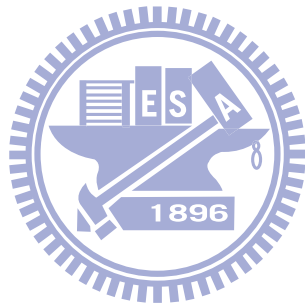
3.1.2	<i>Analysis of Noise Effect</i>	25
3.1.3	<i>Analysis of residual ISI</i>	29
3.2	Proposed Method	32
3.3	Simulations	36
4	IIR Time Domain Equalization for OFDM Systems	49
4.1	Signal Model	50
4.2	Proposed IIR TEQ Method	51
4.2.1	<i>IIR Characteristic of the TEQ</i>	52
4.2.2	<i>Derivation of MS FIR TEQ</i>	53
4.2.3	<i>Derivation of IIR TEQ</i>	55
4.2.4	<i>Complexity Analysis</i>	58
4.3	Simulations	59
5	Time Domain Equalization for OFDM Systems with Unitary Precoding	77
5.1	Motivation	78
5.2	Proposed Method	82
5.2.1	<i>System Model</i>	82
5.2.2	<i>TEQ Design with MSINR Method</i>	84
5.2.3	<i>Detection Methods</i>	87
5.2.4	<i>Computational Complexity Analysis</i>	97
5.3	Simulations	99
6	Conclusions	115
	Bibliography	119



List of Tables

3.1	Throughput for various TEQ design methods (unit: Mbps)	37
4.1	Plot definitions of simulation scenario A (for various IIR order)	75
4.2	Plot definitions of simulation scenario B (for various pole/zero order per stage)	75
4.3	Plot definitions of simulation scenario C (for various TLS per stage)	76
5.1	Complexity comparison for various detection methods (SNR_a is varied)	101
5.2	Complexity comparison for various detection methods (p is varied)	101



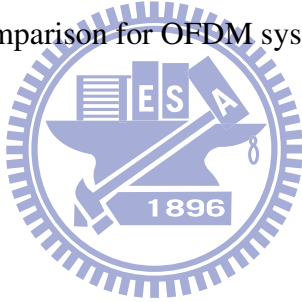


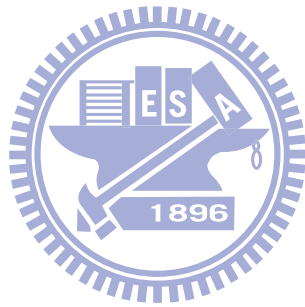
List of Figures

1.1	An OFDM system model.	8
2.1	A DMT model for TEQ design	20
2.2	Block diagram of the MMSE equalizer	21
2.3	(a) Effective channel in a DMT system, (b) Decomposition of received signal: desired signal path, ISI path, and noise path (H is the channel matrix).	22
3.1	Decomposed TEQ-filtered noise powers ($N = 16$, CSA#5 Loop)	38
3.2	Comparison of TEQ-filtered noise powers; power calculated with (3.9), power calculated with (3.8) (correct one), and simulated power ($N = 16$, CSA#5 Loop)	39
3.3	A zoomed view of Figure 3.2	40
3.4	Decomposed residual-ISI powers ($N = 16$, CSA#5 Loop)	41
3.5	Comparison of residual-ISI powers; power calculated with (3.12), power calcu- lated with (3.11) (correct one), and simulated power ($N = 16$, CSA#5 Loop) .	42
3.6	A zoomed view of Figure 3.5	43
3.7	Configuration of various standard test loops defined in ITU-T Recommendation G.996.1. The numbers on a line segment represent the length (feet) and the wire gauge (American wire gauge) of the line. The left side of a loop is connected to a central office.	44
3.8	SINR comparison between TEQs designed for min-ISI method and SEMBR method ($N = 16$, mid-CSA#6 Loop)	45

3.9	Throughput comparison for TEQs designed with min-ISI and SEMBR method ($N = 16$). MFB shows upper bound with no ISI. Loop Index is defined in Table 3.1.	46
3.10	TEQ frequency responses designed with min-ISI and SEMBR method ($N = 16$)	47
4.1	An OFDM system with TEQ	63
4.2	An OFDM system with multistage TEQ	64
4.3	System model for Steiglitz McBride method	65
4.4	A typical wireless channel impulse response	65
4.5	Average-squared-error of IIR TEQ fitted with SMM (for various pole/zero order)	66
4.6	Residual ISI power of IIR TEQ fitted with SMM (for various pole/zero order) .	67
4.7	SER Performance of IIR TEQ fitted with SMM (for various pole/zero order) . .	68
4.8	Impulse response of an FIR TEQ and its fitted IIR TEQ	69
4.9	SER performance of Experiment #1 (for various stage number)	70
4.10	SER performance of Experiment #2 (for various TEQ order in the first stage) .	71
4.11	SER performance of Experiment #3 (for various TEQ order in the second stage)	72
4.12	SER performance of Experiment #4 (for various TLS per Stage)	73
4.13	SER comparison of conventional FIR TEQ and proposed IIR TEQ	74
5.1	(a). A conventional OFDM system, (b). An OFDM system with unitary precoding (UP) and unitary decoding (UD).	102
5.2	Proposed model for OFDM systems with a TEQ	103
5.3	Complexity comparison for various detection methods	104
5.4	Complexity comparison for various detection methods	105
5.5	BER performance comparison for OFDM systems with various unitary precoders	106
5.6	BER performance comparison for precoded OFDM systems with SD detector (QPSK scheme)	107

5.7	BER performance comparison for precoded OFDM systems with SIC detector (QPSK scheme)	108
5.8	BER performance comparison for precoded OFDM systems with SD detector (16-QAM scheme)	109
5.9	BER performance comparison for precoded OFDM systems with SIC detector (16-QAM scheme)	110
5.10	BER performance comparison for precoded systems with various detection methods (QPSK scheme)	111
5.11	BER performance comparison for precoded OFDM systems with various detection methods (16-QAM scheme)	112
5.12	BER performance comparison for OFDM systems with ISI (QPSK scheme) . .	113
5.13	BER performance comparison for OFDM system with ISI (16-QAM)	114





Chapter 1

Introduction

IN recent years, the multicarrier technique has been becoming more and more popular in communication communities [1]- [2]. For example, discrete multitone (DMT) is used in standardized digital subscriber line (DSL) systems, such as asymmetric DSL (ADSL) [3]- [5] and very high speed DSL (VDSL) [6], and orthogonal frequency division multiplexing (OFDM) is used in standardized wireless systems, such as IEEE 802.11g [10], [11], digital audio broadcast (DAB) [8], and digital video broadcast (DVB) [9]. Although DMT and OFDM systems are efficient, there are still many problems not investigated. This chapter gives introduction for the motivation of this research and the contribution of the dissertation. Section 1.1 states the problem we consider, Section 1.2 reviews the related works, and Section 1.3 states the main contributions of this research and give the outline of the dissertation.

§ 1.1 Problem Statement

As the transmission speed of a communication system becomes higher and higher, the undesired effect, intersymbol interference (ISI), becomes more and more serious. A common remedy for ISI is the use of an equalizer. However, for high speed systems, the delay spread of the channel is large and equalization becomes difficult. One effective solution for the problem

is the multicarrier modulation technique. In multicarrier systems, the symbol size is made large and the ISI effect is then reduced. The idea of multicarrier communication is not new. However, it is not popular until the implementation bottleneck was broken by advanced digital signal processing, i.e., multicarrier modulation can be efficiently implemented by fast Fourier transform (FFT). Two multicarrier techniques are well known, i.e, DMT and OFDM. DMT is developed for wireline systems while OFDM for wireless. The modulation technique is essentially the same for both systems. The difference lies in that DMT transmits real signals while OFDM complex signals, and DMT conducts two additional operations, bit loading (at the transmitter) and time-domain equalization (at the receiver).

A block diagram of an OFDM transceiver is shown in Figure 1.1. The key to avoid complicated equalization is the addition of a guard period between two consecutive OFDM symbols, called the cyclic prefix (CP). If the CP length is larger than that of the channel response, no ISI will occur. As a result, the transmit signal in each subcarrier can be easily recovered by a single-tap frequency domain equalizer (FEQ). However, the CP is an overhead and it will reduce the transmission efficiency. In wireline systems, the channel impulse response (CIR) is known to have a low-pass infinite-impulse-response (IIR) characteristic. To avoid ISI, the CP size must be large and this is not desirable. A compromising approach is to use a time-domain equalizer (TEQ) in the receiver side such that the channel response can be shortened and a smaller CP is applicable. Note that the TEQ is usually implemented as a finite-impulse-response (FIR) filter and due to the low-pass IIR characteristic, the required number of filter taps is generally small. The computational complexity of the TEQ is usually low. The design of the TEQ has been a critical problem in DMT systems.

In conventional OFDM systems, the TEQ is not considered. As a result, the choice of the CP size is a compromise between the transmission overhead and system performance. If the CIR length exceeds the CP range, the ISI is induced and the system performance will be degraded. A simple remedy for this problem is also to apply a TEQ such that the CIR can be shortened into the CP range. If the TEQ can be applied for OFDM systems, the CP length

can be reduced without sacrificing the performance. Or, the CP length remains the same and the performance can be improved. There are a couple of reasons why the TEQ is not popular in OFDM systems. The first reason is that for fast fading environments, the TEQ will be fast varying and the calculation of the optimum TEQ will be difficult. The second reason is that the channel response of a wireless system usually does not have the low-pass characteristic and the TEQ cannot be as efficient as that in DMT systems. In other words, the length of the optimum TEQ response can be very long. The third reason is that the optimum TEQ in OFDM systems is difficult to design. In OFDM systems, no bit-loading is conducted. Each subcarrier transmits the same number of bits and the criterion for the TEQ to minimize is the average bit-error-rate (BER). However, the BER is a highly nonlinear function of the TEQ. The optimization is very difficult to conduct if not impossible.

In this dissertation, we will develop new algorithms for the TEQ design in DMT and OFDM systems. For DMT systems, many TEQ design methods have been proposed. As we will show, however, all the methods are not optimal. We will develop the true optimum approach and show the superiority of the proposed algorithm. For OFDM systems, we develop new methods such that the TEQ can be applied in slow fading environments. In slow fading, we do not have to update the TEQ frequently and the system overhead is low. To solve the inefficient TEQ problem, we propose using an IIR TEQ and develop new IIR TEQ design methods. With the IIR TEQ, the operation can be as efficient as that in DMT systems. As to the optimum TEQ, we propose using a precoding scheme such that the optimum TEQ, minimizing the BER, can be derived easily. The proposed precoded OFDM system also outperforms the uncoded OFDM no matter the TEQ is used or not.

§ 1.2 Review of Previous Works

The TEQ development is originated from the community of wireline communications (e.g. ADSL). As mentioned, the multicarrier modulation scheme in wireline applications is called

DMT. The DMT performs bit-loading and the transmission rate can approach the maximum channel capacity. Many algorithms have been proposed for the design of the TEQ in the DMT system [12]- [27].

A conventional method uses the minimum mean square error (MMSE) algorithm [12], [13], which minimizes the mean square error between two responses, one with the TEQ shortened impulse response, and the other a desired impulse response. Treating the TEQ design as a pure channel shortening problem, the work in [14] proposes a criterion to maximize the shortening signal-to-noise ratio (SSNR), defined as the ratio of the energy of the TEQ shortened response inside and outside the CP range. This method was referred to as the maximized SSNR (MSSNR) method. Another shortening method, minimizing the channel delay spread, has also been proposed [20]- [21]. Note that all these methods do not consider the impact of the TEQ on channel capacity, and they are not optimal in general.

The work in [15] first considered capacity maximization in the TEQ design. With a geometric signal-to-noise (SNR) maximization, a constrained nonlinear optimization problem was obtained. Since a closed-form solution did not exist, some numerical method was used in [15]. One drawback to this work is that the residual ISI effect was not considered. A method referred to as maximum bit rate (MBR) [18] was then proposed, taking both residual ISI and channel noise into account. To reduce the computational complexity, a suboptimum method called minimum ISI (min-ISI), which performs similarly to the MBR method, was also developed. Another MBR related method was suggested in [24]. It is known that when the maximum excess delay exceeds the CP range, inter-carrier interference (ICI) will occur in DMT systems. Thus, the residual ISI will induce ICI, and this problem was examined in [17]. It was found that the aforementioned methods shared a common mathematical framework based on the maximization of a product of generalized Rayleigh quotients [22].

The methods mentioned above conducted the TEQ design entirely in the time-domain. Another approach, treating the problem in the frequency-domain, was first proposed in [23] for DMT systems, and later in [28] for MIMO OFDM systems. This method, referred to as per-

tone equalization (PTEQ), allows an equalizer designed for the signal in each tone. By taking the computational advantage of fast Fourier transform (FFT), TEQ filtering operations can be effectively implemented in the discrete Fourier transform (DFT) domain. It was shown that the PTEQ scheme can outperform conventional TEQ schemes. However, the PTEQ requires a large quantity of memory for storage and potentially greater computational complexity [22]. Another method, called subsymbol equalization [25], also design the TEQ in the frequency domain. It used the conventional zero-forcing (ZF) FEQ to obtain the equalized time-domain signal. The drawback of this approach is that it is only applicable to a certain type of channels.

Recently, some TEQ design methods developed for DMT systems have been extended to OFDM systems [28]- [33]. The MSSNR TEQ for OFDM systems has been studied in [29]. In the original MSSNR method, the TEQ length is constrained to be smaller than or equal to the CP length. In [29], a modified MSSNR TEQ method was proposed to solve the problem. Using this method, the limitation on the TEQ tap length can be removed. In [29], an adaptive TEQ method based on the least mean-square (LMS) algorithm was also proposed to track the channel variation. Since the convergence of the LMS algorithm is slow, the QR-recursive least square (QR-RLS) algorithm was further proposed in [33] for TEQ adaptation.

There are some precoder designs for OFDM systems proposed in [46]- [52]. In [46], it is shown that the OFDM system with a unitary precoder can improve system performance and a simple decision-feedback detector can further enhances the performance. A special and simple precoder was proposed in [47]- [48] such that blind channel estimation for OFDM systems can be conducted. When the channel has nulls close to or on the FFT grids, OFDM faces serious symbol recovery problems. As an alternative to error control coding (ECC), [49] proposed a unitary precoding to solve the problem. The work in [50] also considers the OFDM systems with unitary precoding. It proves that when the receiver is the MMSE, the optimum precoding matrix is the DFT matrix. In this case, the OFDM system becomes a single carrier system. The works in [51] and [52] combines ECC and unitary precoding in order to obtain a high diversity and low complexity system. The overall diversity was shown [51] to be the product of the

individual diversity achievable by the ECC and that by the precoder, while the complexity is just a linear multiple of the sum of their individual complexities.

§ 1.3 Contributions and Dissertation Organization

The MBR design method [18] has proved to be an effective TEQ design method in DMT systems. Unfortunately, we have found that in the derivation of the MBR method, the TEQ-filtered noise and the ISI powers were not properly evaluated. As a result, the MBR method, claimed to be optimal, is not truly optimal. This is due to the assumption made in [18] (also in [15]) that the DFT of the TEQ-filtered noise is equal to the DFT of the TEQ response multiplied by that of the noise sequence (in a DMT symbol). This is equivalent to saying that the TEQ-filtered noise is obtained with a circular convolution of the TEQ response and the noise sequence. However, the noise sequence does not have a CP, and the TEQ-filtered noise corresponds to a linear convolution of the TEQ response and the noise sequence, instead of a circular convolution. This problem was first discovered by us [26], [27], and it was also briefly mentioned in a recently published work [25] (no detailed discussions and derivations were reported). A similar assumption was also made for the residual ISI [18]. Note that the residual ISI is the ISI response outside the CP range. As a result, the residual ISI cannot be obtained with a circular convolution of the input signal and the residual ISI response. This dissertation attempts to resolve the problems not considered previously. We give a detailed analysis of the TEQ-filtered noise and residual ISI in a DMT system, and derive precise formulae for the calculation of the noise and residual ISI powers. It turns out that these powers are larger than those previously calculated [15], [18]. With the analytic results, we further re-formulate the capacity criterion to design the true optimum TEQ.

It is well known that the wireline channel has an IIR characteristic. Consequently, conventional TEQs use in DMT systems are treated as a FIR filter. However, a wireless channel typically has the multi-path response, exhibiting a FIR characteristic. It can be shown that the

ideal TEQ for a wireless channel has an IIR characteristic. If the delay spread of a wireless channel is larger than the CP size, the ISI will occur. The TEQ, designed to shorten the CIR in DMT systems, can also be used to in OFDM systems. However, the corresponding TEQ will tend to have an IIR response. If the TEQ is still modeled as an FIR filter, the required order for the TEQ will be high. Conventional approaches then suffer from the high computational complexity problem, both in the derivation of TEQ and in the operation of channel shortening. We then propose using an IIR TEQ to overcome these problems. Since the ideal TEQ exhibits a low-order IIR characteristic, the order of the proposed IIR TEQ can be much lower than the FIR TEQ.

In OFDM systems, the signal band is divided into multiple subbands and a subcarrier is used in each subband. In each subcarrier, signal is modulated independently. For a frequency-selective fading channel, the channel response for some subcarriers may be poor. Signal recovery in those subcarriers is then difficult. It can be shown that the frequency diversity of a subcarrier is one. The conventional OFDM system does not fully explore the frequency diversity the channel provides. We propose an OFDM system with a unitary precoding. We show that the frequency diversity of the precoded system can be greatly enhanced. Note that the precoded OFDM system is different from that in [46]- [52]. In our system, the coding block does not require having the same size as that of the OFDM symbol. Another advantage of the precoded OFDM system is that the TEQ design becomes simple and the resultant performance is better. We propose a TEQ design method called the maximum signal-to-interference-plus-noise ratio (MSINR). It is shown that the optimum TEQ, maximizing the SINR of all subcarriers, can be easily derived. To fully explore the diversity the channel provides, the detector used at the receiver must be the maximum-likelihood (ML). The computational complexity of the ML detector for the precoded OFDM system can be very high. We then propose a detection method, called the sphere-decoding-and-successive-interference-cancelation (SDSIC) method. The proposed method can have near-optimal performance but the computational complexity is low.

This dissertation is organized as follows. In Chapter 2, we briefly review some conventional TEQ designs. In Chapter 3, we present the detailed analysis of the TEQ-filtered noise and residual ISI in a DMT system, and derive the precise formulae for the calculation of the noise and residual ISI powers. With the result, we further re-formulate the capacity criterion to design the true optimum TEQ. In Chapter 4, we describe the proposed IIR TEQ. Using the TEQ, we can conduct the equalization operation in an efficient way. In Chapter 5, we detail the proposed precoded OFDM system, and present the proposed MSINR TEQ design method. The SDSIC, an efficient ML-type detection algorithm, is also described. Finally, we draw the conclusions in Chapter 6.

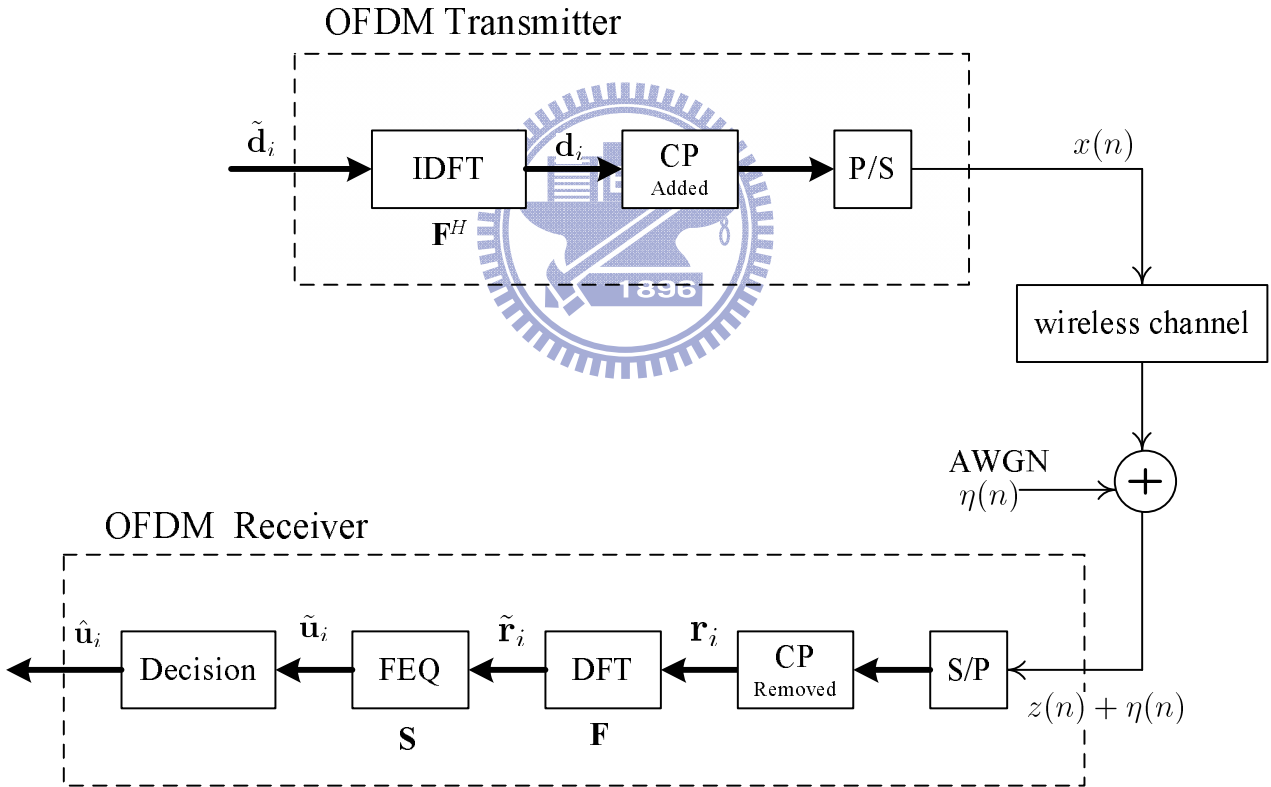
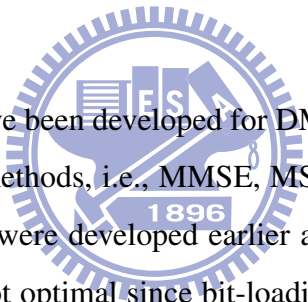


Figure 1.1: An OFDM system model.

Chapter 2

Conventional Time Domain Equalization for DMT Systems



Many TEQ design methods have been developed for DMT systems. This chapter reviews three commonly used TEQ design methods, i.e., MMSE, MSSNR, and MBR. The designs with the MMSE and MSSNR methods were developed earlier and the solutions are simpler to derive. However, these methods are not optimal since bit-loading is conducted in DMT systems. The TEQ designed with the MBR method is theoretically optimal since it maximizes channel capacity. This chapter reviews the methods reported in [12], [14], and [18]. In Section 2.1, we give the signal model for a DMT system with a TEQ. In Section 2.2, 2.3 and 2.4, we briefly review the MMSE, MSSNR, and the MBR TEQ design methods.

§ 2.1 Signal Model

First we define variables and symbols used throughout this work. Let M be the DFT size, L the CP length, $K = M + L$ the DMT symbol length, I the channel length, and N the TEQ length. In addition, let n be the time index, i the DMT symbol index, both in the time domain, and k the subchannel index in the DFT domain. Since DMT is a real modulation scheme,

$0 \leq k \leq M/2 - 1$. For OFDM systems, however, $0 \leq k \leq M - 1$. Denote $*$ as the operation of linear convolution while \otimes as that of circular convolution. As for vector or matrix operations, we denote $[\cdot]^T$, $[\cdot]^*$, and $[\cdot]^H$ as the transpose, the complex conjugate, and the Hermitian operations for a vector or matrix, respectively. Also, denote $\mathbf{0}_p$ as the $p \times 1$ zero column vector, $\mathbf{1}_p$ the $p \times 1$ unity column vector, $\mathbf{0}_{p \times q}$ the $p \times q$ zero matrix, \mathbf{I}_p the $p \times p$ identity matrix, and $\text{diag}[\cdot]$ as either the vector formed by the diagonal elements of a matrix, or a diagonal matrix formed by a vector. For notational convenience, we also define $[\mathbf{a}]^2 = \mathbf{a}\mathbf{a}^H$, and $\langle \mathbf{a} \rangle^2 = \text{diag}[\mathbf{a}\mathbf{a}^H]$, where \mathbf{a} is a vector. Note that $[\mathbf{a}]^2$ is a matrix while $\langle \mathbf{a} \rangle^2$ is a vector. Also, these operations are applicable to matrices.

A common model of a DMT system with a TEQ design is shown in Figure 2.1. At the DMT transmitter side, we denote the i th transmitted data symbol as

$$\tilde{\mathbf{d}}_i = [\tilde{d}_i(0), \dots, \tilde{d}_i(M-1)]^T,$$

where $\tilde{d}_i(k)$ is the $(k+1)$ th element of $\tilde{\mathbf{d}}_i$. Taking the M -point inverse DFT (M -IDFT) of $\tilde{\mathbf{d}}_i$, we can then obtain the corresponding time domain signal, denoted as \mathbf{d}_i . Then,

$$\mathbf{d}_i = [d_i(0), \dots, d_i(M-1)]^T = \mathbf{F}^H \tilde{\mathbf{d}}_i,$$

where \mathbf{F} is an $M \times M$ DFT matrix. Let

$$\alpha = e^{-j2\pi/M}, \quad (2.1)$$

and

$$\mathbf{f}(k) = \frac{1}{\sqrt{M}} [1, \alpha^k, \dots, \alpha^{(M-1)k}]^T. \quad (2.2)$$

We then have

$$\mathbf{F} = [\mathbf{f}(0), \mathbf{f}(1), \dots, \mathbf{f}(M-1)]. \quad (2.3)$$

Appending the CP and conducting the parallel-to-serial conversion, we can obtain the transmitted signal $x(n)$. Here, $n = iK + l$, and

$$\begin{cases} x(iK + l) = d_i(l + M - L), & \text{for } 0 \leq l \leq L - 1, \\ x(iK + l) = d_i(l - L), & \text{for } L \leq l \leq K - 1, \end{cases}$$

where $d_i(l)$ is the $(l + 1)$ th element of \mathbf{d}_i . The signal $x(n)$ is then transmitted over an FIR channel and corrupted by additive white Gaussian noise (AWGN).

Let the channel response be represented as

$$\mathbf{h} = [h(0), \dots, h(I - 1)]^T,$$

the AWGN as $\eta(n)$, and the noise-free channel output signal as $z(n)$. Then,

$$z(n) = x(n) * h(n).$$

At the receiver side, both $z(n)$ and $\eta(n)$ are first filtered by an N -tap TEQ. Let the TEQ coefficients be denoted as

$$\mathbf{w} = [w(0), \dots, w(N - 1)]^T, \quad (2.4)$$

the corresponding TEQ-filtered output of $z(n)$, and that of the channel noise be $y(n)$ and $v(n)$, respectively. Thus, $y(n) = z(n) * w(n)$ and $v(n) = \eta(n) * w(n)$. Performing the serial-to-parallel conversion, and removing the CP, we can obtain the i th received signal-only DMT symbol as

$$\mathbf{y}_i = [y(iK + \Delta + L), \dots, y(iK + \Delta + K - 1)]^T. \quad (2.5)$$

where Δ is the optimum delay. With the M -DFT operation, we have the frequency domain signal vector as

$$\tilde{\mathbf{y}}_i = [\tilde{y}_i(0), \dots, \tilde{y}_i(M - 1)]^T = \mathbf{F}\mathbf{y}_i,$$

where $\tilde{y}_i(k)$ is the $(k + 1)$ th element of $\tilde{\mathbf{y}}_i$. Let the corresponding i th noise vector at the TEQ input and output be

$$\boldsymbol{\eta}_i = [\eta(iK + \Delta + L), \dots, \eta(iK + \Delta + K - 1)]^T, \quad (2.6)$$

and

$$\mathbf{v}_i = [v(iK + \Delta + L), \dots, v(iK + \Delta + K - 1)]^T, \quad (2.7)$$

respectively. We can obtain their M -DFT transformed vectors as

$$\tilde{\boldsymbol{\eta}}_i = [\tilde{\eta}_i(0), \dots, \tilde{\eta}_i(M - 1)]^T = \mathbf{F}\boldsymbol{\eta}_i,$$

and

$$\tilde{\mathbf{v}}_i = [\tilde{v}_i(0), \dots, \tilde{v}_i(M-1)]^T = \mathbf{F}\mathbf{v}_i,$$

respectively.

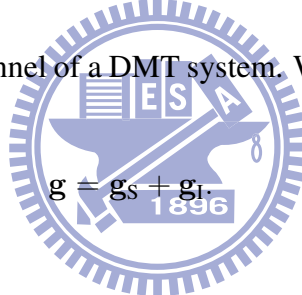
From Figure 2.1, we can see that the transmitted signal $x(n)$ is passed through the channel $h(n)$ and the TEQ $w(n)$. Let $g(n)$ be the equivalent channel response (ECR) where

$$g(n) = h(n) * w(n),$$

and the length of $g(n)$ be J where $J = I + N - 1$. Here, we assume that $J < M$. The ECR can be represented by a vector, \mathbf{g} , and

$$\mathbf{g} = [g(0), g(1), \dots, g(J-1)]^T.$$

Figure 2.3(a) shows the effective channel of a DMT system. We can then decompose \mathbf{g} into two parts,



The first part,

$$\mathbf{g}_s = [\mathbf{0}_{\Delta}^T, \mathbf{g}_{\Delta}^T, \mathbf{0}_{J-\Delta-L}^T]^T,$$

corresponds to the desired shortened channel response (in the CP range). Thus,

$$\mathbf{g}_{\Delta} = [g(\Delta), g(\Delta+1), \dots, g(\Delta+L-1)]^T.$$

If we let

$$g_{\Delta}(i) = g(\Delta+i),$$

then we have

$$\mathbf{g}_{\Delta} = [g_{\Delta}(0), g_{\Delta}(1), \dots, g_{\Delta}(L-1)]^T.$$

The second part,

$$\mathbf{g}_I = [g(0), \dots, g_{\Delta}(-1), \mathbf{0}_L^T, g_{\Delta}(L), \dots, g(J-1)]^T,$$

is the ECR outside the CP region.

We can express \mathbf{g}_s and \mathbf{g}_l in terms of the channel matrix \mathbf{H} and the TEQ vector \mathbf{w} as

$$\begin{aligned}\mathbf{g}_s &= \mathbf{D}_s \mathbf{H} \mathbf{w}, \\ \mathbf{g}_l &= \mathbf{D}_l \mathbf{H} \mathbf{w},\end{aligned}\tag{2.8}$$

where

$$\begin{aligned}\mathbf{D}_s &= \text{diag} [\mathbf{0}_{\Delta}^T, \mathbf{1}_L^T, \mathbf{0}_{J-\Delta-L}^T], \\ \mathbf{D}_l &= \mathbf{I}_J - \mathbf{D}_s = \text{diag} [\mathbf{1}_{\Delta}^T, \mathbf{0}_L^T, \mathbf{1}_{J-\Delta-L}^T],\end{aligned}\tag{2.9}$$

and

$$\mathbf{H} = \begin{bmatrix} h(0) & 0 & \cdots & 0 \\ h(1) & h(0) & \cdots & 0 \\ \vdots & \vdots & \ddots & \vdots \\ h(I-1) & h(I-2) & \cdots & h(I-N) \\ 0 & h(I-1) & \cdots & h(I-N+1) \\ \vdots & \vdots & \ddots & \vdots \\ 0 & 0 & \cdots & h(I-1) \end{bmatrix}_{J \times N}.\tag{2.10}$$

Define an $M \times J$ matrix \mathbf{T}_G such that when \mathbf{g}_l and \mathbf{g}_s are multiplied by \mathbf{T}_G , they will be shifted with the optimal delay Δ , and then padded with zeros to have a size of M . That is,

$$\mathbf{T}_G = \begin{bmatrix} \mathbf{0}_{(J-\Delta) \times \Delta} & \mathbf{I}_{J-\Delta} \\ \mathbf{I}_{\Delta} & \mathbf{0}_{\Delta \times (J-\Delta)} \\ \mathbf{0}_{(M-J) \times J} \end{bmatrix}_{M \times J}\tag{2.11}$$

Additionally, let $\tilde{\mathbf{g}}_s$, $\tilde{\mathbf{g}}_l$ be the DFT of \mathbf{g}_s , and \mathbf{g}_l , respectively. Then, we have

$$\begin{aligned}\tilde{\mathbf{g}}_s &= [\tilde{g}_s(0), \dots, \tilde{g}_s(M-1)]^T = \mathbf{F} \mathbf{T}_G \mathbf{g}_s, \text{ and} \\ \tilde{\mathbf{g}}_l &= [\tilde{g}_l(0), \dots, \tilde{g}_l(M-1)]^T = \mathbf{F} \mathbf{T}_G \mathbf{g}_l,\end{aligned}\tag{2.12}$$

where

$$\begin{aligned}\tilde{g}_S(k) &= \mathbf{f}^T(k)\mathbf{T}_G\mathbf{D}_S\mathbf{H}\mathbf{w}, \text{ and} \\ \tilde{g}_I(k) &= \mathbf{f}^T(k)\mathbf{T}_G\mathbf{D}_I\mathbf{H}\mathbf{w}\end{aligned}\quad (2.13)$$

are the $(k + 1)$ th elements of $\tilde{\mathbf{g}}_S$, and $\tilde{\mathbf{g}}_I$, respectively. We can re-express \mathbf{g}_S and \mathbf{g}_I as $\mathbf{g}_S = [g_S(0), \dots, g_S(J - 1)]^T$, and $\mathbf{g}_I = [g_I(0), \dots, g_I(J - 1)]^T$, respectively, where $g_S(l)$, $g_I(l)$ are the $(l + 1)$ th elements of \mathbf{g}_S , and \mathbf{g}_I , respectively. Let $y_S(n)$ and $y_I(n)$ be the desired and residual ISI components of $y(n)$, respectively. Thus we have

$$y(n) = y_S(n) + y_I(n),$$

where $y_S(n) = x(n) * g_S(n)$, and $y_I(n) = x(n) * g_I(n)$. Consequently, we can also decompose \mathbf{y}_i as

$$\mathbf{y}_i = \mathbf{y}_{S,i} + \mathbf{y}_{I,i}, \quad (2.14)$$

where

$$\begin{aligned}\mathbf{y}_{S,i} &= [y_S(iK + \Delta + L), \dots, y_S(iK + \Delta + K - 1)]^T, \text{ and} \\ \mathbf{y}_{I,i} &= [y_I(iK + \Delta + L), \dots, y_I(iK + \Delta + K - 1)]^T.\end{aligned}$$

Let

$$\begin{aligned}\tilde{\mathbf{y}}_{S,i} &= [\tilde{y}_{S,i}(0), \dots, \tilde{y}_{S,i}(M - 1)]^T, \\ \tilde{\mathbf{y}}_{I,i} &= [\tilde{y}_{I,i}(0), \dots, \tilde{y}_{I,i}(M - 1)]^T\end{aligned}$$

be the M -DFT of $\mathbf{y}_{S,i}$, and $\mathbf{y}_{I,i}$, respectively. Then, $\tilde{\mathbf{y}}_{S,i} = \mathbf{F}\mathbf{y}_{S,i}$, $\tilde{\mathbf{y}}_{I,i} = \mathbf{F}\mathbf{y}_{I,i}$, and $\tilde{\mathbf{y}}_i$ can be rewritten as $\tilde{\mathbf{y}}_i = \tilde{\mathbf{y}}_{S,i} + \tilde{\mathbf{y}}_{I,i}$. Figure 2.3(b) shows the decomposition of $y(n) + \eta(n)$.

§ 2.2 Minimum Mean Squared Error (MMSE) Method

The block diagram of the MMSE TEQ design method is shown in Figure 2.2. As we can see, the upper branch of the system consists of the channel and an FIR TEQ, and the lower branch

consists of a delay and an FIR filter with a target impulse response (TIR). The MMSE TEQ \mathbf{w} is designed to minimize the MSE between the output of the TEQ and the TIR. If the ECR is equal to the delayed TIR, the error signal e_i will be zero. For a given length of the TIR, the MMSE TEQ tend to make the ECR to have the same response length. Note that to avoid an all-zero trivial solution, there must be some constraint on \mathbf{w} or the TIR. Commonly used constraints include unit-energy constraint (UEC) and unit-tap constraint (UTC) [16].

From Figure 2.2, we see that the signal at the receiver is given by

$$z(n) = h(n) * x(n) + \eta(n). \quad (2.15)$$

Using the matrix-form expression, we have

$$\mathbf{z}_i = \mathbf{H}^T \mathbf{x}_i + \boldsymbol{\eta}_i, \quad (2.16)$$

where \mathbf{H} is the channel matrix defined in (2.10), $\mathbf{x}_i = [x(iK + \Delta + L), \dots, x(iK + \Delta + K - 1)]^T$, $\mathbf{z}_i = [z(iK + \Delta + L), \dots, z(iK + \Delta + K - 1)]^T$, and $\boldsymbol{\eta}_i$ defined in (2.6). Let the TIR be denoted as $\mathbf{b} = [b(0), \dots, b(L - 1)]^T$. Note here that the TIR length is chosen to be the CP size L . The error signal $e(n)$ can then be defined as

$$\begin{aligned} e(n) &= r(n) - \zeta(n) = w(n) * z(n) + \zeta(n) \\ &= \sum_{i=0}^{N-1} w(i)z(n + N - 1 - i) - \sum_{j=0}^L b_j x(n + N - 1 - \Delta - j) \\ &= \mathbf{w}^T \mathbf{z}_n - [\mathbf{0}_{1 \times \Delta}, \mathbf{b}^T, \mathbf{0}_{1 \times (N + I - \Delta - L - 1)}] \mathbf{x}_n, \end{aligned} \quad (2.17)$$

where $\mathbf{z}_n = [z(n + N - 1), \dots, z(n)]^T$ and $\mathbf{x}_n = [x(n + N - 1), \dots, x(n - I)]^T$. If we let $\mathbf{b}_\Delta = [\mathbf{0}_{\Delta \times 1}, \mathbf{b}, \mathbf{0}_{(N + I - \Delta - L - 1) \times 1}]$, the MSE can then have the following expression:

$$\text{MSE} = \text{E}\{e(n)^2\} = \mathbf{b}_\Delta^T \mathbb{R}_{\mathbf{z}\mathbf{z}} \mathbf{b}_\Delta - \mathbf{b}_\Delta^T \mathbb{R}_{\mathbf{z}\mathbf{x}} \mathbf{w} - \mathbf{w}^T \mathbb{R}_{\mathbf{x}\mathbf{z}} \mathbf{b}_\Delta + \mathbf{w}^T \mathbb{R}_{\mathbf{x}\mathbf{x}} \mathbf{w}, \quad (2.18)$$

where $\mathbb{R}_{\mathbf{x}\mathbf{x}} = \text{E}\{\mathbf{x}\mathbf{x}^T\}$, $\mathbb{R}_{\mathbf{x}\mathbf{z}} = \text{E}\{\mathbf{x}\mathbf{z}^T\}$, $\mathbb{R}_{\mathbf{z}\mathbf{x}} = \text{E}\{\mathbf{z}\mathbf{x}^T\}$, and $\mathbb{R}_{\mathbf{z}\mathbf{z}} = \text{E}\{\mathbf{z}\mathbf{z}^T\}$, respectively.

Taking the derivative with respect to \mathbf{w} and setting the result to zero, we have

$$\mathbf{b}_\Delta^T \mathbb{R}_{\mathbf{z}\mathbf{z}} = \mathbf{w}^T \mathbb{R}_{\mathbf{z}\mathbf{x}} \quad (2.19)$$

Substituting (2.19) into (2.18), we further have

$$\text{MSE} = \mathbf{b}_\Delta^T [\mathbb{R}_{xx} - \mathbb{R}_{xz}\mathbb{R}_{zz}^{-1}\mathbb{R}_{zx}] \mathbf{b}_\Delta \quad (2.20)$$

Define \mathbb{R}_Δ as

$$\begin{aligned} \mathbb{R}_\Delta = & \left[\mathbf{0}_{(L+1) \times \Delta}, \mathbf{I}_{(L+1) \times (L+1)}, \mathbf{0}_{(L+1) \times (N+I-\Delta-L-1)} \right]^T [\mathbb{R}_{xx} - \mathbb{R}_{xz}\mathbb{R}_{zz}^{-1}\mathbb{R}_{zx}] \cdot \\ & \left[\mathbf{0}_{(L+1) \times \Delta}, \mathbf{I}_{(L+1) \times (L+1)}, \mathbf{0}_{(L+1) \times (N+I-\Delta-L-1)} \right]. \end{aligned} \quad (2.21)$$

Thus, the MSE can be written as

$$\text{MSE} = \mathbf{b}^T \mathbb{R}_\Delta \mathbf{b} \quad (2.22)$$

As mentioned, some constraint must be posed to avoid the trivial solution. Here, we pose the UTC on \mathbf{b} , i.e., $\mathbf{b}^T \mathbf{i}_k = 1$. Thus, the Lagrangian can be formed as

$$\mathbb{L}_{\text{UT}}(\mathbf{b}, \lambda) = \mathbf{b}^T \mathbb{R}_\Delta \mathbf{b} + \lambda(\mathbf{b}^T \mathbf{i}_k - 1), \quad (2.23)$$

where \mathbf{i}_k is $(k+1)$ th column vector of the identity matrix \mathbf{I}_M . Setting the derivative with respect to \mathbf{b} , $\partial \mathbb{L}_{\text{UT}}(\mathbf{b}, \lambda) / \partial \mathbf{b}$, to zero, we have

$$\frac{\partial \mathbb{L}_{\text{UT}}(\mathbf{b}, \lambda)}{\partial \mathbf{b}} = 2\mathbb{R}_\Delta \mathbf{b}_o + \lambda \mathbf{i}_k = 0. \quad (2.24)$$

Thus, the optimal TIR, denoted as \mathbf{b}_o , can be found as

$$\mathbf{b}_o = \frac{\mathbb{R}_\Delta^{-1} \mathbf{i}_{k_o}}{\mathbb{R}_\Delta^{-1}(k_o, k_o)}, \quad (2.25)$$

where $\mathbb{R}_\Delta^{-1}(k, k)$ is the $(k+1)$ th element in the diagonal of the matrix \mathbb{R}_Δ^{-1} , and k_o can be obtained as

$$k_o = \arg \max_{0 \leq k \leq L} \{\mathbb{R}_\Delta^{-1}(k, k)\}. \quad (2.26)$$

The solution given by (2.25) yields an MMSE of

$$\text{MMSE}^{\text{UT}} = \frac{1}{\mathbb{R}_\Delta^{-1}(k_o, k_o)}, \quad (2.27)$$

The optimum TEQ, denoted as \mathbf{w}_o , can be obtained from (2.19) by setting $\mathbf{b} = \mathbf{b}_o$, i.e.,

$$\mathbf{w}_o = \mathbf{b}_o^T \mathbb{R}_{xz} \mathbb{R}_{zz}^{-1} \quad (2.28)$$

If the UEC is posed on \mathbf{b} , then the Lagrangian will become

$$\mathbb{L}_{\text{UE}}(\mathbf{b}, \lambda) = \mathbf{b}^T \mathbb{R}_{\Delta} \mathbf{b} + \lambda(\mathbf{b}^T \mathbf{b} - 1) \quad (2.29)$$

Setting $\partial \mathbb{L}_{\text{UE}}(\mathbf{b}, \lambda) / \partial \mathbf{b}$ to zero, we then have

$$\mathbb{R}_{\Delta} \mathbf{b}_o = \lambda \mathbf{b}_o. \quad (2.30)$$

Equation (2.30) implies that \mathbf{b}_o is an eigenvector of \mathbb{R}_{Δ} . From (2.30), we have the MSE as

$$\text{MSE} = \mathbf{b}_o^T \mathbb{R}_{\Delta} \mathbf{b}_o = \mathbf{b}_o^T \lambda \mathbf{b}_o = \lambda. \quad (2.31)$$

Therefore, we can choose \mathbf{b}_o as the eigenvector corresponding to the minimum eigenvalue of \mathbb{R}_{Δ} , denoted by λ_{\min} , to minimize the MSE. Thus, the minimum MSE is

$$\text{MMSE}_{\text{UE}} = \lambda_{\min}. \quad (2.32)$$

§ 2.3 Maximum Shortened SNR (MSSNR) Method

The work in [14] treats the TEQ design problem as a pure channel shortening problem. It proposes a criterion to minimize the energy of the ECR outside the target window, while keeping the energy inside constant. The SSNR is defined as the ratio of the energy of the ECR inside and outside the CP range. In [14], a method is proposed to find a TEQ that maximizes the SSNR. From (2.35), the ECR inside the target window can be written as

$$\mathbf{g}_s = \mathbf{D}_s \mathbf{H} \mathbf{w}, \quad (2.33)$$

and the ECR outside the target window as

$$\mathbf{g}_I = \mathbf{D}_I \mathbf{H} \mathbf{w}. \quad (2.34)$$

Therefore, the energy inside and outside the target window is

$$\begin{aligned} \mathbf{g}_I^T \mathbf{g}_I &= \mathbf{w}^T \mathbf{H}^T \mathbf{D}_I^T \mathbf{D}_I \mathbf{H} \mathbf{w} = \mathbf{w}^T \mathbf{A} \mathbf{w}, \\ \mathbf{g}_S^T \mathbf{g}_S &= \mathbf{w}^T \mathbf{H}^T \mathbf{D}_S^T \mathbf{D}_S \mathbf{H} \mathbf{w} = \mathbf{w}^T \mathbf{B} \mathbf{w}, \end{aligned} \quad (2.35)$$

respectively, where \mathbf{A} and \mathbf{B} are symmetric and positive semi-definite matrices.

Optimum shortening is achieved if we choose \mathbf{w} to minimize $\mathbf{w}^T \mathbf{A} \mathbf{w}$ while satisfying a constraint on $\mathbf{w}^T \mathbf{B} \mathbf{w}$. Using mathematical expression, we have

$$\min_{\mathbf{w}} \mathbf{w}^T \mathbf{A} \mathbf{w} \text{ such that } \mathbf{w}^T \mathbf{B} \mathbf{w} = 1. \quad (2.36)$$

This is equivalent to maximizing the SSNR given by

$$\text{SSNR} = \frac{\mathbf{w}^T \mathbf{B} \mathbf{w}}{\mathbf{w}^T \mathbf{A} \mathbf{w}} \quad (2.37)$$

Since \mathbf{B} is positive definite, \mathbf{B} can have a Cholesky decomposition. Employing Cholesky decomposition, we have

$$\mathbf{B} = \sqrt{\mathbf{B}} \sqrt{\mathbf{B}}^T \quad (2.38)$$

The optimum solution for the TEQ vector \mathbf{w} is then

$$\mathbf{w}_{\text{opt}} = \left(\sqrt{\mathbf{B}} \right)^{-1} \mathbf{p}_{\text{min}}, \quad (2.39)$$

where \mathbf{p}_{min} is the eigenvector corresponding to the minimum eigenvalue of the composite matrix $(\sqrt{\mathbf{B}})^{-1} \mathbf{A} (\sqrt{\mathbf{B}}^T)^{-1}$. Note that \mathbf{B} is invertible only when $N < L$. The solution when \mathbf{B} is singular is a more complicated problem which has been discussed in [14].

§ 2.4 Maximum Bit Rate (MBR) Method

Let $s_d(k)$ be the signal power in the $(k + 1)$ th subchannel. Then,

$$s_d(k) = \text{E}\{|\tilde{d}_i(k)|^2\}, \quad (2.40)$$

where $E\{\cdot\}$ is the expectation operation. Also, let $s_\eta(k)$ be the corresponding noise power. Then,

$$s_\eta(k) = E\{|\tilde{\eta}_i(k)|^2\}. \quad (2.41)$$

It is generally assumed that the transmit data are white, and hence the power is identical for each subchannel; that is, $s_d(k) = s_d$, where s_d is a constant. Similarly, the subchannel noise power $s_\eta(k) = s_\eta$, where s_η is a constant. From the definitions shown above, it is straightforward to have

$$E\{|\tilde{y}_{s,i}(k)|^2\} = s_d |\tilde{g}_s(k)|^2, E\{|\tilde{y}_{l,i}(k)|^2\} = s_d |\tilde{g}_l(k)|^2, \text{ and } E\{|\tilde{v}_i(k)|^2\} = s_\eta |\tilde{w}(k)|^2,$$

where

$$\tilde{w}(k) = \mathbf{f}^T(k) \mathbf{T}_W \mathbf{w}.$$

Here, $\tilde{w}(k)$ is the $(k + 1)$ th component of the M -DFT of \mathbf{w} , and \mathbf{T}_W is an $M \times N$ matrix padding zeros in \mathbf{w} to a size of M , i.e.,

$$\mathbf{T}_W = [\mathbf{I}_N, \mathbf{0}_{(M-N) \times N}]^T.$$

The subchannel signal-to-interference plus noise ratio (SINR) at the DFT output is then

$$\text{SINR}(k) = \frac{E\{|\tilde{y}_{s,i}(k)|^2\}}{E\{|\tilde{v}_i(k)|^2\} + E\{|\tilde{y}_{l,i}(k)|^2\}} = \frac{s_d |\tilde{g}_s(k)|^2}{s_\eta |\tilde{w}(k)|^2 + s_d |\tilde{g}_l(k)|^2}. \quad (2.42)$$

After some mathematical manipulations, the subchannel SINR can be rewritten as

$$\text{SINR}(k) = \frac{s_d(k) |\mathbf{f}^T(k) \mathbf{T}_G \mathbf{D}_S \mathbf{H} \mathbf{w}|^2}{s_\eta(k) |\mathbf{f}^T(k) \mathbf{T}_W \mathbf{w}|^2 + s_d(k) |\mathbf{f}^T(k) \mathbf{T}_G \mathbf{D}_I \mathbf{H} \mathbf{w}|^2} = \frac{\mathbf{w}^T \mathbf{A}(k) \mathbf{w}}{\mathbf{w}^T \mathbf{B}(k) \mathbf{w}} \quad (2.43)$$

where

$$\mathbf{A}(k) = s_d(k) \mathbf{H}^T \mathbf{D}_S^T \mathbf{T}_G^T \mathbf{f}^*(k) \mathbf{f}^T(k) \mathbf{T}_G \mathbf{D}_S \mathbf{H}, \text{ and}$$

$$\mathbf{B}(k) = s_\eta(k) \mathbf{T}_W^T \mathbf{f}^*(k) \mathbf{f}^T(k) \mathbf{T}_W + s_d(k) \mathbf{H}^T \mathbf{D}_I^T \mathbf{T}_G^T \mathbf{f}^*(k) \mathbf{f}^T(k) \mathbf{T}_G \mathbf{D}_I \mathbf{H}.$$

Using the result shown above, we can express the capacity for a DMT system as

$$B = \sum_{k \in \Omega} \log_2 \left(1 + \frac{1}{\Gamma} \frac{\mathbf{w}^T \mathbf{A}(k) \mathbf{w}}{\mathbf{w}^T \mathbf{B}(k) \mathbf{w}} \right) \text{ bits/symbol}, \quad (2.44)$$

where Ω is the set of total usable subchannels, namely,

$$\Omega = \{0, 1, \dots, M/2 - 1\},$$

and Γ the SNR gap [18]. Thus, we can obtain the optimum TEQ vector \mathbf{w} by maximizing (2.44). This method is called MBR [18]. Note that (2.44) is a nonlinear function of \mathbf{w} . It can only be solved by some nonlinear optimization methods, such as the quasi-Newton or simplex algorithms. Since the nonlinear optimization method often requires extensive computations, a suboptimal method, referred to as min-ISI, was then developed in [18]. It was shown that the performance of min-ISI can effectively approach the performance of MBR.

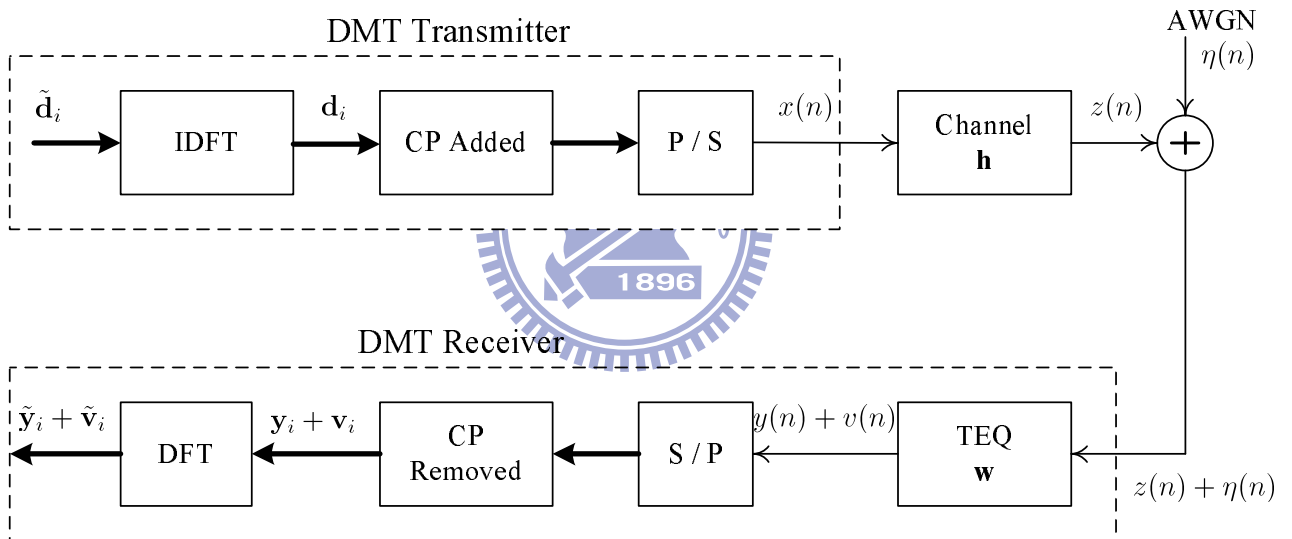


Figure 2.1: A DMT model for TEQ design

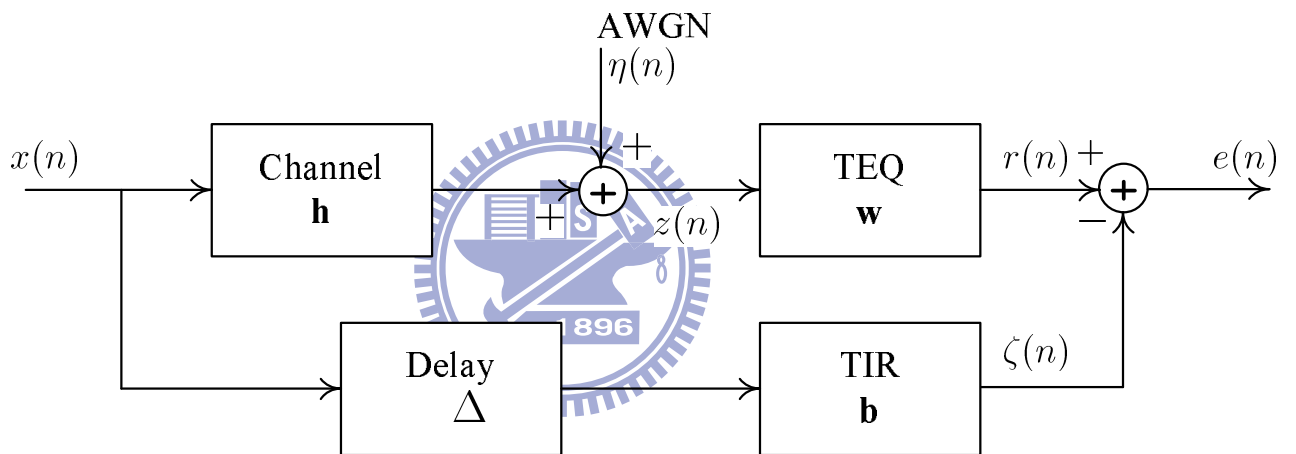


Figure 2.2: Block diagram of the MMSE equalizer

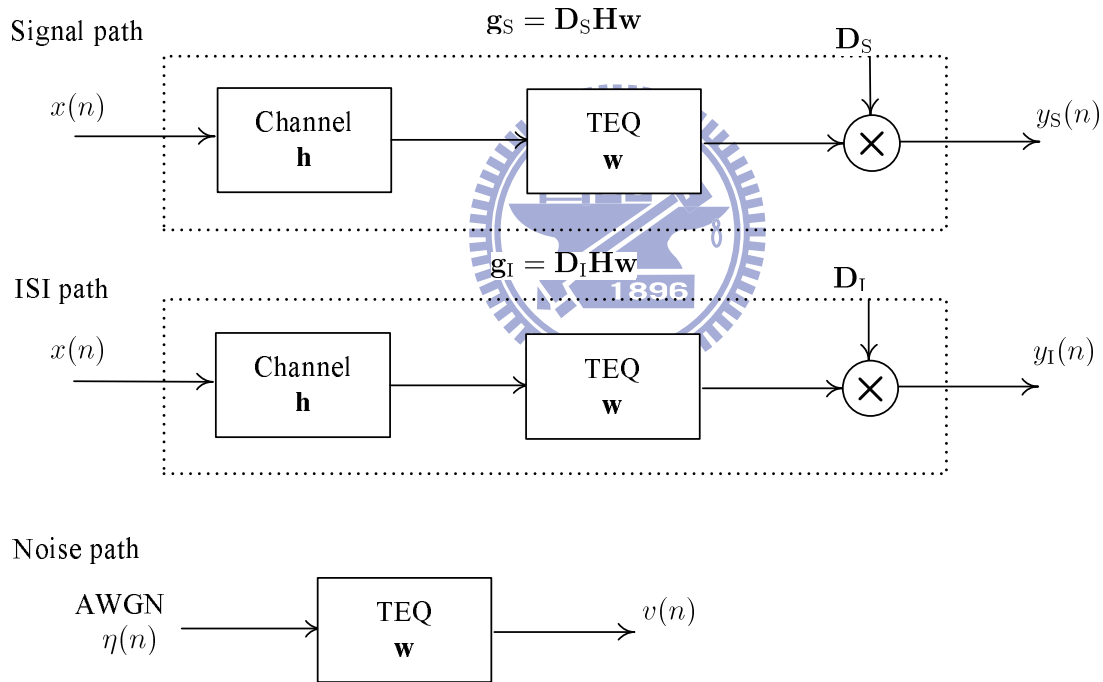
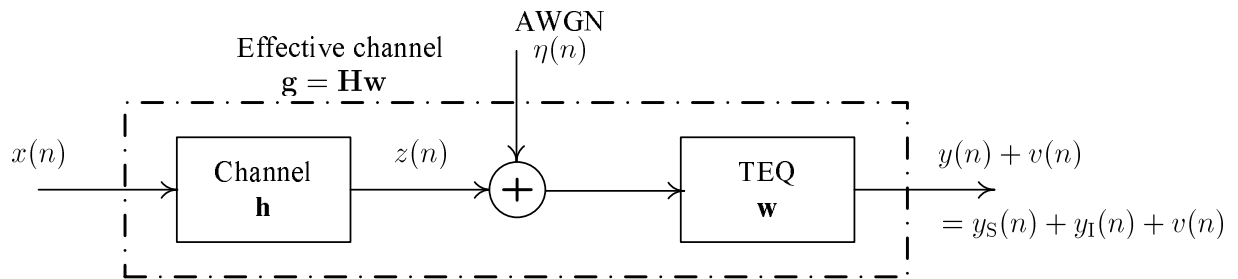


Figure 2.3: (a) Effective channel in a DMT system, (b) Decomposition of received signal: desired signal path, ISI path, and noise path (\mathbf{H} is the channel matrix).

Chapter 3

Time Domain Equalization for DMT Systems with Enhanced MBR Method



As shown in Section 2.4, to use the MBR method we have to evaluate the TEQ-filtered noise and the ISI powers. Unfortunately, we have found that, the TEQ-filtered noise and the ISI powers were not properly evaluated in existing works. As a result, the MBR method, claimed to be optimal, is not truly optimal. In this chapter, we attempt to resolve the problems not considered in previous works [15], [18]. We present a detailed analysis of the TEQ-filtered noise and residual ISI in a DMT system, and derive correct formulae for the calculation of the noise and residual ISI powers. With the analytic results, we further re-formulate the capacity function, and then propose a new method for TEQ design, called the enhanced MBR (EMBR) method. This chapter is organized as follows. In Section 3.1, we analyze the impact of the noise and residual ISI to the TEQ design, and derive correct formulae for the calculation of noise and residual ISI powers. In Section 3.2, we re-formulate the conventionally used cost function and propose a new TEQ design method. Section 3.3 gives simulation results.

§ 3.1 Analysis of Noise/Residual ISI Effect

§ 3.1.1 Conventional SINR calculation

As discussed in Section 2.4, interference in a subchannel consists of noise and residual ISI. Let

$$\mathbf{x}_i = [x(iK + L), \dots, x(iK + K - 1)]^T$$

be the i th data symbol at the DMT transmitter output. Since \mathbf{x}_i contains a CP, the desired signal component in (4.2) can be expressed as

$$\mathbf{y}_{s,i} = \mathbf{x}_i \circledast \mathbf{g}.$$

Here, we extend the circular convolution operation to vectors for notational simplicity. With the M -DFT operation,

$$\tilde{\mathbf{y}}_{s,i} \equiv \tilde{\mathbf{x}}_i \bullet \tilde{\mathbf{g}}$$

where \bullet is defined as the element-by-element vector multiplication. Note that noise does not contain CPs; thus, $\mathbf{v}_i \neq \boldsymbol{\eta}_i \circledast \mathbf{w}$, and $\tilde{\mathbf{v}}_i \neq \tilde{\boldsymbol{\eta}}_i \bullet \tilde{\mathbf{w}}$. As a result,

$$\mathbb{E}\{|\tilde{v}_i(k)|^2\} \neq s_\eta |\tilde{w}(k)|^2.$$

Also, the residual ISI response is the ISI response outside the CP region. The corresponding residual ISI cannot be obtained from the circular convolution of the input signal and \mathbf{g}_i . Thus,

$$\mathbb{E}\{|\tilde{y}_{i,i}(k)|^2\} \neq s_d |\tilde{g}_i(k)|^2.$$

From these facts, we conclude that SINR calculated with (2.42) is not correct. In other words,

$$\text{SINR}(k) \neq \frac{s_d |\tilde{g}_s(k)|^2}{s_\eta |\tilde{w}(k)|^2 + s_d |\tilde{g}_i(k)|^2} \quad (3.1)$$

Although the properties analyzed above are simple, they were not discovered until recently [26]. It was also independently observed in [25]. Since the SINR is erroneously calculated, the optimum solution obtained with (2.44) is no longer optimal. In the following section, we will analyze the effect of the non-cyclic noise and residual ISI, and derive correct formulae for their power calculations.

§ 3.1.2 Analysis of Noise Effect

Let

$$\begin{aligned}\mathbf{s}_d &= [s_d(0), s_d(1), \dots, s_d(M-1)]^T = s_d \cdot \mathbf{1}_M, \text{ and} \\ \mathbf{s}_\eta &= [s_\eta(0), s_\eta(1), \dots, s_\eta(M-1)]^T = s_\eta \cdot \mathbf{1}_M,\end{aligned}$$

where

$$\begin{aligned}s_d &= M \cdot \mathbf{E}\{x^2(n)\} = M\sigma_d^2, \text{ and} \\ s_\eta &= M \cdot \mathbf{E}\{\eta^2(n)\} = M\sigma_\eta^2.\end{aligned}$$

Recall \mathbf{g}_Δ defined in Section 2.1, and define \mathbf{G}_Δ as an $M \times M$ circular channel matrix:

$$\mathbf{G}_\Delta = \begin{bmatrix} g_\Delta(0) & 0 & \dots & 0 & g_\Delta(L-1) & \dots & g_\Delta(2) & g_\Delta(1) \\ g_\Delta(1) & g_\Delta(0) & \dots & 0 & 0 & \dots & g_\Delta(3) & g_\Delta(2) \\ \vdots & \vdots & \ddots & \vdots & \vdots & \ddots & \ddots & \vdots \\ 0 & 0 & \dots & g_\Delta(L-2) & g_\Delta(L-3) & \dots & g_\Delta(0) & 0 \\ 0 & 0 & \dots & g_\Delta(L-1) & g_\Delta(L-2) & \dots & g_\Delta(1) & g_\Delta(0) \end{bmatrix}. \quad (3.2)$$

We first consider a scenario in which \mathbf{g} does not have residual ISI. The DFT output of the received symbol $\tilde{\mathbf{y}}_i = \tilde{\mathbf{y}}_{S,i}$ can be written as

$$\tilde{\mathbf{y}}_{S,i} = \mathbf{F}\mathbf{y}_{S,i} = \mathbf{F}\mathbf{G}_\Delta\mathbf{x}_i = \tilde{\mathbf{G}}_\Delta\mathbf{x}_i,$$

where $\tilde{\mathbf{G}}_\Delta = \mathbf{F}\mathbf{G}_\Delta$. Define the vector consisting of the subchannel received signal powers as \mathbf{s}_y . Then,

$$\mathbf{s}_y = \mathbf{E}\{\langle \tilde{\mathbf{y}}_{S,i} \rangle^2\}.$$

It follows that

$$\mathbf{E}\{\langle \tilde{\mathbf{y}}_{S,i} \rangle^2\} = \langle \mathbf{E}\{\tilde{\mathbf{G}}_\Delta\mathbf{x}_i\} \rangle^2 = \sigma_d^2 \langle \tilde{\mathbf{G}}_\Delta \rangle^2.$$

Let

$$\mathbf{G}_\Delta = [\boldsymbol{\rho}(0), \dots, \boldsymbol{\rho}(M-1)],$$

where $\boldsymbol{\rho}(l)$ is the $(l + 1)$ th column of \mathbf{G}_Δ . Then,

$$\tilde{\mathbf{G}}_\Delta = [\tilde{\boldsymbol{\rho}}(0), \dots, \tilde{\boldsymbol{\rho}}(M - 1)],$$

where $\tilde{\boldsymbol{\rho}}(k) = \mathbf{F}\boldsymbol{\rho}(k)$ is the $(k + 1)$ th column vector of $\tilde{\mathbf{G}}_\Delta$. Thus,

$$\mathbf{s}_y = \mathbf{E} \{ \langle \tilde{\mathbf{y}}_{S,i} \rangle^2 \} = \sigma_d^2 \sum_{k=0}^{M-1} \langle \tilde{\boldsymbol{\rho}}(k) \rangle^2. \quad (3.3)$$

From (3.2), we find that each $\boldsymbol{\rho}(k)$ in \mathbf{s}_y contains a circular shift of the ECR vector \mathbf{g}_Δ . Thus,

$$\langle \tilde{\boldsymbol{\rho}}(k) \rangle^2 = \langle \tilde{\mathbf{g}}_\Delta \rangle^2$$

for all k 's, where

$$\tilde{\mathbf{g}}_\Delta = \mathbf{F}\mathbf{T}_\Delta\mathbf{g}_\Delta = \mathbf{F}\boldsymbol{\rho}(0)$$

and \mathbf{T}_Δ is an $M \times L$ zero padding matrix used to increase the size of \mathbf{g}_Δ to M . Consequently,

$$\mathbf{s}_y = M\sigma_d^2 \langle \tilde{\mathbf{g}}_\Delta \rangle^2 = s_d \langle \tilde{\mathbf{g}}_\Delta \rangle^2$$

for all k 's.

Without loss of generality, we let the TEQ length, N , be smaller than the CP length, L . Furthermore, let

$$\boldsymbol{\eta}_{C,i} = [\eta(iK + \Delta), \eta(iK + \Delta + 1), \dots, \eta(iK + \Delta + L - 1)]^T,$$

which is the noise sequence in the CP region of the i th symbol. Thus, the noise vector in the i th DMT symbol can be defined as

$$\tilde{\boldsymbol{\eta}}_i = [\tilde{\boldsymbol{\eta}}_{C,i}^T, \boldsymbol{\eta}_i^T]^T.$$

Then, we can denote the TEQ-filtered noise vector as

$$\mathbf{v}_i = \mathbf{W}\tilde{\boldsymbol{\eta}}_i,$$

where \mathbf{W} is an $M \times K$ matrix composing of TEQ coefficients as

$$\mathbf{W} = \begin{bmatrix} 0 & \dots & w(N-1) & w(N-2) & \dots & 0 & \dots & 0 & 0 \\ 0 & \dots & 0 & w(N-1) & \dots & 0 & \dots & 0 & 0 \\ \vdots & \ddots & \vdots & \vdots & \ddots & \vdots & \ddots & \vdots & \vdots \\ 0 & \dots & 0 & 0 & \dots & w(N-1) & \dots & w(0) & 0 \\ 0 & \dots & 0 & 0 & \dots & 0 & \dots & w(1) & w(0) \end{bmatrix}_{M \times K}. \quad (3.4)$$

Note that the first $(L - N)$ column vectors of \mathbf{W} are zero vectors, $\mathbf{0}_M$. The DFT of the TEQ-filtered noise vector in the i symbol, denoted as $\tilde{\mathbf{v}}_i$, is then

$$\tilde{\mathbf{v}}_i = \mathbf{F}\mathbf{v}_i = \mathbf{F}\mathbf{W}\tilde{\boldsymbol{\eta}}_i = \tilde{\mathbf{W}}\tilde{\boldsymbol{\eta}}_i,$$

where $\tilde{\mathbf{W}} = \mathbf{F}\mathbf{W}$ is the DFT of \mathbf{W} . Note that \mathbf{W} is not a circular matrix like \mathbf{G}_Δ , and \mathbf{W} can be expressed in another form $[\mathbf{u}(0), \dots, \mathbf{u}(K-1)]$, where $\mathbf{u}(p)$ is

$$\mathbf{u}(p) = \begin{cases} \mathbf{0}_M & \text{if } 0 \leq p \leq L - N \\ [w(L-p), \dots, w(N-1), \mathbf{0}_{K-N-p}^T]^T & \text{if } L - N + 1 \leq p \leq L - 1 \\ [\mathbf{0}_{p-L}^T, \mathbf{w}^T, \mathbf{0}_{K-N-p}^T]^T & \text{if } L \leq p \leq K - N \\ [\mathbf{0}_{p-L}^T, w(0), w(1), \dots, w(K-1-p)]^T & \text{if } K - N + 1 \leq p \leq K - 1 \end{cases} \quad (3.5)$$

Let \mathbf{s}_v denote the vector containing the power of TEQ-filtered noise in subchannels. Thus,

$$\mathbf{s}_v = \mathbf{E}\{\langle \tilde{\mathbf{v}}_i \rangle^2\} = \mathbf{E}\{\langle \tilde{\mathbf{W}}\tilde{\boldsymbol{\eta}}_i \rangle^2\} = \sigma_\eta^2 \langle \tilde{\mathbf{W}} \rangle^2 = \sigma_\eta^2 \sum_{p=0}^{K-1} \langle \tilde{\mathbf{u}}(p) \rangle^2, \quad (3.6)$$

where $\tilde{\mathbf{u}}(p) = \mathbf{F}\mathbf{u}(p)$ is the DFT of $\mathbf{u}(p)$, and

$$\mathbf{E}\{\langle \tilde{\boldsymbol{\eta}}_i \rangle^2\} = \sigma_\eta^2 \cdot \mathbf{1}_K.$$

For simplicity, we let \mathbf{W}_1 be the matrix formed by $\mathbf{u}(p)$ for $L - N + 1 \leq p \leq L - 1$, \mathbf{W}_2 be formed by $\mathbf{u}(p)$ for $L \leq p \leq K - N$, and \mathbf{W}_3 be formed by $\mathbf{u}(p)$ for $K - N + 1 \leq p \leq K - 1$, respectively. Then, we can rewrite \mathbf{W} as

$$\mathbf{W} = [\mathbf{0}_{M \times (L-N)}, \mathbf{W}_1, \mathbf{W}_2, \mathbf{W}_3]. \quad (3.7)$$

From (3.5), note that column vectors in \mathbf{W}_2 contain the complete TEQ vector \mathbf{w} , which implies that

$$\langle \tilde{\mathbf{u}}(p) \rangle^2 = \langle \tilde{\mathbf{w}} \rangle^2,$$

for $L \leq p \leq K - N$. Each column vector in \mathbf{W}_1 and \mathbf{W}_3 , however, contains only partial \mathbf{w} . As a result, \mathbf{s}_v can be expressed as

$$\mathbf{s}_v = \sigma_\eta^2 \left(\sum_{p=L-N+1}^{L-1} \langle \tilde{\mathbf{u}}(p) \rangle^2 + (M - N + 1) \langle \tilde{\mathbf{w}} \rangle^2 + \sum_{p=K-N+1}^{K-1} \langle \tilde{\mathbf{u}}(p) \rangle^2 \right). \quad (3.8)$$

Equation (3.8) gives the exact calculation of the noise power after TEQ. From (3.4), we can see that if the channel noise is cyclic, \mathbf{W} can be folded to become an $M \times M$ circular matrix. In this case, we have

$$\mathbf{s}_v = M \sigma_\eta^2 \langle \tilde{\mathbf{w}} \rangle^2 = s_\eta \langle \tilde{\mathbf{w}} \rangle^2. \quad (3.9)$$

Conventional SINR calculation, as shown (2.42), uses (3.9). However, the channel noise is not cyclic; (3.9) is incorrect. From (3.8), we can clearly see that two more terms are induced due to the non-cyclic noise problem.

Now, we use some experimental results to show the differences between (3.8) and (3.9). The experiment settings are the standard ADSL environments [5], and will be described later in detail in Section 3.3. These experiments are all obtained with the standard test loop CSA #5, and the vector of the TEQ coefficients \mathbf{w} is obtained with the min-ISI method [18]. As we can see from (3.9), \mathbf{s}_v , representing the TEQ-filtered noise spectrum, is equal to the multiplication of s_η and $\langle \tilde{\mathbf{w}} \rangle^2$. Thus, if the TEQ induces a null in its spectrum, it will also do that in \mathbf{s}_v . However, it is not the case in (3.8). Figure 3.1 shows the contribution of \mathbf{W}_1 , \mathbf{W}_2 , and \mathbf{W}_3 , to \mathbf{s}_v , respectively. Only \mathbf{W}_2 shows the same spectrum characteristic as that of \mathbf{w} . As mentioned previously, column vectors of both \mathbf{W}_1 and \mathbf{W}_3 contain only partial \mathbf{w} , and their spectrum characteristics are different from those of \mathbf{w} . As we can see from the figure, spectrum nulls introduced by the TEQ disappeared in spectrums yielded by \mathbf{W}_1 and \mathbf{W}_3 . Figure 3.2 shows the TEQ-filtered noise spectrums calculated with (3.8) and (3.9), and Figure 3.3 shows the zoomed spectrum around nulls. The simulated noise power is also shown in the figures, which

are obtained with 500 DMT symbols. It is apparent that the magnitudes at TEQ-induced nulls increase in the spectrum calculated with (3.8), and it is accurate. We then conclude that noise power tends to be higher in the spectrum with (3.8). This will have a great impact on the signal to noise ratio (SNR) at spectrum nulls induced by the TEQ.

§ 3.1.3 Analysis of residual ISI

In general, a TEQ can not be designed to shorten the channel into the CP range completely. The resultant channel response outside the CP range consists of the residual ISI. Let the transmit signal in the CP range of the i th DMT symbol be

$$\mathbf{x}_{C,i} = [x(iK), x(iK + 1), \dots, x(iK + L - 1)]^T.$$

We then have the complete i th DMT symbol,

$$\check{\mathbf{x}}_i = [\mathbf{x}_{C,i}^T, \mathbf{x}_i^T]^T,$$

which is a $K \times 1$ column vector. Due to the delay Δ , the i th received DMT symbol $\check{\mathbf{x}}_i$ receives interference from $\check{\mathbf{x}}_{i-1}$ and $\check{\mathbf{x}}_{i+1}$. Define an extended symbol as

$$\check{\mathbf{x}}_{3,i} = [\check{\mathbf{x}}_{i-1}^T, \check{\mathbf{x}}_i^T, \check{\mathbf{x}}_{i+1}^T]^T,$$

and the response of \mathbf{g}_1 can be ignored when it exceeds M ; that is,

$$\mathbf{g}_1 = [g(0), \dots, g_{\Delta}(-1), \mathbf{0}_L^T, g_{\Delta}(L), \dots, g(M - 1)]^T,$$

which can be expressed in another form as

$$\mathbf{g}_1 = [g_1(0), \dots, g_1(\Delta), g_1(\Delta + 1), \dots, g_1(M - 1)]^T.$$

Thus, the power of $\check{\mathbf{x}}_{3,i}$ is

$$\mathbb{E}\{[\check{\mathbf{x}}_{3,i}]^2\} = \sigma_d^2 \cdot \begin{bmatrix} \mathbf{C}_S & \mathbf{0}_{K \times K} & \mathbf{0}_{K \times K} \\ \mathbf{0}_{K \times K} & \mathbf{C}_S & \mathbf{0}_{K \times K} \\ \mathbf{0}_{K \times K} & \mathbf{0}_{K \times K} & \mathbf{C}_S \end{bmatrix},$$

where

$$\mathbf{C}_S = \mathbf{I}_{K \times K} + \begin{bmatrix} \mathbf{0}_{L \times M} & \mathbf{I}_{L \times L} \\ \mathbf{0}_{M \times M} & \mathbf{0}_{M \times L} \end{bmatrix}.$$

Using vector representation, we can express the residual ISI $\mathbf{y}_{1,i}$ in (4.2) as

$$\mathbf{y}_{1,i} = \mathbf{C}_I \check{\mathbf{x}}_{3,i},$$

where

$$\mathbf{C}_I = [\mathbf{c}_I(0), \dots, \mathbf{c}_I(3K - 1)]$$

is the matrix with residual ISI coefficients. We have the following decomposition:

$$\mathbf{C}_I = [\mathbf{0}_{M \times (2L + \Delta + 1)}, \mathbf{C}_1, \mathbf{C}_2, \mathbf{C}_3, \mathbf{0}_{M \times (K - \Delta)}]_{M \times 3K},$$

where

$$\begin{aligned} \mathbf{C}_1 &= \begin{bmatrix} g_I(M-1) & \dots & g_I(1) \\ \mathbf{0} & \dots & g_I(2) \\ \vdots & & \vdots \\ 0 & \dots & g_I(M-1) \\ 0 & \dots & 0 \end{bmatrix}_{M \times (M-1)} \\ \mathbf{C}_2 &= \begin{bmatrix} g_I(0) & g_I(1) & \dots & g_I(M-1) \end{bmatrix}_{M \times 1}^T \\ \mathbf{C}_3 &= \begin{bmatrix} 0 & \dots & 0 & 0 \\ g_I(0) & \dots & 0 & 0 \\ \vdots & \ddots & \vdots & \vdots \\ g_I(M-2) & \dots & g_I(1) & g_I(0) \end{bmatrix}_{M \times (M-1)}. \end{aligned} \quad (3.10)$$

Let

$$\tilde{\mathbf{C}}_I = \mathbf{F} \mathbf{C}_I = [\mathbf{0}_{M \times (2L + \Delta + 1)}, \tilde{\mathbf{c}}_I(1), \dots, \tilde{\mathbf{c}}_I(2M - 1), \mathbf{0}_{M \times (K - \Delta)}]$$

be the DFT of \mathbf{C}_I , where

$$\tilde{\mathbf{c}}_I(p) = \mathbf{F} \mathbf{c}_I(2L + \Delta + p), \text{ for } 1 \leq p \leq 2M - 1.$$

At the DFT output, we have the residual ISI component of the received signal,

$$\tilde{\mathbf{y}}_{1,i} = \mathbf{F}\mathbf{y}_{1,i} = \mathbf{F}\mathbf{C}_1\tilde{\mathbf{x}}_{3,i} = \tilde{\mathbf{C}}_1\tilde{\mathbf{x}}_{3,i}.$$

Denote \mathbf{s}_1 as the vector containing residual ISI power in subchannels. Then,

$$\begin{aligned} \mathbf{s}_1 &= \mathbf{E} \{ \langle \tilde{\mathbf{y}}_{1,i} \rangle^2 \} = \mathbf{E} \{ \langle \mathbf{F}\mathbf{C}_1\tilde{\mathbf{x}}_{3,i} \rangle^2 \} \\ &= \sigma_d^2 \sum_{p=1}^{2M-1} \langle \tilde{\mathbf{c}}_1(p) \rangle^2 + \sigma_d^2 \sum_{p=M-L-\Delta}^{M-\Delta-1} \langle \tilde{\mathbf{c}}_1(p) \rangle^2 + \sigma_d^2 \sum_{p=2M-\Delta}^{2M+L-\Delta-1} \langle \tilde{\mathbf{c}}_1(p) \rangle^2, \end{aligned} \quad (3.11)$$

where the last two terms in (3.11) are the interference power induced from the off-diagonal terms of $\mathbf{E} \{ [\tilde{\mathbf{x}}_{3,i}]^2 \}$. Observe that only \mathbf{C}_2 has the complete residual ISI vector \mathbf{g}_1 . Thus,

$$\langle \tilde{\mathbf{C}}_2 \rangle^2 = \langle \tilde{\mathbf{g}}_1 \rangle^2,$$

where

$$\tilde{\mathbf{C}}_2 = \mathbf{F}\mathbf{C}_2 = \tilde{\mathbf{c}}_1(K+L).$$

Column vectors in \mathbf{C}_1 and \mathbf{C}_3 contain only partial \mathbf{g}_1 . If \mathbf{g}_1 is in the CP range, then the circular convolution property can be applied. Then,

$$\mathbf{s}_1 = M\sigma_d^2 \langle \tilde{\mathbf{g}}_1 \rangle^2 = s_d \langle \tilde{\mathbf{g}}_1 \rangle^2. \quad (3.12)$$

This is the result used in (2.42). However, the residual ISI is the ISI outside the CP range, and (3.12) is not valid in practice.

Here, we also use some experimental results to show the difference between (3.11) and (3.12). The experiment settings are the same as those in Section 3.1.2. Figure 3.4 shows the spectrums yielded by \mathbf{C}_1 , \mathbf{C}_2 , and \mathbf{C}_3 in (3.10), respectively. We can see that spectrums yielded by \mathbf{C}_1 and \mathbf{C}_3 are larger than that by \mathbf{C}_2 , which is directly related to \mathbf{g}_1 . This phenomenon is more apparent in regions with spectrum nulls. Figure 3.5 shows the spectrums obtained with (3.11) and (3.12), and Figure 3.6 is a zoomed spectrum. The simulated ISI power is also shown in the figures, which are obtained with 500 DMT symbols. As revealed with the figures, the magnitudes at the nulls are significantly raised in the spectrum calculated with (3.11). Also, the

spectrum agrees with that simulation very well. Similar to the case in Section 3.1.2, the SINR is reduced at spectrum nulls.

Combining the results in Section 3.1.2 and Section 3.1.3, we conclude that the SINR calculation in (2.43) is not correct. To have better loading performance, noise and residual ISI powers should be revised to those in (3.8) and (3.11). In the next section, we will use the corrected formula to propose a new TEQ scheme.

§ 3.2 Proposed Method

The formulations in (3.8) and (3.11) is meant to demonstrate the effect of the non-cyclic property of noise and the residual ISI. To derive the optimum TEQ, we have to use another formulation. Rewrite the TEQ-filtered noise vector \mathbf{v}_i as $\mathbf{v}_i = \mathbf{N}_i \mathbf{w}$, where \mathbf{N}_i is a matrix with noise samples, i.e.,

$$\mathbf{N}_i = \begin{bmatrix} \eta(iK + \Delta + L) & \dots & \eta(iK + \Delta + L - N + 1) \\ \vdots & \ddots & \vdots \\ \eta(iK + \Delta + K - 1) & \dots & \eta(iK + \Delta + K - N + 1) \end{bmatrix}_{M \times N}. \quad (3.13)$$

The DFT of the i th TEQ-filtered noise symbol at the $(k + 1)$ th subchannel is

$$\tilde{v}_i(k) = \mathbf{f}^T(k) \mathbf{v}_i = \mathbf{f}^T(k) \mathbf{N}_i \mathbf{w},$$

and the corresponding power is

$$\mathbb{E}\{|\tilde{v}_i(k)|^2\} = \mathbb{E}\left\{|\mathbf{f}^T(k) \mathbf{N}_i \mathbf{w}|^2\right\} = \mathbf{w}^T \mathbf{R}(k) \mathbf{w},$$

where

$$\mathbf{R}(k) = \mathbb{E}\{[\tilde{\mathbf{N}}_i^T(k)]^2\},$$

and

$$\tilde{\mathbf{N}}_i(k) = \mathbf{f}^T(k) \mathbf{N}_i.$$

Similarly, we can rewrite the residual ISI, $\mathbf{y}_{1,i}$, in (4.2) as

$$\mathbf{y}_{1,i} = \mathbf{X}_i \mathbf{g}_i,$$

where

$$\mathbf{X}_i = \begin{bmatrix} x(iK + L - J + 1) & \dots & x(iK + L) \\ \vdots & \ddots & \vdots \\ x(iK + K - J) & \dots & x(iK + K - 1) \end{bmatrix}_{M \times J}. \quad (3.14)$$

The DFT of the residual ISI at the $(k + 1)$ th subchannel is

$$\tilde{y}_{1,i}(k) = \mathbf{f}^T(k) \mathbf{y}_{1,i} = \mathbf{f}^T(k) \mathbf{X}_i \mathbf{D}_1 \mathbf{H} \mathbf{w},$$

and the corresponding power is

$$\mathbb{E}\{|\tilde{y}_{1,i}(k)|^2\} = \mathbb{E}\{|\mathbf{f}^T(k) \mathbf{X}_i \mathbf{D}_1 \mathbf{H} \mathbf{w}|^2\} = \mathbf{w}^T \mathbf{Q}(k) \mathbf{w},$$

where

$$\mathbf{Q}(k) = \mathbf{H}^T \mathbf{D}_1^T \mathbb{E}\{|\tilde{\mathbf{X}}_i^T(k)|^2\} \mathbf{D}_1 \mathbf{H},$$

and

$$\tilde{\mathbf{X}}_i(k) = \mathbf{f}^T(k) \mathbf{X}_i.$$

Then, the subchannel SINR can be revised from (2.42) as

$$\text{SINR}(k) = \frac{\mathbb{E}\{|\tilde{y}_{s,i}(k)|^2\}}{\mathbb{E}\{|\tilde{v}_i(k)|^2\} + \mathbb{E}\{|\tilde{y}_{1,i}(k)|^2\}} = \frac{\mathbf{w}^T \mathbf{A}(k) \mathbf{w}}{\mathbf{w}^T \mathbf{Y}(k) \mathbf{w}} \quad (3.15)$$

where $\mathbf{A}(k)$ is defined as that in (2.43), and

$$\mathbf{w}^T \mathbf{Y}(k) \mathbf{w} = \mathbf{w}^T [\mathbf{R}(k) + \mathbf{Q}(k)] \mathbf{w}$$

includes the noise power $\mathbf{w}^T \mathbf{R}(k) \mathbf{w}$ and residual ISI power $\mathbf{w}^T \mathbf{Q}(k) \mathbf{w}$. Finally, the capacity can be expressed in terms of the subchannel SINR (3.15) as

$$B = \sum_{k \in \Omega} \log_2 \left(1 + \frac{1}{\Gamma} \frac{\mathbf{w}^T \mathbf{A}(k) \mathbf{w}}{\mathbf{w}^T \mathbf{Y}(k) \mathbf{w}} \right) \text{ bits/symbol}. \quad (3.16)$$

The optimum \mathbf{w} can then be obtained by maximizing B . To distinguish from the MBR method [18], we called the proposed method the enhanced MBR (EMBR) method.

The proposed EMBR method requires the use of a nonlinear optimization method to search the optimum solution and its computational complexity is high. To reduce the complexity, (3.16) must be simplified. Here, we use the procedure outlined in [18] to do the work. To avoid the trivial all-zero solution, a constraint must be imposed. Using the constraint that

$$\sum_{k \in \Omega} \mathbf{w}^T \mathbf{A}(k) \mathbf{w} = 1,$$

we define the TEQ optimization problem as

$$\text{Minimize } \mathbf{w}^T \left(\sum_{k \in \Omega} \mathbf{Y}(k) \right) \mathbf{w}, \text{ subject to } \mathbf{w}^T \left(\sum_{k \in \Omega} \mathbf{A}(k) \right) \mathbf{w} = 1. \quad (3.17)$$

From results derived previously, we have

$$\sum_{k \in \Omega} \mathbf{w}^T \mathbf{Y}(k) \mathbf{w} = \mathbf{w}^T \sum_{k \in \Omega} \mathbf{E}\{[\tilde{\mathbf{N}}_i(k)]^2\} \mathbf{w} + \mathbf{w}^T \mathbf{H}^T \mathbf{D}_1^T \sum_{k \in \Omega} \mathbf{E}\{[\tilde{\mathbf{X}}_i(k)]^2\} \mathbf{D}_1 \mathbf{H} \mathbf{w} \quad (3.18)$$

From the definition of $\mathbf{E}\{[\tilde{\mathbf{N}}_i(k)]^2\}$, we can derive its closed-form expression as

$$\mathbf{E}\{[\tilde{\mathbf{N}}_i(k)]^2\} = \sigma_\eta^2 \begin{bmatrix} a_1 & b_{1,2} & \dots & b_{1,N} \\ b_{2,1} & a_2 & \dots & b_{2,N} \\ \vdots & \vdots & \ddots & \vdots \\ b_{N,1} & b_{N,2} & \dots & a_N \end{bmatrix}, \quad (3.19)$$

where

$$\begin{cases} a_i = M & \text{for all } i, \\ b_{i,j} = (M - i + j) \alpha^{(j-i)k} & \text{for } i > j, \\ b_{i,j} = (M + i - j) \alpha^{(j-i)k} & \text{for } i < j. \end{cases}$$

Similarly, we have $E\{[\tilde{\mathbf{X}}_i(k)]^2\}$ as

$$\sigma_d^2 \begin{bmatrix} a_1 & b_{1,2} & \dots & b_{1,L+1} & b_{1,L+2} + c_{1,L+2} & \dots & b_{1,M} + c_{1,M} \\ b_{2,1} & a_2 & \dots & b_{2,L+1} & b_{2,L+2} & \dots & b_{2,M} + c_{2,M} \\ \vdots & \vdots & \ddots & \vdots & \vdots & \ddots & \vdots \\ b_{L+1,1} & b_{L+1,2} & \dots & a_{L+1} & b_{L+1,L+2} & \dots & b_{L+1,M} + c_{L+1,M} \\ b_{L+2,1} + c_{L+2,1} & b_{L+2,2} & \dots & b_{L+2,L+1} & a_{L+2} & \dots & b_{L+2,M} + c_{L+2,M} \\ b_{L+3,1} + c_{L+3,1} & b_{L+3,2} + c_{L+3,2} & \dots & b_{L+3,L+1} & b_{L+3,L+2} & \dots & b_{L+3,M} + c_{L+3,M} \\ \vdots & \vdots & \ddots & \vdots & \vdots & \ddots & \vdots \\ b_{M,1} + c_{M,1} & b_{M,2} + c_{M,2} & \dots & b_{M,L+1} + c_{M,L+1} & b_{M,L+2} + c_{M,L+2} & \dots & a_M \end{bmatrix} \quad (3.20)$$

where

$$\begin{cases} c_{i,j} = (i-j-L)\alpha^{(M+L+j-i)k} & \text{for } i > j, \\ c_{i,j} = (j-i-L)\alpha^{-(M+L-j+i)k} & \text{for } i < j. \end{cases}$$

The maximization problem in (3.17) is known to be a Rayleigh quotient problem, and the solution can be obtained with the eigen-decomposition method. Let

$$\mathbf{A} = \sum_{k \in \Omega} \mathbf{A}(k), \quad \mathbf{Y} = \sum_{k \in \Omega} \mathbf{Y}(k).$$

Using the Cholesky decomposition, we have

$$\mathbf{A} = \mathbf{A}_{CD}^T \mathbf{A}_{CD}.$$

The optimal TEQ solution to (3.17) is known to be

$$\mathbf{w}_{opt} = \mathbf{A}_{CD}^{-1} \mathbf{p}_{min}, \quad (3.21)$$

where \mathbf{p}_{min} is the eigenvector corresponding to the minimum eigenvalue of a composite matrix $\mathbf{A}_{CD}^{-1} \mathbf{Y} (\mathbf{A}_{CD}^T)^{-1}$ [14]. We refer to the EMBR solved with the suboptimum method as simplified EMBR (SEMBR). The SEMBR method avoids the complicated nonlinear optimization problem. Simulations show that the TEQ designed with the SEMBR method is close to the optimum.

§ 3.3 Simulations

In this section, we report some simulation results to demonstrate the effectiveness of the proposed TEQ method. We use the 12 standard test loops defined in the ITU ADSL specification [7], including 3 revised resistance design (RRD) loops, 8 carrier serving area (CSA) loops, and one Mid-CSA loop. Figure 3.7 shows the configuration of these test loops. In this figure, the numbers specified for a link represent the wire length and the wire gauge of the link. The performance of the proposed SEMBR method and that of the original min-ISI method [18] is compared. The channel noise was modeled as AWGN with a flat power spectrum density of -140 dBm/Hz, and near-end-cross-talk (NEXT) noise from 5 integrated services digital network (ISDN) disturbers. The transmit signal power was set to 23 dBm. The DFT/IDFT size, as defined in the ITU ADSL standard, is 512, and the CP size is 32. In addition, the sampling rate was set to 2.208 MHz, and the overall SNR gap Γ is 11.6 dB [12].

Figure 3.8 shows the subchannel SINRs with TEQs obtained by the min-ISI and the SEMBR methods for mid-CSA loop #6. Both SINR plots are evaluated with 500 DMT symbols. As we can see, these two SINR distributions are very close. However, some nulls appear in the SINR plot associated with the min-ISI method. Bit loading in these subchannels are then seriously affected. Figure 3.9 shows the throughput comparison for the DMT systems with TEQs designed by the min-ISI and SEMBR methods. All 12 test loops mentioned above were evaluated, and the size of the TEQ used here was set to 16. Note that the loop index in Figure 3.9 is defined in Table 3.1 and the table also shows the detailed throughput in Figure 3.9. The matched filter bound (MFB) in Figure 3.9, calculated without the ISI effect, serves as the theoretical upper bound. From the figure, we can observe that the throughput of the DMT system with the TEQ designed by the SEMBR method is consistently higher than that generated by the min-ISI method. Figure 3.10 shows the frequency responses of TEQs designed with the min-ISI and SEMBR methods for CSA loop #6 and T1.601 loop #9. From the figure, we can clearly tell the difference between these two methods. The TEQ responses yielded by the proposed

Table 3.1: Throughput for various TEQ design methods (unit: Mbps)

Loop Index	Test Loop	min-ISI	SEMBR	MFB
1	CSA Loop #1	8.6045	9.0972	9.2306
2	CSA Loop #2	9.7885	10.321	10.548
3	CSA Loop #3	8.3222	8.7051	8.8715
4	CSA Loop #4	8.2342	8.7314	8.8668
5	CSA Loop #5	8.8369	9.1219	9.3507
6	CSA Loop #6	8.0701	8.4261	8.5745
7	CSA Loop #7	7.8381	8.4464	8.5303
8	CSA Loop #8	7.1301	7.4443	7.5482
9	midCSA Loop	9.7429	10.114	10.182
10	T1.601 Loop #7	2.1658	2.2491	2.4220
11	T1.601 Loop #9	2.5006	2.7647	2.9412
12	T1.601 Loop #13	2.5112	2.7635	2.9090

SEMBR method do not have the spectrum nulls as those observed from the min-ISI method. The appearance of the nulls is due to the underestimate of the noise and residual ISI powers.

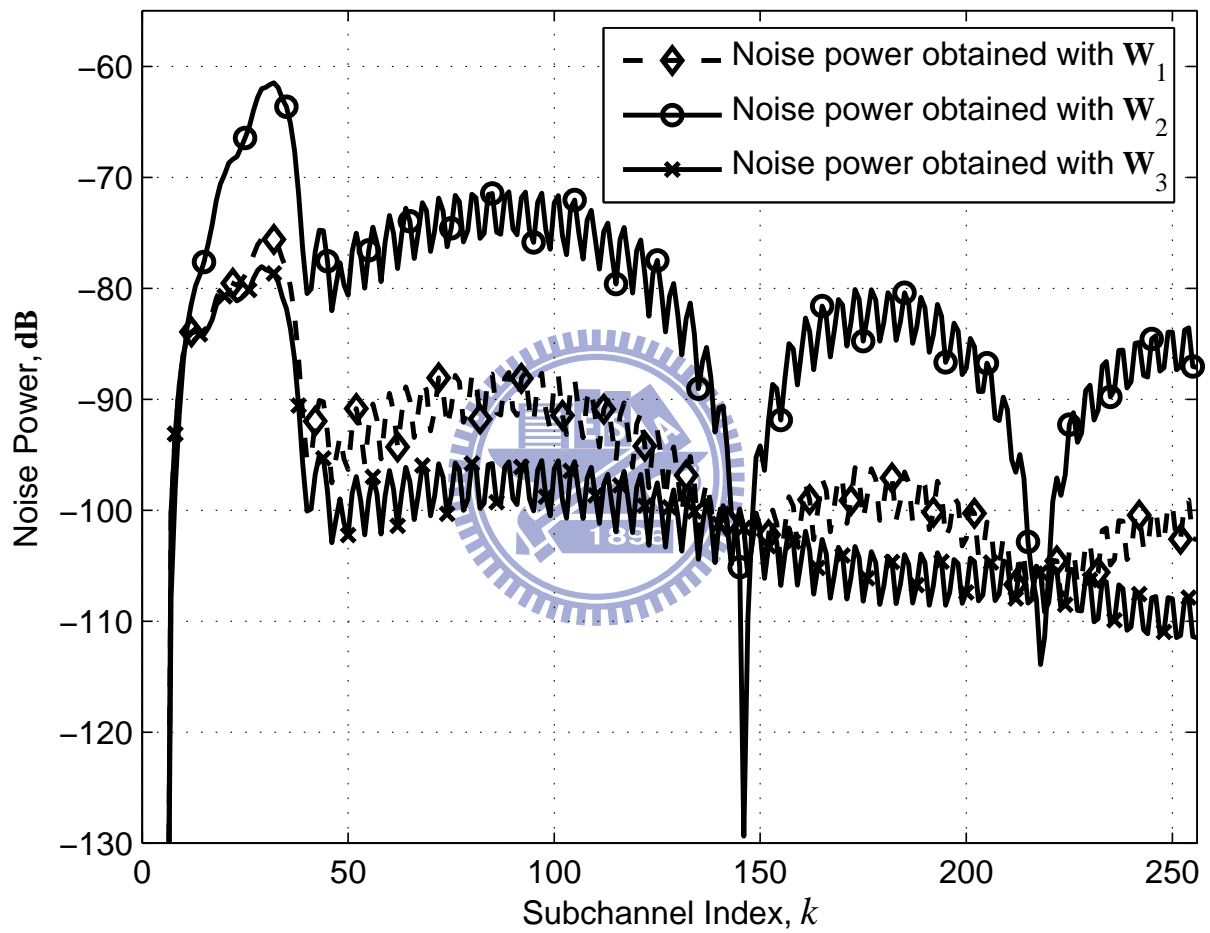


Figure 3.1: Decomposed TEQ-filtered noise powers ($N = 16$, CSA#5 Loop)

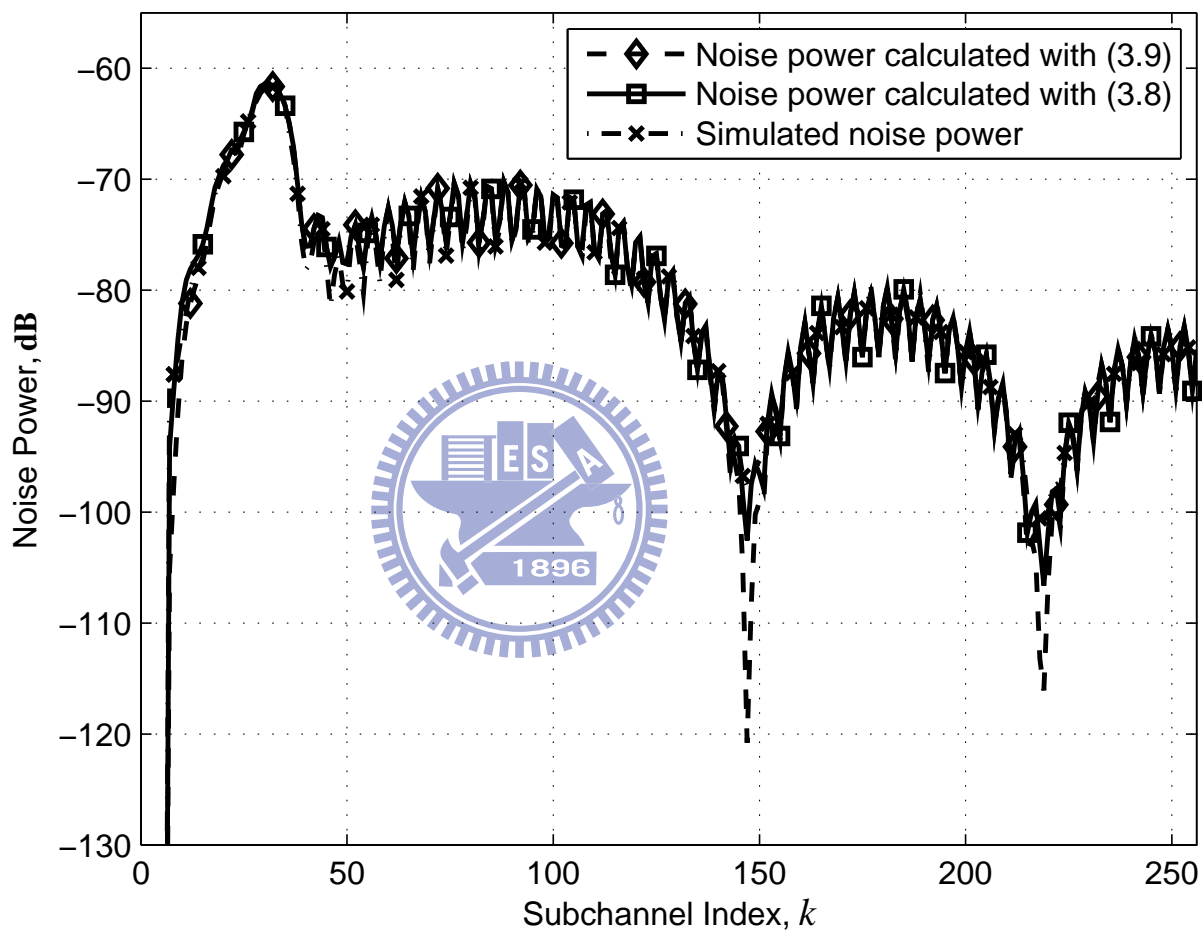


Figure 3.2: Comparison of TEQ-filtered noise powers; power calculated with (3.9), power calculated with (3.8) (correct one), and simulated power ($N = 16$, CSA#5 Loop)

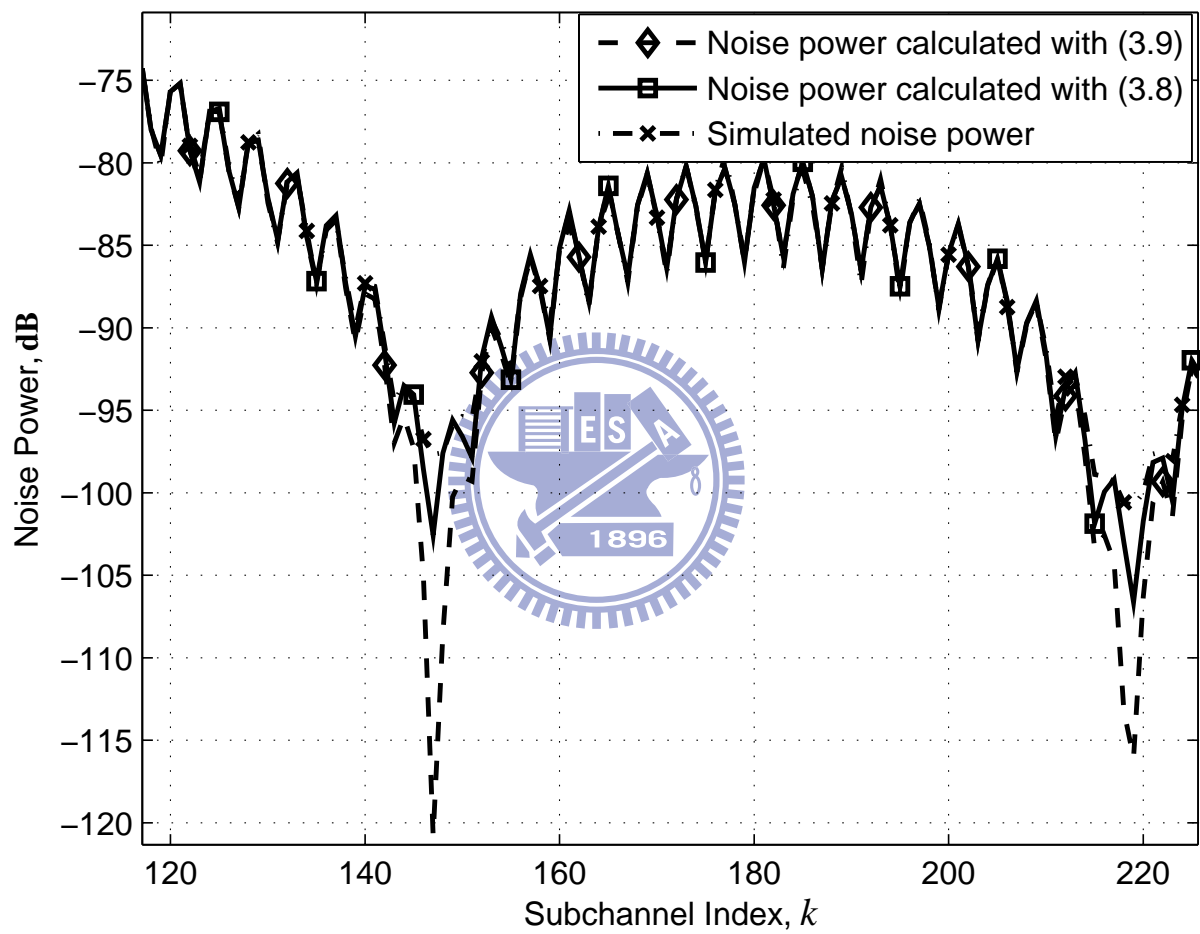


Figure 3.3: A zoomed view of Figure 3.2

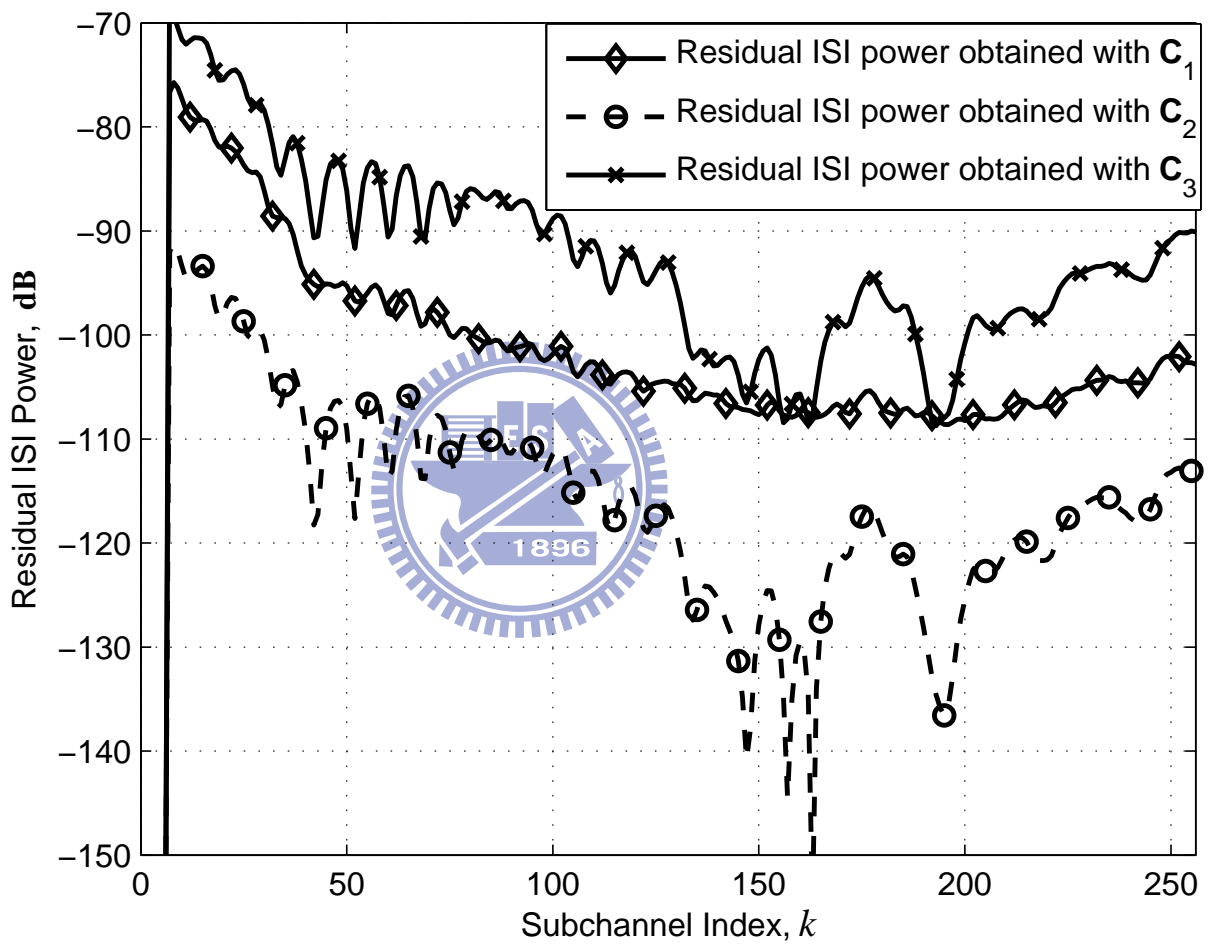


Figure 3.4: Decomposed residual-ISI powers ($N = 16$, CSA#5 Loop)

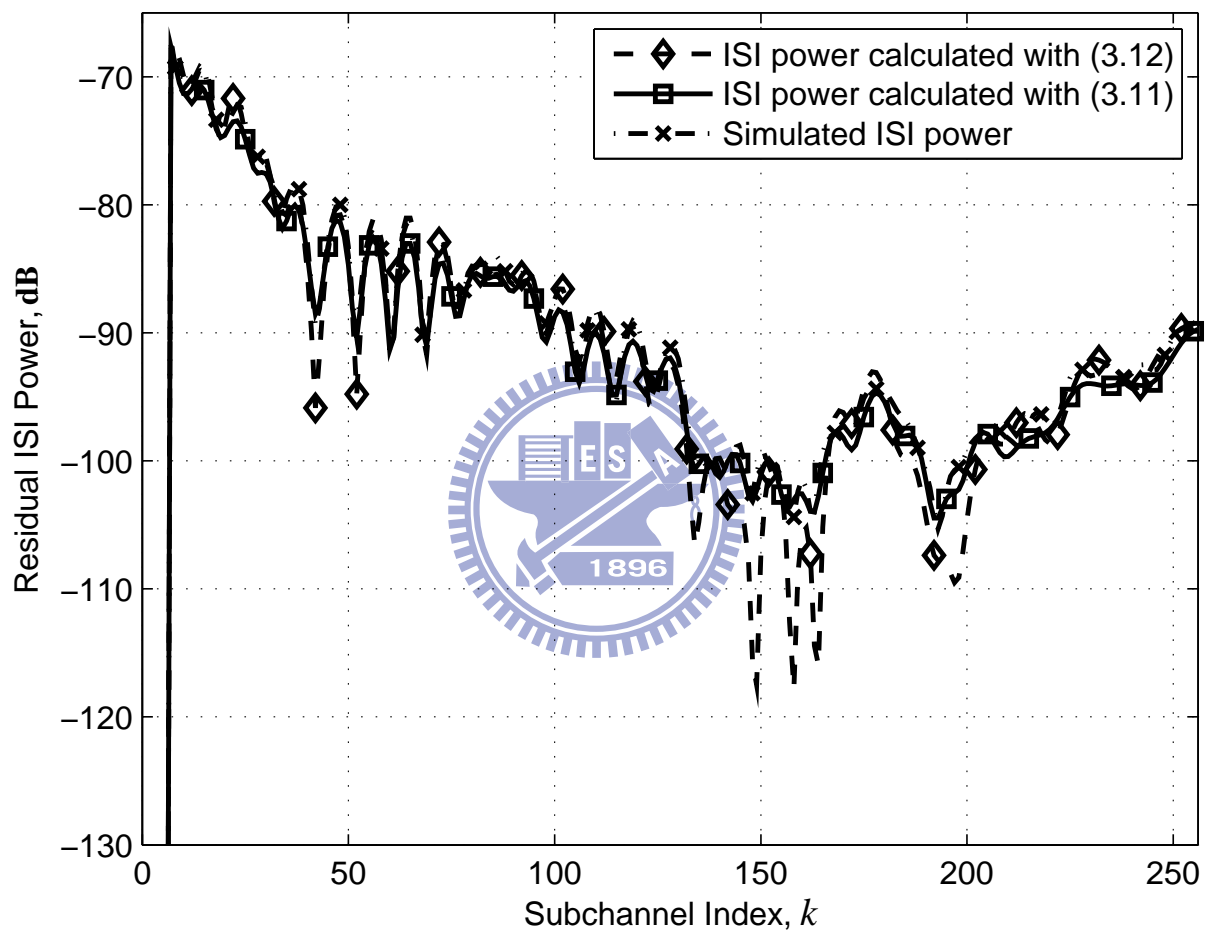


Figure 3.5: Comparison of residual-ISI powers; power calculated with (3.12), power calculated with (3.11) (correct one), and simulated power ($N = 16$, CSA#5 Loop)

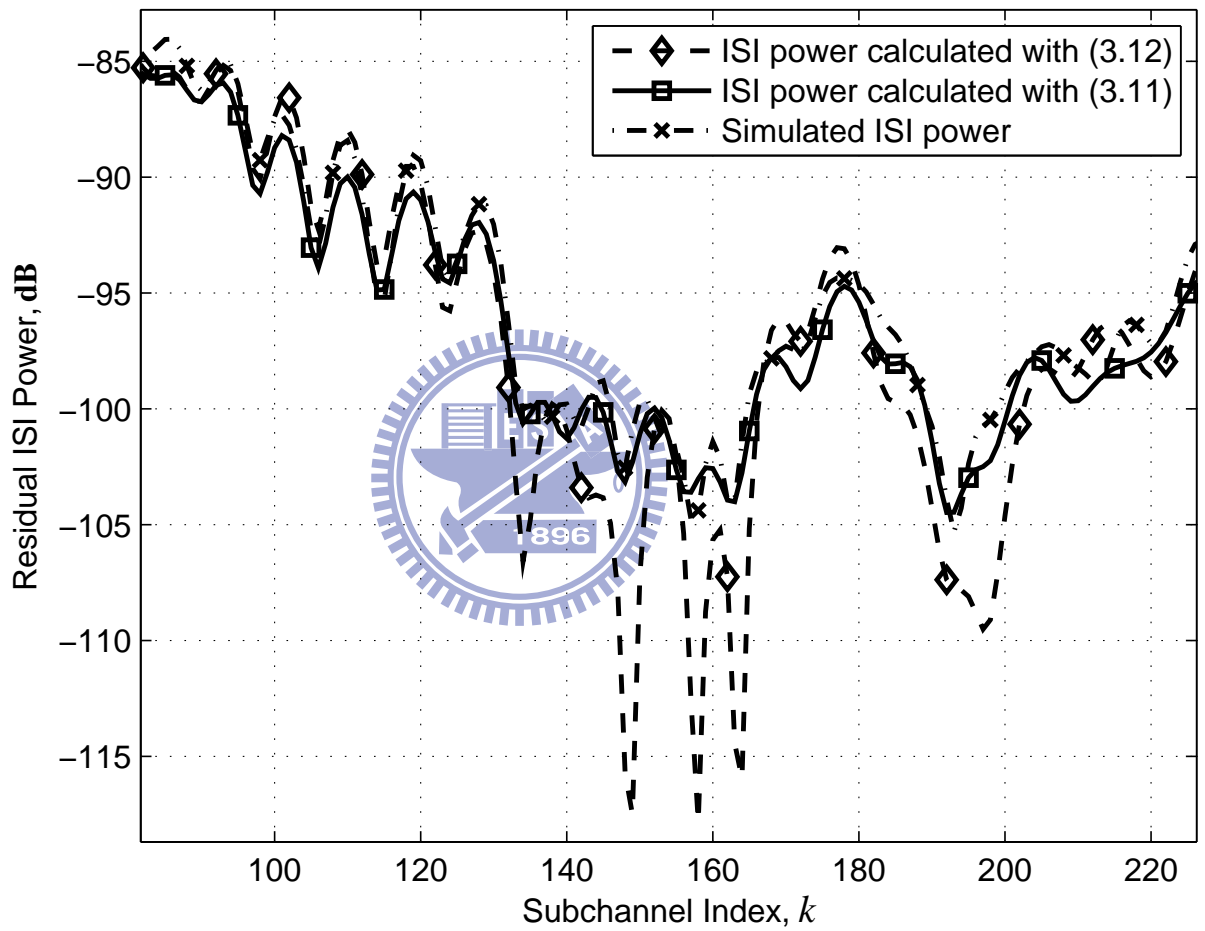


Figure 3.6: A zoomed view of Figure 3.5

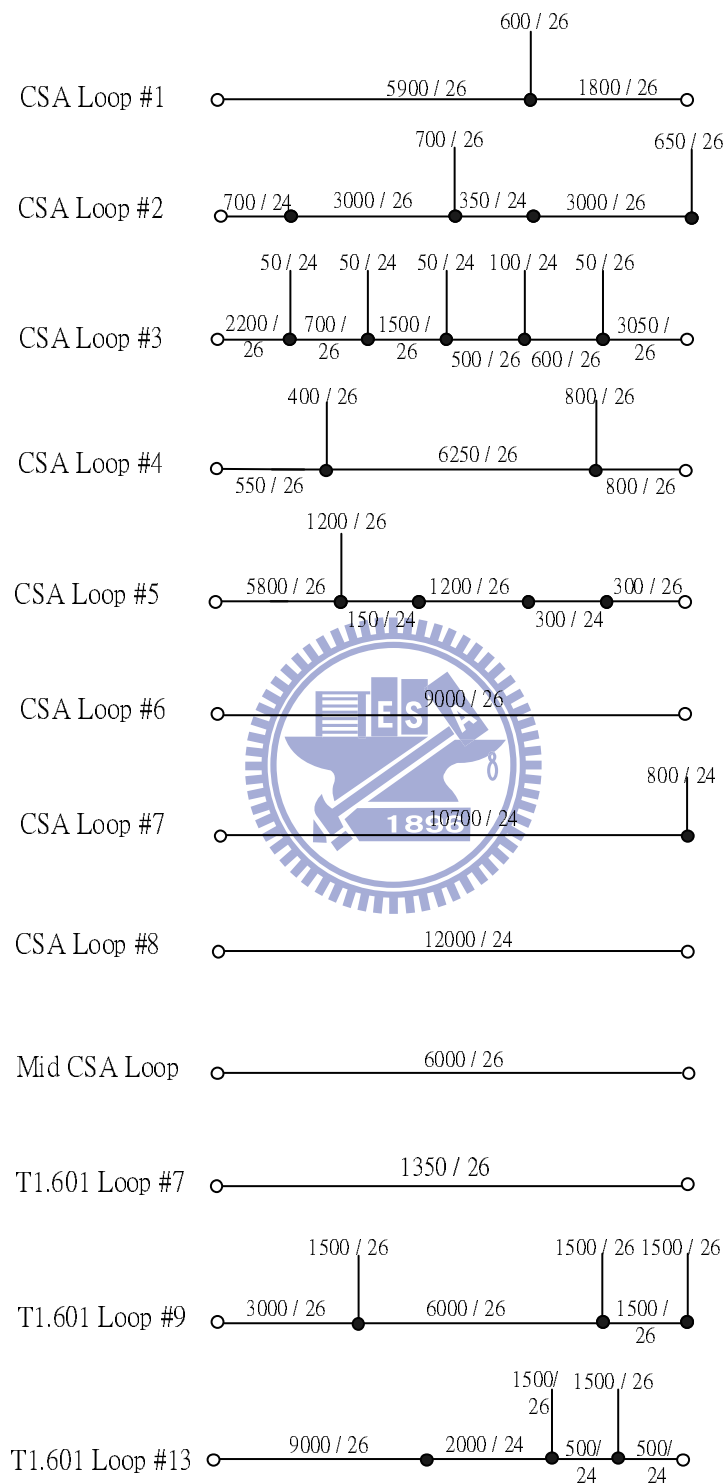


Figure 3.7: Configuration of various standard test loops defined in ITU-T Recommendation G.996.1. The numbers on a line segment represent the length (feet) and the wire gauge (American wire gauge) of the line. The left side of a loop is connected to a central office.

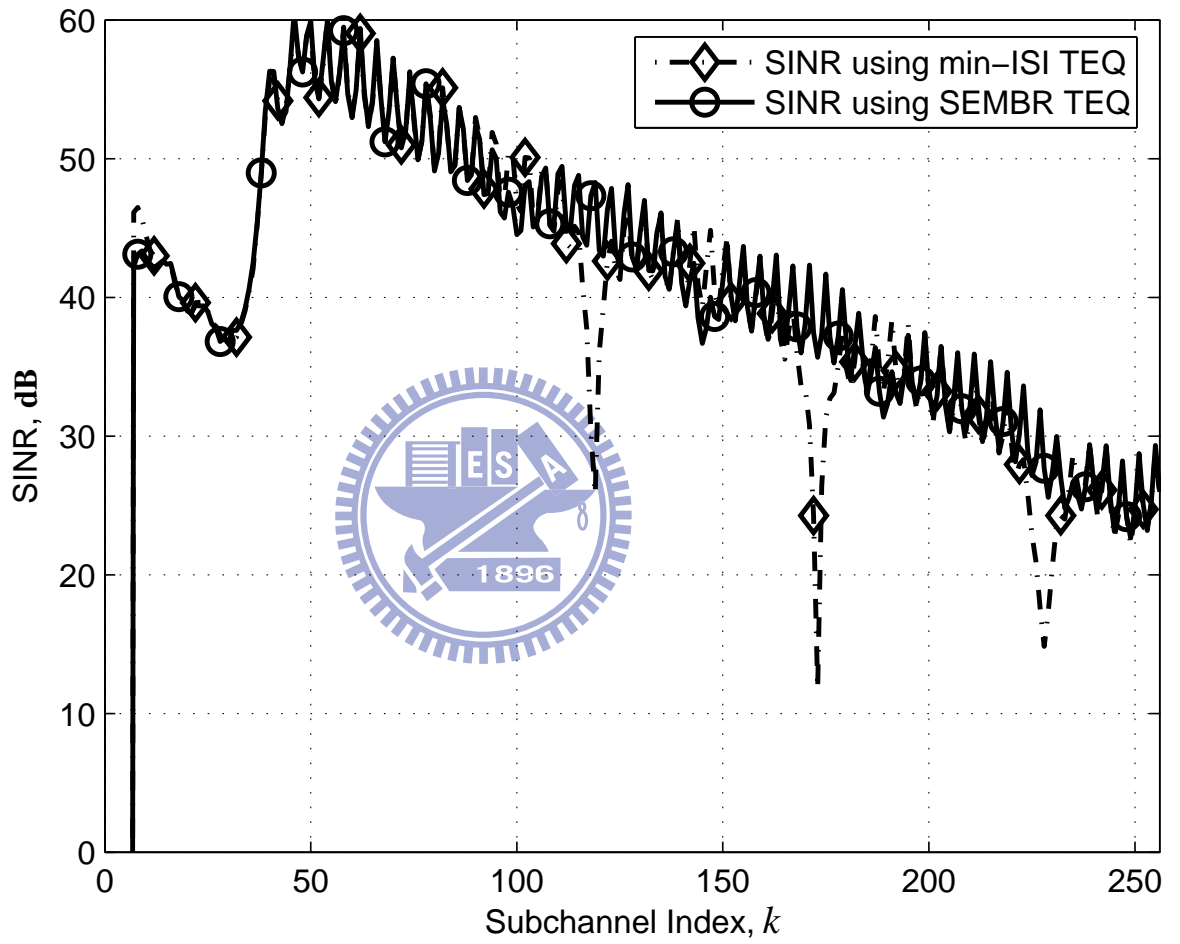


Figure 3.8: SINR comparison between TEQs designed for min-ISI method and SEMBR method ($N = 16$, mid-CSA#6 Loop)

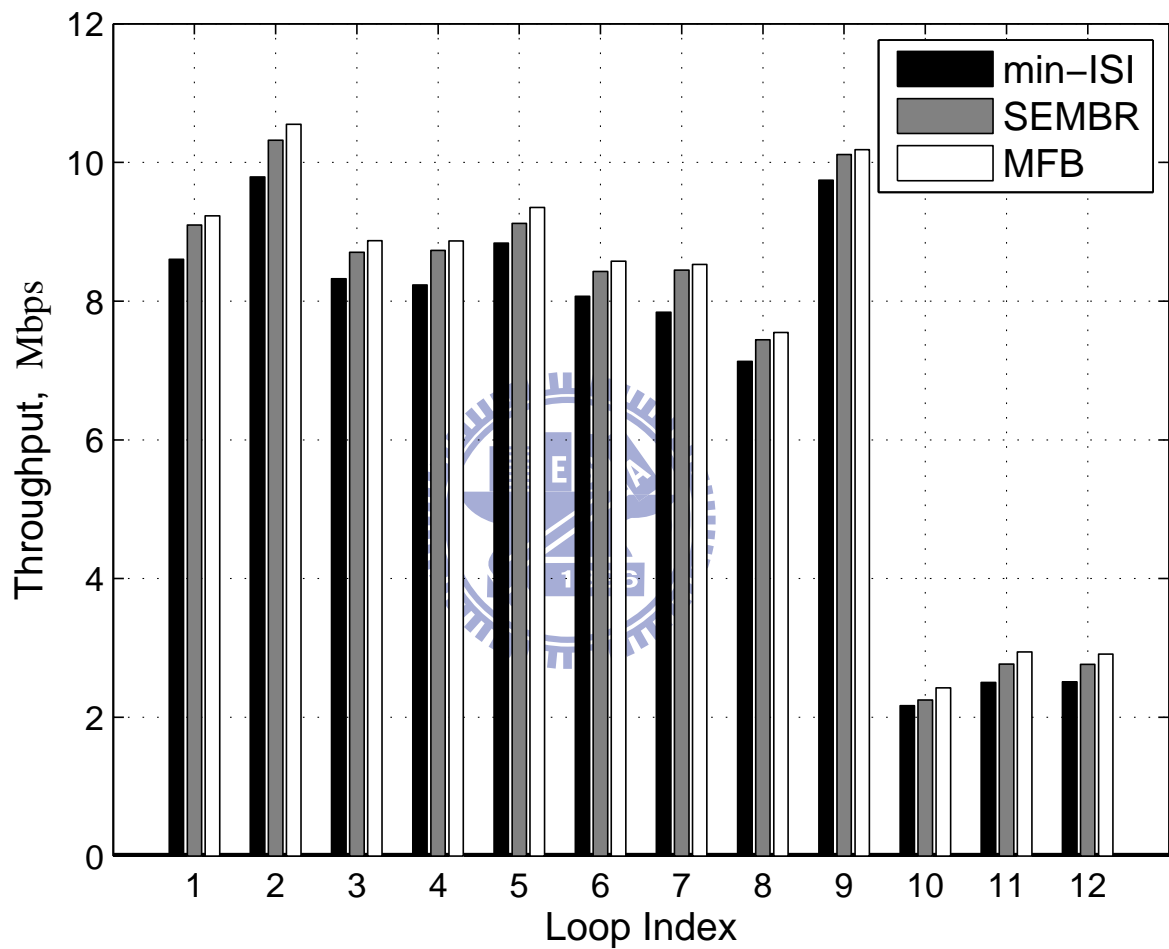


Figure 3.9: Throughput comparison for TEQs designed with min-ISI and SEMBR method ($N = 16$). MFB shows upper bound with no ISI. Loop Index is defined in Table 3.1.

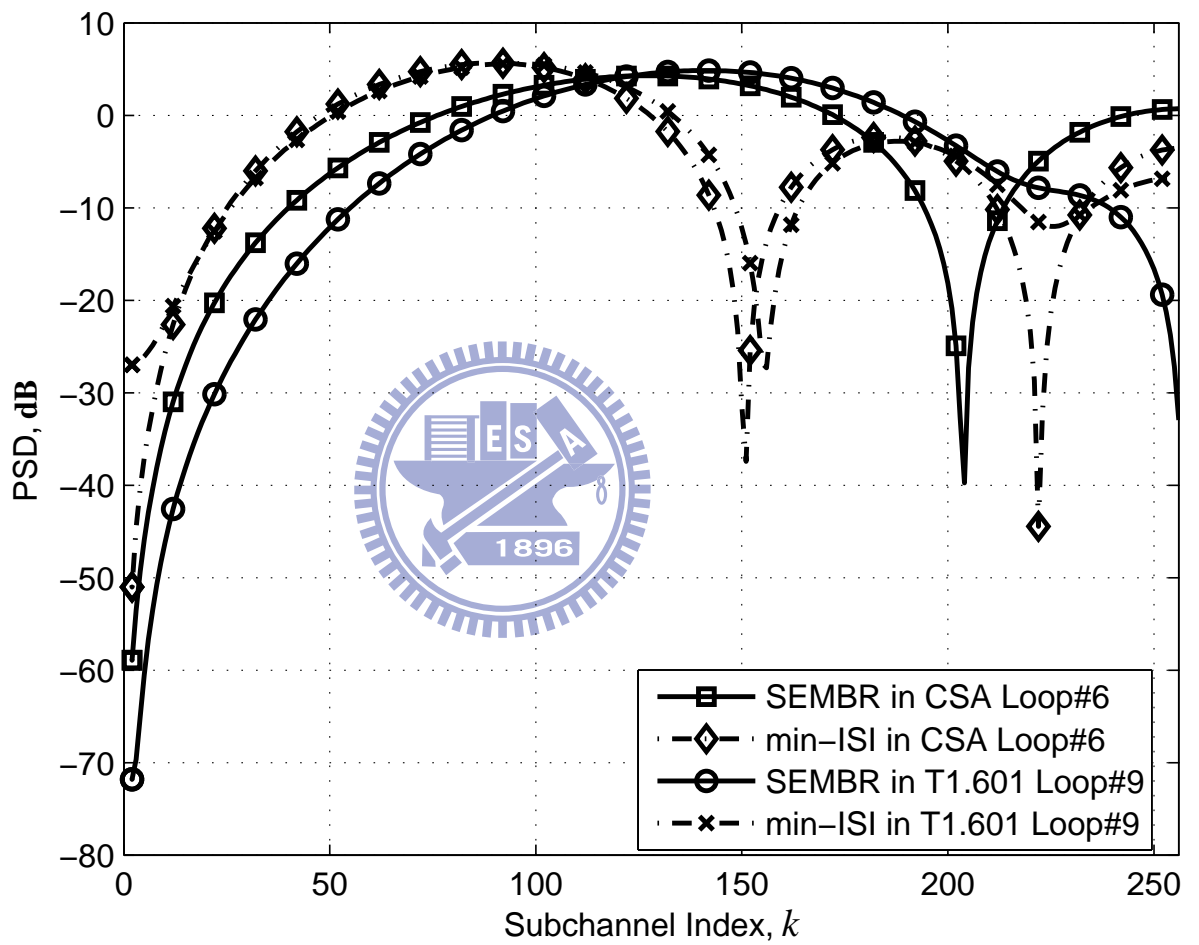
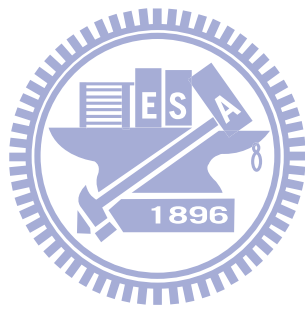
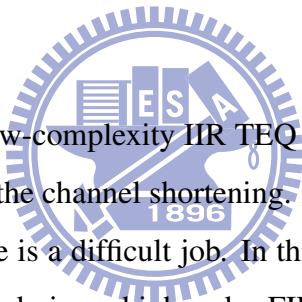


Figure 3.10: TEQ frequency responses designed with min-ISI and SEMBR method ($N = 16$)



Chapter 4

IIR Time Domain Equalization for OFDM Systems



In this chapter, we propose a low-complexity IIR TEQ scheme. The basic idea is to use an IIR TEQ instead of an FIR one for the channel shortening. However, the direct derivation of an IIR TEQ from the channel response is a difficult job. In this chapter, we propose using a two-step approach. In the first step, we derive a high-order FIR TEQ. In the second step, we convert the FIR TEQ into a low-order IIR TEQ. In the derivation of the FIR TEQ, we propose using a multi-stage (MS) structure. Instead of a single-stage (SS) high-order TEQ, we propose using a cascade of several low-order TEQs. For conventional TEQ design methods such as [14] or [18], matrix operations are frequently required, and the computational complexity is $O(N^3)$ [29] where N is the TEQ order. Thus, if N is large, the required computational complexity is high. With our MS structure, the computational complexity for the FIR TEQ derivation can be dramatically reduced. Since the ideal TEQ exhibits the low-order IIR characteristic, the order required for an IIR TEQ will be much lower than that of an FIR TEQ. To convert an FIR filter into an equivalent IIR form, we apply the Steiglitz McBride method (SMM) [35] to do the job. Simulations show that while the proposed method can reduce the computational complexity significantly, its performance is almost unaffected. In this chapter, we will mainly use the

MSSNR method [14] as our TEQ design method. It can have a good BER performance for OFDM systems [29]. Note that the idea of the IIR TEQ was first proposed by in [31] and [32]. In [34], an IIR TEQ based on the QR-RLS adaptive algorithm was also proposed. However, it is well-known that the stability of an adaptive IIR filter cannot be guaranteed. This is different from the SMM we use, where the convergence is guaranteed [36]- [39].

This chapter is organized as follows. In Section 4.1, we give the general signal model of an OFDM system. In Section 4.2, we briefly review the IIR characteristic of the TEQ, derive the MS FIR TEQ, detail the proposed IIR TEQ scheme, and analyze its complexity. Section 4.3 shows the simulation results.

§ 4.1 Signal Model

A common model of an OFDM system with the TEQ design is shown in Figure 4.1. At the OFDM transmitter side, denote the i -th transmitted data symbol as $\tilde{\mathbf{d}}_i = [\tilde{d}_i(0), \dots, \tilde{d}_i(M-1)]^T$, where $\tilde{d}_i(k)$ is the $(k+1)$ -th element of $\tilde{\mathbf{d}}_i$. Taking the M -point inverse DFT (M -IDFT) to $\tilde{\mathbf{d}}_i$, we can then obtain the corresponding time domain signal, denoted as \mathbf{d}_i . That is, $\mathbf{d}_i = [d_i(0), \dots, d_i(M-1)]^T = \mathbf{F}^H \tilde{\mathbf{d}}_i$ where \mathbf{F} is an $M \times M$ DFT matrix defined in (2.3). Subsequently, appending the CP and conducting the parallel-to-serial conversion, we obtain the transmitted signal $x(n)$. Here, $n = iK + l$, and

$$x(iK + l) = \begin{cases} d_i(l + M - L), & \text{for } 0 \leq l \leq L - 1, \\ d_i(l - L), & \text{for } L \leq l \leq K - 1. \end{cases} \quad (4.1)$$

where $d_i(l)$ is the $(l+1)$ -th element of \mathbf{d}_i . The signal $x(n)$ is then transmitted over a wireless channel with FIR and corrupted by AWGN.

Let the wireless CIR be represented as $\mathbf{h} = [h(0), \dots, h(I-1)]^T$, and AWGN as $\eta(n)$. $x(n)$ is assumed independent to the noise $\eta(n)$. Denote the noise-free channel output signal as $z(n)$, where $z(n) = x(n) * h(n)$. At the receiver side, both $z(n)$ and $\eta(n)$ are first filtered by an N -tap TEQ. Let the TEQ coefficients be denoted as $\mathbf{w} = [w(0), \dots, w(N-1)]^T$. Also let

the corresponding TEQ-filtered output of $z(n)$ and that of the channel noise be $y(n)$ and $v(n)$, where $y(n) = z(n) * w(n)$ and $v(n) = \eta(n) * w(n)$, respectively. Moreover, without loss of generality, let the synchronization delay be zero in the following paragraphs. Performing the serial-to-parallel conversion and removing the CP, we can obtain the i -th received signal-only OFDM symbol as $\mathbf{y}_i = [y(iK + L), \dots, y((i + 1)K - 1)]^T$. Let the corresponding i -th noise symbol vector at the TEQ input and output be $\boldsymbol{\eta}_i = [\eta(iK + L), \dots, \eta((i + 1)K - 1)]^T$ and $\mathbf{v}_i = [v(iK + L), \dots, v((i + 1)K - 1)]^T$, respectively.

From Figure 4.1, we can see that the transmitted signal $x(n)$ passes the wireless channel, $h(n)$, and the TEQ, $w(n)$. Let $g(n) = h(n) * w(n)$ be the ECR, and $\mathbf{g} = [g(0), \dots, g(J - 1)]^T$ where $J = I + N - 1$. Assume that $J < M$, and we can decompose \mathbf{g} into $\mathbf{g} = \mathbf{g}_S + \mathbf{g}_I$, where $\mathbf{g}_S = [g(0), \dots, g(L - 1), \mathbf{0}_{J-L}^T]^T$ is the desired shortened channel response, and $\mathbf{g}_I = [\mathbf{0}_L^T, g(L), \dots, g(J - 1)]^T$ the residual ISI response. Both the responses \mathbf{g}_S and \mathbf{g}_I are defined in (2.35), and the channel matrix \mathbf{H} is in (2.10).

We can reexpress \mathbf{g}_S and \mathbf{g}_I as $\mathbf{g}_S = [g_S(0), \dots, g_S(J - 1)]^T$, and $\mathbf{g}_I = [g_I(0), \dots, g_I(J - 1)]^T$, respectively, where $g_S(l)$ is the $(l + 1)$ -th element of \mathbf{g}_S , and $g_I(l)$ that of \mathbf{g}_I . Let $y_S(n)$, $y_I(n)$ be the desired part and the residual ISI part of $y(n)$. Thus we have $y(n) = y_S(n) + y_I(n)$, where $y_S(n) = x(n) * g_S(n)$, and $y_I(n) = x(n) * g_I(n)$. Consequently, we can also decompose \mathbf{y}_i as

$$\mathbf{y}_i = \mathbf{y}_{S,i} + \mathbf{y}_{I,i}, \quad (4.2)$$

where $\mathbf{y}_{S,i} = [y_S(iK + L), \dots, y_S((i + 1)K - 1)]^T$, and $\mathbf{y}_{I,i} = [y_I(iK + L), \dots, y_I((i + 1)K - 1)]^T$.

§ 4.2 Proposed IIR TEQ Method

In this section, we first describe the IIR characteristic of the TEQ in Section 4.2.1. Then we derive the MS FIR TEQ in Section 4.2.2. Based on the result, we then derive the proposed IIR TEQ scheme in Section 4.2.3. Finally, we analyze the computational complexity of the

proposed scheme in Section 4.2.4.

§ 4.2.1 IIR Characteristic of the TEQ

The typically wireless channel generally has a multipath response, which can be modeled as an FIR system. In this paragraph, we show that the TEQ for an FIR channel will exhibit an IIR characteristic. Recall that a wireless CIR \mathbf{h} has an FIR where the channel length exceeds the CP size, that is, $I > L$. Without loss of generality, we let $h(0) = 1$. Denote the transfer function of the channel as $H(z)$. Then,

$$\begin{aligned} H(z) &= 1 + h(1)z^{-1} + \cdots + h(I-1)z^{-I+1} \\ &= (1 - z_1z^{-1})(1 - z_2z^{-1}) \cdots (1 - z_{I-1}z^{-1}) \end{aligned} \quad (4.3)$$

where z_1, \cdots, z_{I-1} are $I-1$ zeros of $H(z)$ and $|z_1| \leq |z_2| \leq \cdots \leq |z_{I-1}|$. We can further express $H(z)$ as a cascade of three FIR channels, i.e., $H(z) = H_0(z)H_1(z)H_2(z)$ where $H_0(z)$ have m_0 zeros all located inside the unit circle, $H_1(z)$ have m_1 zeros all located on the unit circle, and $H_2(z)$ have m_2 zeros all located outside the unit circle. Note that $m_0 + m_1 + m_2 = I-1$. Now, suppose we want to shorten the wireless channel into the CP range. In other words, the TEQ must shorten at least $I-L$ channel taps. We have three cases to discuss, i.e., (1) $I-L \leq m_0$, (2) $m_0 < I-L \leq m_0 + m_2$, (3) $m_0 + m_2 < I-L$. For Case 1, the TEQ can be an IIR filter having $I-L$ poles of $\{z_1, \cdots, z_{I-L}\}$. Denoting the transfer function of the TEQ as $W(z)$, we can have

$$W(z) = \frac{1}{(1 - z_1z^{-1})(1 - z_2z^{-1}) \cdots (1 - z_{I-L}z^{-1})}. \quad (4.4)$$

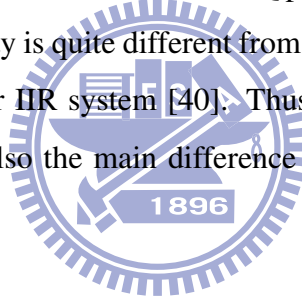
In this case, $I-L$ zeros of $H(z)$ is canceled by $I-L$ poles of $W(z)$, and the channel response can be perfectly shortened. For Case 2, we can let m_0 zeros of $H(z)$ be canceled by m_0 poles of $W(z)$ obtained from $H_0(z)$. However, there are $I-L-m_0$ zeros cannot be canceled. Note that if we substitute z with z^{-1} in $H_2(z)$, the resultant transfer function will have its zeros located inside the unit circle. This indicates that the zeros of $H_2(z^{-1})$ can also be canceled by an IIR

filter if the time index goes from 0 to $-\infty$. Although the IIR filter is not realizable, it can be approximated by a non-causal FIR filter. Thus, we have the TEQ as

$$W(z) = \frac{W_0(z)}{(1 - z_1 z^{-1})(1 - z_2 z^{-1}) \cdots (1 - z_{m_0} z^{-1})}. \quad (4.5)$$

where $W_0(z)$ is the FIR filter designed to cancel the response of the $I - L - m_0$ zeros. In this case, the channel can be shortened, but not perfectly. The performance depends on the dimension of $W_0(z)$. As known, zeros on the unit circle cannot be canceled. Thus, for Case 3, the channel response cannot be shortened into the CP range. Since the number of the taps to be shortened is generally much smaller than the channel length itself, Case 1 will be observed in most environments.

From above discussion, we conclude that the TEQ possesses an IIR characteristic in wireless channels. Note that this property is quite different from the wireline applications where the CIR can be modeled as a low-order IIR system [40]. Thus, a low-order FIR TEQ can effectively shorten the channel. This is also the main difference between the application of the TEQ in DMT and OFDM systems.



§ 4.2.2 Derivation of MS FIR TEQ

As shown in Figure 4.1, the objective of the TEQ is to shorten the CIR length I to the CP size, L . As discussed, for wireless channels, the required FIR TEQ order for the desired shortening may be long. As we will see, the derivation of the MSSNR TEQ relies on matrix operations having the computational complexity of $O(N^3)$. If N is large, the computational complexity will be high. Here, we propose an MS structure to alleviate this problem. We approach the original SS TEQ with a cascade of multiple TEQs. It is simple to see that the TEQ order in each stage can be made much smaller than that of the original one. Let the number of stages be V , the TEQ vector in the l -th stage be \mathbf{w}_l , and its order be N_l , that is, $\mathbf{w}_l = [w_l(0), \cdots, w_l(N_l - 1)]^T$ where $1 \leq l \leq V$. In each stage, we can derive the TEQ using the conventional MSSNR method.

For each individual stage of the MS structure, let the ECR at the l -th stage be denoted as

\mathbf{g}_l . Then, $\mathbf{g}_l = \mathbf{g}_{l-1} * \mathbf{w}_l$, where $\mathbf{g}_0 = \mathbf{h}$ and $1 \leq l \leq V$. Here, the convolution operator ‘*’ is applied for vectors. In the l -th stage, the TEQ shortens the CIR for a designated P_l taps. In other words, after the l -th TEQ, the length of target-impulse-response becomes $I - \sum_{i=1}^l P_i$. Hence, the total target-shortening-length is $\sum_{l=1}^V P_l = I - L$ and the overall equivalent TEQ length is $\sum_{l=1}^V N_l - V + 1$. Furthermore, the overall TEQ response \mathbf{w} is equal to the cascade of the individual TEQs, that is, $\mathbf{w} = \mathbf{w}_1 * \mathbf{w}_2 * \cdots * \mathbf{w}_V$.

As mentioned in Section 4.1, assume that the synchronization delay is zero, and let $\mathbf{g}_l = [g_l(0), \dots, g_l(J_l - 1)]^T$, where J_l is the ECR length at the l -th stage, and $J_l = J_{l-1} + N_l - 1$, $1 \leq l \leq V$. Note that $J_0 = I$ is the original CIR length. We can then decompose \mathbf{g}_l into two parts, the desired shortened channel response $\mathbf{g}_{S,l} = [g_l(0), \dots, g_l(L_l - 1), \mathbf{0}_{J_l - L_l}^T]^T$, and the residual ISI $\mathbf{g}_{I,l} = [\mathbf{0}_{L_l}^T, g_l(L_l), \dots, g_l(J_l - 1)]^T$, where $L_l = I - \sum_{j=1}^l P_j$. That is, $\mathbf{g}_l = \mathbf{g}_{S,l} + \mathbf{g}_{I,l}$. Then, we can rewrite $\mathbf{g}_{S,l}$ and $\mathbf{g}_{I,l}$ as

$$\begin{aligned} \mathbf{g}_{S,l} &= \mathbf{D}_{S,l} \mathbf{H}_l \mathbf{w}_l \\ \mathbf{g}_{I,l} &= \mathbf{D}_{I,l} \mathbf{H}_l \mathbf{w}_l, \end{aligned} \quad (4.6)$$

where $\mathbf{D}_{S,l} = \text{diag}[\mathbf{1}_{L_l}^T, \mathbf{0}_{J_l - L_l}^T]$, $\mathbf{D}_{I,l} = \text{diag}[\mathbf{0}_{L_l}^T, \mathbf{1}_{J_l - L_l}^T]$, and \mathbf{H}_l a $J_l \times N_l$ matrix consisting of a shift version of the ECR \mathbf{g}_{l-1} ,

$$\mathbf{H}_l = \begin{bmatrix} g_{l-1}(0) & 0 & \dots & 0 \\ g_{l-1}(1) & g_{l-1}(0) & \dots & 0 \\ \vdots & \vdots & \ddots & \vdots \\ g_{l-1}(J_{l-1} - 1) & g_{l-1}(J_{l-1} - 2) & \dots & g_{l-1}(J_{l-1} - N_l) \\ 0 & g_{l-1}(J_{l-1} - 1) & \dots & g_{l-1}(J_{l-1} - N_l + 1) \\ \vdots & \vdots & \ddots & \vdots \\ 0 & 0 & \dots & g_{l-1}(J_{l-1} - 1) \end{bmatrix}_{J_l \times N_l}. \quad (4.7)$$

The SSNR at the TEQ output of the l -th stage for the OFDM receiver is then defined as

$$\text{SSNR}_l = \frac{\mathbf{g}_{S,l}^H \mathbf{g}_{S,l}}{\mathbf{g}_{I,l}^H \mathbf{g}_{I,l}} = \frac{\mathbf{w}_l^H \mathbf{H}_l^H \mathbf{D}_{S,l}^H \mathbf{D}_{S,l} \mathbf{H}_l \mathbf{w}_l}{\mathbf{w}_l^H \mathbf{H}_l^H \mathbf{D}_{I,l}^H \mathbf{D}_{I,l} \mathbf{H}_l \mathbf{w}_l} = \frac{\mathbf{w}_l^H \mathbf{A}_l \mathbf{w}_l}{\mathbf{w}_l^H \mathbf{B}_l \mathbf{w}_l}, \quad (4.8)$$

where $\mathbf{g}_{S,l}^H \mathbf{g}_{S,l}$ is the desired signal power, $\mathbf{g}_{I,l}^H \mathbf{g}_{I,l}$ the residual ISI power, $\mathbf{A}_l = \mathbf{H}_l^H \mathbf{D}_{S,l}^H \mathbf{D}_{S,l} \mathbf{H}_l$, and $\mathbf{B}_l = \mathbf{H}_l^H \mathbf{D}_{I,l}^H \mathbf{D}_{I,l} \mathbf{H}_l$.

The optimal TEQ for the MSSNR method can be obtained through the maximization of the SSNR. The rows of $\mathbf{D}_{I,l} \mathbf{H}_l$ are formed by the shifted version of the CIR and the rank of $\mathbf{D}_{I,l} \mathbf{H}_l$ is $J_l \times N_l$. Consequently, the matrix \mathbf{B}_l is of full rank $N_l \times N_l$ and also positive definite. Hence, \mathbf{B}_l can be decomposed by using the Cholesky decomposition, that is, $\mathbf{B}_l = \mathbb{B}_l \mathbb{B}_l^H$. We can define a vector $\mathbf{y}_l = \mathbb{B}_l^H \mathbf{w}_l$, and then $\mathbf{w}_l = (\mathbb{B}_l^H)^{-1} \mathbf{y}_l$. Thus, $\mathbf{w}_l^H \mathbf{B}_l \mathbf{w}_l = \mathbf{y}_l^H \mathbf{y}_l$, and $\mathbf{w}_l^H \mathbf{A}_l \mathbf{w}_l = \mathbf{y}_l^H (\mathbb{B}_l)^{-1} \mathbf{A}_l (\mathbb{B}_l^H)^{-1} \mathbf{y}_l = \mathbf{y}_l^H \mathbb{A}_l \mathbf{y}_l$, where $\mathbb{A}_l = (\mathbb{B}_l)^{-1} \mathbf{A}_l (\mathbb{B}_l^H)^{-1}$. As a result, $\text{SSNR}_l = \mathbf{y}_l^H \mathbb{A}_l \mathbf{y}_l / \mathbf{y}_l^H \mathbf{y}_l$ has a form of Raleigh quotient. It is well known that optimal $\mathbf{y}_{l,0}$ maximizing the quotient SSNR_l can be obtained by choosing the eigenvector corresponding to the maximum eigenvalue of \mathbb{A}_l [41]. Thus, we can have the optimal TEQ vector $\mathbf{w}_{l,0}$ is

$$\mathbf{w}_{l,0} = (\mathbb{B}_l^H)^{-1} \mathbf{y}_{l,0}, \quad (4.9)$$

and the corresponding optimal SSNR_l is

$$\text{SSNR}_{l,0} = \frac{\mathbf{w}_{l,0}^H \mathbf{A}_l \mathbf{w}_{l,0}}{\mathbf{w}_{l,0}^H \mathbf{B}_l \mathbf{w}_{l,0}} = \lambda_l \quad (4.10)$$

where λ_l is the maximum eigenvalue of \mathbb{A}_l . Different from that in DMT systems, the MSSNR TEQ has been shown to have good performance in OFDM systems [29].

After deriving TEQ vectors $\{\mathbf{w}_{1,0}, \mathbf{w}_{2,0}, \dots, \mathbf{w}_{V,0}\}$ for all V stages, we can have the equivalent optimal TEQ vector \mathbf{w}_0 as

$$\mathbf{w}_0 = \mathbf{w}_{1,0} * \mathbf{w}_{2,0} * \dots * \mathbf{w}_{V,0} \quad (4.11)$$

This result is also shown in Figure 4.2.

§ 4.2.3 Derivation of IIR TEQ

As shown in Sec 4.2.1, the TEQ for the wireless channel possesses a low-order IIR property. Thus, a conventional FIR TEQ achieving satisfactory performance requires a high order. This

will consume heavy computations in the shortening operation. To solve the problem, we then propose converting the FIR TEQ obtained in (4.11) to an equivalent IIR one. By doing so, we can effectively reduce the required computational complexity for the shortening operation. Here, we use the SMM to do the job.

The SMM is an iterative method for the IIR system identification [35]. Its structure is shown in Figure 4.3, in which $c(n)$, $x(n)$, and $r(n)$ denote the impulse response, the input signal, and the output signal of the plant, respectively. Here, the plant is an IIR system and its transfer function can be represented as a rational function as

$$C(z) = \frac{A(z)}{B(z)}. \quad (4.12)$$

Also let

$$C_m(z) = \frac{A_m(z)}{B_m(z)} \quad (4.13)$$

be the estimated transfer function of the plant in the m -th iteration, where $A_m(z) = \sum_{j=0}^Q \alpha_j(m)z^{-j}$, $B_m(z) = 1 - \sum_{j=1}^P \beta_j(m)z^{-j}$. Note that Q and P are the order of $A(z)$ and $B(z)$, respectively. Assume that in the $(m-1)$ -th iteration, optimal $B_{m-1}(z)$ and $A_{m-1}(z)$ have been obtained. To conduct the m -th iteration, the SMM first filters the plant output, $r(n)$, and its input, $x(n)$, with $1/B_{m-1}(z)$. The resultant outputs, $u(n)$ and $v(n)$, are then fed to $B_m(z)$ and $A_m(z)$, respectively. Optimal $B_m(z)$ and $A_m(z)$ can then be obtained by minimizing the average-squared-error (ASE) power of the two outputs. It is simple to see that if the algorithm converges, i.e., $B_{m-1}(z) = B_m(z)$, then the plant is identified as $A_m(z)/B_m(z)$.

Put the unknown parameters $\beta_j(m)$ and $\alpha_j(m)$ together to form a vector $\Theta(m)$ as

$$\Theta(m) = [\beta_1(m), \dots, \beta_P(m), \alpha_0(m), \dots, \alpha_Q(m)]^T, \quad (4.14)$$

and also define a vector $\Phi(n)$ as

$$\Phi(n) = [v(n-1), \dots, v(n-P), u(n), \dots, u(n-Q)]^T. \quad (4.15)$$

Define the error signal between the filtered outputs of $u(n)$ and $v(n)$ as $e_m(n)$. Then, we have

$$\begin{aligned} e_m(n) &= \sum_{j=0}^Q \alpha_j(m)v(n-j) - u(n) + \sum_{j=1}^P \beta_j(m)u(n-j) \\ &= \mathbf{\Phi}^T(n)\mathbf{\Theta}(m) - u(n). \end{aligned} \quad (4.16)$$

If we collect the observations of $u(n)$ and $v(n)$ in a time window with size N' , we can then have N' samples of the error signal which can be expressed as

$$\mathbf{\epsilon}_m(n) = \mathbf{\Psi}(n)\mathbf{\Theta}(m) - \mathbf{u}(n), \quad (4.17)$$

where $\mathbf{\epsilon}_m(n) = [e_m(n), e_m(n-1), \dots, e_m(n-N'+1)]^T$, $\mathbf{u}(n) = [u(n), u(n-1), \dots, u(n-N'+1)]^T$, and $\mathbf{\Psi}(n) = [\mathbf{\Phi}(n), \mathbf{\Phi}(n-1), \dots, \mathbf{\Phi}(n-N'+1)]^T$. Thus, we can use the least-squares (LS) method to obtain the optimal estimate of $\mathbf{\Theta}(m)$. The criterion for the LS method is to minimize the ASE power, denoted as $\xi[\mathbf{\Theta}(m)]$, given by [35],

$$\xi[\mathbf{\Theta}(m)] = \|\mathbf{\epsilon}_m(n)\|^2 = \|\mathbf{\Psi}(n)\mathbf{\Theta}(m) - \mathbf{u}(n)\|^2, \quad (4.18)$$

The solution to the LS problem (4.18) can be written as

$$\mathbf{\Theta}(m) = (\mathbf{\Psi}^T(n)\mathbf{\Psi}(n))^{-1} \mathbf{\Psi}^T(n)\mathbf{u}(n). \quad (4.19)$$

Then, $1/B_m(z)$ is used to filter $r(n)$ and $x(n)$, and $u(n)$ and $v(n)$ is obtained for the LS solution in the next iteration. Since the SMM is an iterative algorithm, it requires an initial estimate of $B_0(z)$. A simple method for this problem is just to let $B_0(z) = 1$. In this case, $v(n)$ is the input of the plant which is $x(n)$, and $u(n)$ is the corresponding output, i.e., $u(n) = r(n)$. For IIR filter design, the stability is always an issue. The stability and the convergence of the SMM have been investigated. Interested readers may refer to [36] - [39].

We summarize the procedure of the proposed TEQ design method as follows. Firstly, we apply the MS structure and use the conventional MSSNR method to obtain an FIR TEQ $\mathbf{w}_{l,0}$ for each stage, where $1 \leq l \leq V$. By cascading the multiple stages of TEQs $\mathbf{w}_{l,0}$, we can obtain the equivalent optimal TEQ \mathbf{w}_0 in (4.11). Treating \mathbf{w}_0 as the impulse response of an IIR plant, we can then apply the SMM to convert the FIR TEQ into an equivalent IIR TEQ, efficiently.

§ 4.2.4 Complexity Analysis

In this paragraph, we discuss the issue of computational complexity of the proposed algorithm. We first compare the design complexity of the conventional SS and the proposed MS FIR TEQ. For fair comparison, we let the order of the conventional SS TEQ be equal to the equivalent order of the MS TEQ. The computational complexity of the SS MSSNR TEQ method is shown to be $38N^3/3 + IN^2$ [29], where N is the SS TEQ length. Thus, that of the proposed MS method is $38 \sum_{l=1}^V N_l^3/3 + I \sum_{l=1}^V N_l^2$, where N_l is the proposed l -th stage TEQ length, V the number of multi-stages, and I the CIR length. Hence, the MS approach can greatly reduce the required computational complexity. As an example, we let $N = 16$, $V = 3$ and $I = 25$. The computational complexity of the MS TEQ is only 13.8% of that of the SS TEQ. The improvement comes from the fact that the computational complexity of the MSSNR method is $\mathcal{O}(N^3)$. As a result, when N is large, the complexity grows fast.

We now consider the computational complexity of the SMM. For simplicity, let the data window size of the SMM, denoted as N' , be equal to the FIR TEQ filter order N . It can be shown that the computational complexity of the SMM is $\mathcal{O}(m[(P+Q+1)^3 + (P+Q+1)^2N + (P+Q+1)N])$, where m is the iteration number. Although the computational complexity of the SMM has the same order as that of the MSSNR, its actual complexity will be much lower. This is due to two facts. First, as we will see in the next section, the SMM converges very fast, usually within five iterations. Second, in typical applications, $P+Q$ is usually much smaller than N . As a result, the overhead introduced by the SMM is not significant.

We now evaluate the computational complexity during the shortening operation. Note that the shortening operation has to be conducted for every input data sample. It solely depends on the number of taps in the TEQ. Thus, the computational complexity for the conventional FIR TEQ is $\mathcal{O}(N)$, while that for the proposed IIR TEQ is $\mathcal{O}(P+Q+1)$. Since $P+Q$ is usually much smaller than N , the computational complexity of the IIR TEQ is much smaller than the FIR TEQ. Using a typical example, the proposed algorithm can save approximately up to 70%

of the computations without compromising the SER performance [32]. When M and L are large, as found in many practical OFDM systems, the reduction in computational complexity can be more significant.

§ 4.3 Simulations

The simulation setup is described as follows. The OFDM system we use has the symbol size of 64, and the CP size of 16. The wireless channel is generated using an exponential-decay power profile. The channel is quasi-static and its response changes for every OFDM packet. In our simulations, we assume that the CIR is known or can be well estimated. The wireless CIR length is assumed to be 25, exceeding the CP size. A typical wireless CIR is shown in Figure 4.4. Channel noise is modeled as the AWGN, and added at the channel output. All FIR TEQs considered in the simulations have an order of 16. They are designed with the MSSNR method [14], which has been shown to have a good compromise between the complexity and the SER performance [29]. In the figures shown, N and D stand for the number of zeros and poles used in the IIR TEQ, respectively.

In the first set of simulations, we evaluate the impact of the number of poles and zeros used in the IIR TEQ, and the convergence rate of the SMM. Figure 4.5 shows the relationship between the ASE power and the iteration numbers, under the variation of the pole/zero order of the IIR TEQ. We can see that as the number of poles (or zeros) increases, the error power decreases. This is not surprising since more degree of freedom can be used to reduce the ASE power. Figure 4.6 shows the relationship between the residual ISI power and the iteration numbers, under the same setting as that in Figure 4.5. Since the residual ISI power is not the criterion to be minimized, an IIR TEQ with higher order does not necessarily yield a smaller residual ISI power. Note that the residual ISI power relates to the SER, directly. Also shown in Figure 4.5 and Figure 4.6, we can see that the SMM converges to a stable value very quick. The required number for iteration is typically below 5. We then consider the SER performance of the IIR

TEQs discussed above, as shown in Figure 4.7. The behavior of the SER performance in Figure 4.7 is similar to that of the residual ISI power in Figure 4.6. This is consistent with the assertion we just mentioned. Note that the choice of the order of the IIR TEQ is a compromise between the SER performance and the computational complexity. From simulations, we found that a good choice for the numbers of zeros and poles are 3 and 3, respectively. Figure 4.8 shows an example of the impulse responses of the FIR filter and its equivalent IIR one (fitted with the SMM). Here, the number of poles is 3, that of zeros is also 3, and the iteration number used in the SMM is 5. We can see that the fitted IIR TEQ can approach the original FIR TEQ well.

The performance and the computational complexity of the proposed algorithm depend on the parameters it uses such as the number of stage, the filter order at each stage, and the target channel length to be shortened (TLS) at each stage. Before the actual application of the proposed algorithm, we need to determine those parameters. We then need some design guidelines in order to obtain optimal results. Since theoretical analysis is difficult, we use simulations to do the job here. Table 4.1, 4.2, and 4.3 show the different parameter settings for simulations. The second column in the tables numbers the test TEQs used in the simulations, and the third column gives the number of stages used in the MS structure. The fourth column gives the order of the TEQ used at each stage, in which the notation $[a, b, \dots]$ indicates that the TEQ order for the first stage is a , that for the second stage is b , and so on. The last column gives the TLS, where the notation $[c, d, \dots]$ indicates that the TLS for the first stage is c , that for the 2nd stage is d , and so on.

The SER performance of the MSSNR [14] and the proposed method are then evaluated. All the simulations are evaluated with 1000 OFDM packets, where each OFDM packet contains 60 OFDM symbols. We first see the effect of the number of processing stages. Table 4.1 shows the parameter setting for this purpose. Here, we let the equivalent order of the MS TEQ be the same in all settings. The number of stages we tried are 2, 3, 4, and 5, corresponding to TEQ #1a, #1b, #1c, and #1d, respectively. The equivalent TEQ filter order is 16 for all 4 test TEQs. The TEQ filter orders are $[8, 9]$, $[6, 6, 6]$, $[5, 5, 5, 4]$, and $[4, 4, 4, 4, 4]$, respectively. And the TLSs

for the test TEQs are $[4, 5]$, $[3, 3, 3]$, $[3, 2, 2, 2]$, $[2, 2, 2, 2, 1]$, respectively. Figure 4.9 shows the SER performance comparison for settings in Table 4.1. We can see that as the number of stages increases, although it can reduce more computations, the SER performance degrades. It is apparently that the BER performance for the SS TEQ (the plot of MSSNR TEQ) is superior to that of the multistage ones. This is not surprising since the original MSSNR design is a joint optimization approach (for all tap weights), while the MS structure is not. From Figure 4.9, we can see that it is adequate to let the number of stages be 2 or 3 (that is, TEQ #1a and #1b), a good compromise between the complexity and BER performance.

We then evaluate the effect of the filter order used at each stage. Table 4.2 gives the setting for simulations. Here, the number of stage is set as 2, and the highest order for each stage is set as 16. The TLSs for the test TEQs are all fixed to $[4, 5]$. Figure 4.10 and Figure 4.11 show the simulation results. From the figures, we can see that the larger the filter order, the better the BER performance we can have. However, as the filter order of one stage increases, the computational complexity increases accordingly. Thus, there is a compromise between the TEQ order and the performance. Also from Figure 4.11, we can see that as the filter order at the second stage decreases (that in the first stage is fixed), the performance degrades, but the degradation is not severe. In contrast, from Figure 4.10, we see that as the filter order of the first stage decreases (that in the second stage is fixed), the performance degradation is more severe. This is because the residual ISI of the first stage will propagate to the second stage, and the TEQ in the second stage cannot compensate for that effect completely. Thus, the TEQs in early stages play more important roles than those in following stages. We should give a higher order for the TEQs in the early stages. On the other hand, the shortening work is also relatively easier at early stages, and a higher order for the TEQ may not require. In summary, we may let the TEQ order be roughly equal for all stages. This is an important property the MS structure has.

Table 4.3 shows the settings of the TEQ in scenarios with various TLSs. Here, the number of stages is still set to 2, and the TEQ tap length for both stages is set to 16. Figure 4.12 shows the simulation results. We see that if the TLS of the first stage is in a smaller order, such as the

case of TEQ #4d, #4e and #4f, the SER performance is generally better than that of other cases. The reason is similar to the results in Figure 4.10 and Figure 4.11. As the TLS of the first stage increases, the residual ISI of the first stage will become larger and it propagates to the second stage. The TEQ in the second stage cannot compensate for that effect. However, if the TLS of the first stage becomes too small, the corresponding TLS of the second stage becomes large and the required filter order of the second stage will become high. Then the computational complexity of the TEQ will be increased. With a larger residual ISI, no matter in the first or second stage, the performance of the TEQ will be degraded. Thus, it is better to distribute the required TLS to all stages, evenly. This is another important property the MS structure has.

Based on the simulation results, we can obtain some design guidelines for the MS design. Firstly, the number of stages used should not be too large, i.e., 2 or 3. Secondly, the filter order for each stage can be made roughly equal. The order is selected with a compromise between complexity and performance. For example, an appropriate filter order for a two-stage structure may be $[8, 9]$. Thirdly, the total TLS can also be evenly distributed to all TEQs. In other words, the TLS for each stage can also be set roughly equal. Or, that in early stages is somewhat lower. For example, an appropriate TLS value for a two-stage structure can be $[4, 5]$ or $[3, 6]$.

According to the above design guidelines, we can determine proper values for the parameters. It turns out that the number of stages is 2, the filter order per stage is $[8, 9]$, the TLS is $[4, 5]$. Figure 4.13 shows the simulation results with the settings. As we can see, the SER performance of the proposed IIR TEQ is slightly worse than that of the original FIR TEQ. The complexity ratio of the IIR TEQ to that of the FIR TEQ in TEQ derivation, and in shortening operation, is only 33% and 37%, respectively. We can then conclude that the proposed IIR TEQ is much more efficient than the conventional FIR TEQ.

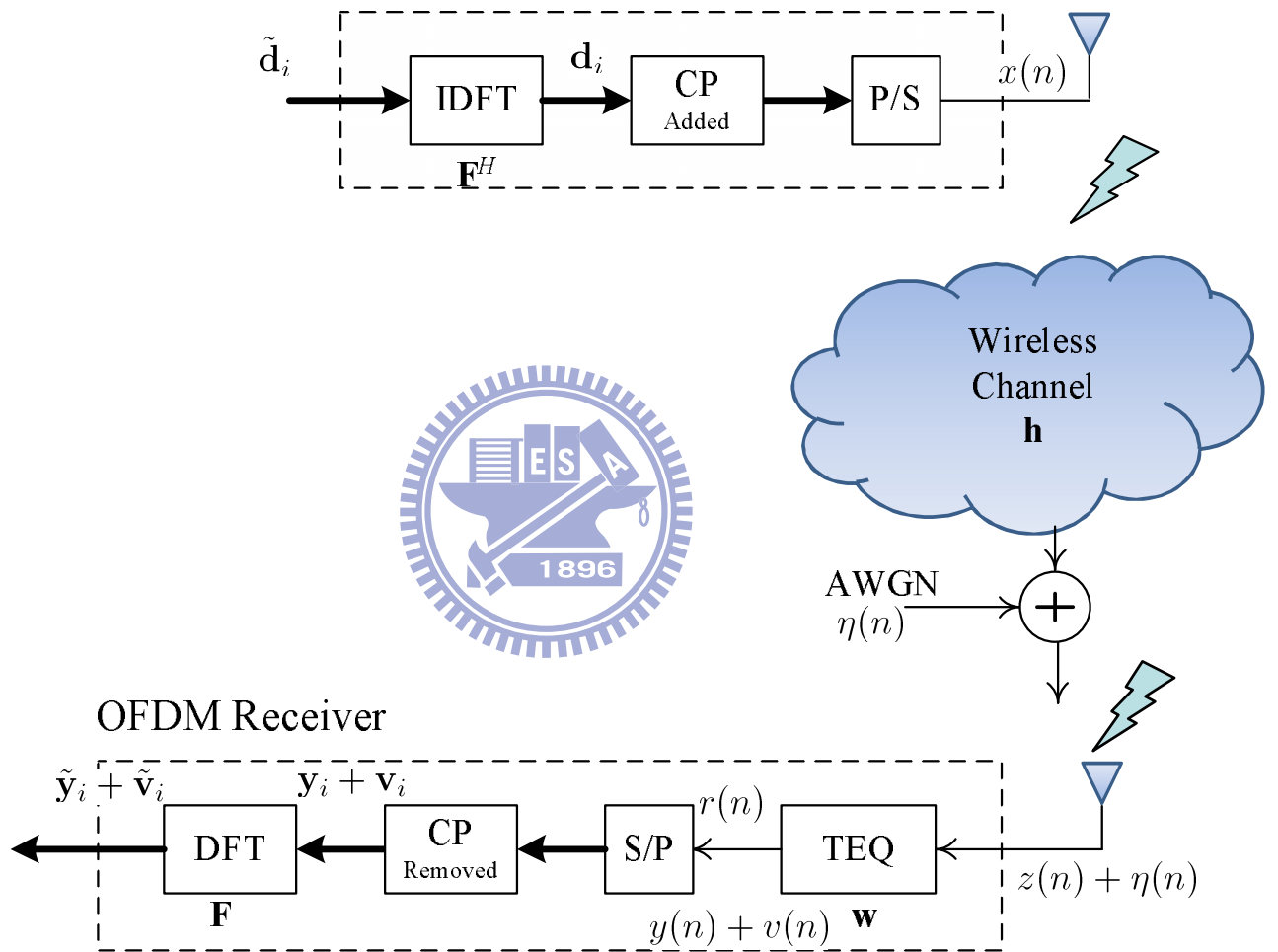


Figure 4.1: An OFDM system with TEQ

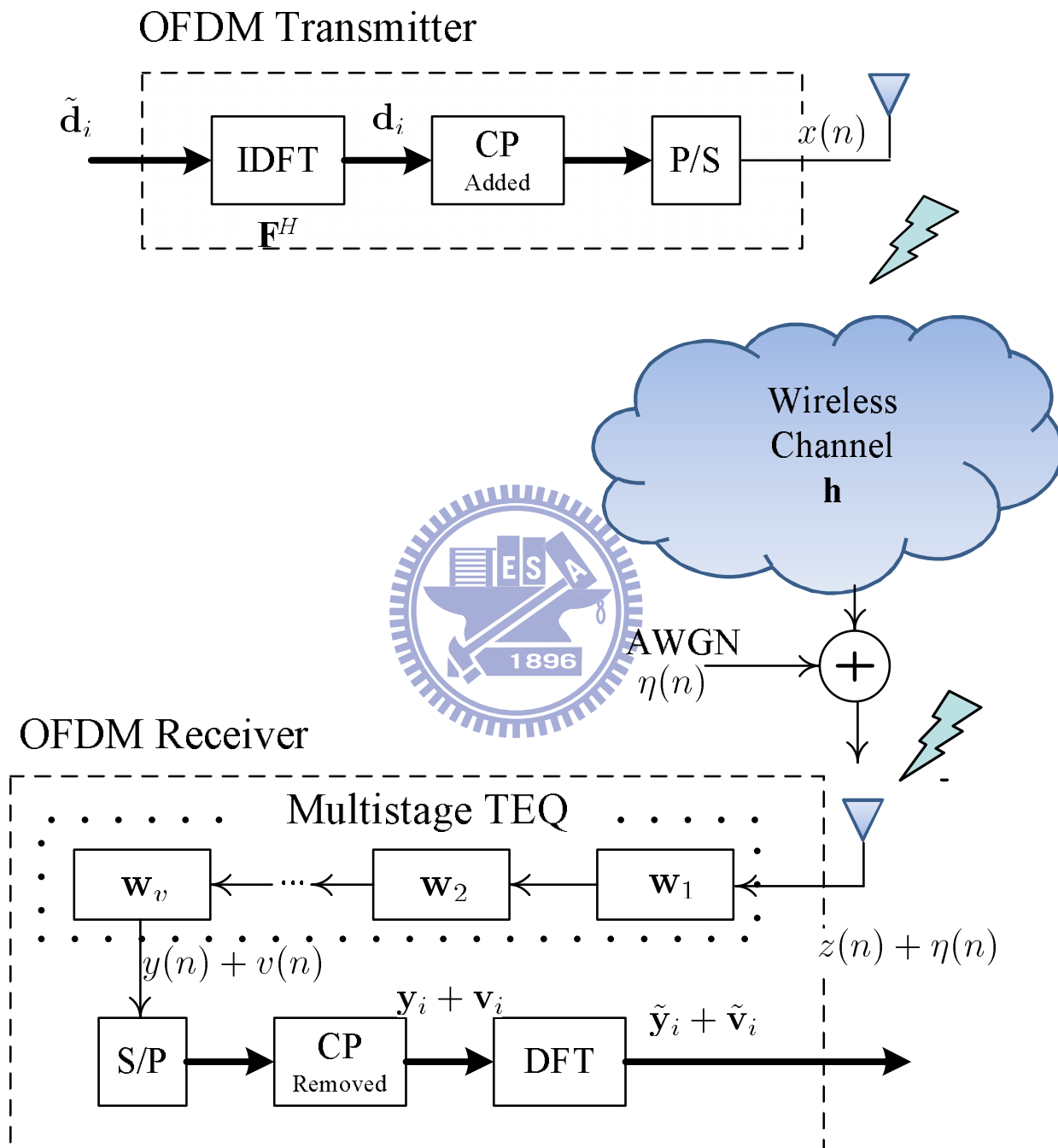


Figure 4.2: An OFDM system with multistage TEQ

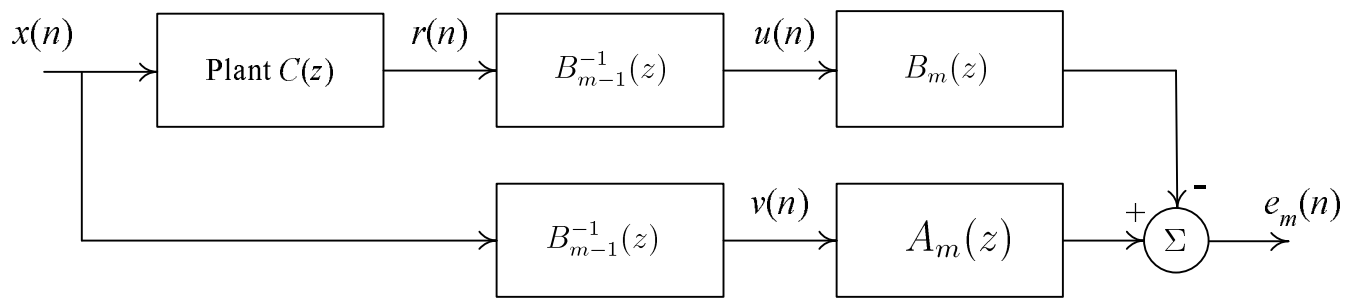


Figure 4.3: System model for Steiglitz McBride method

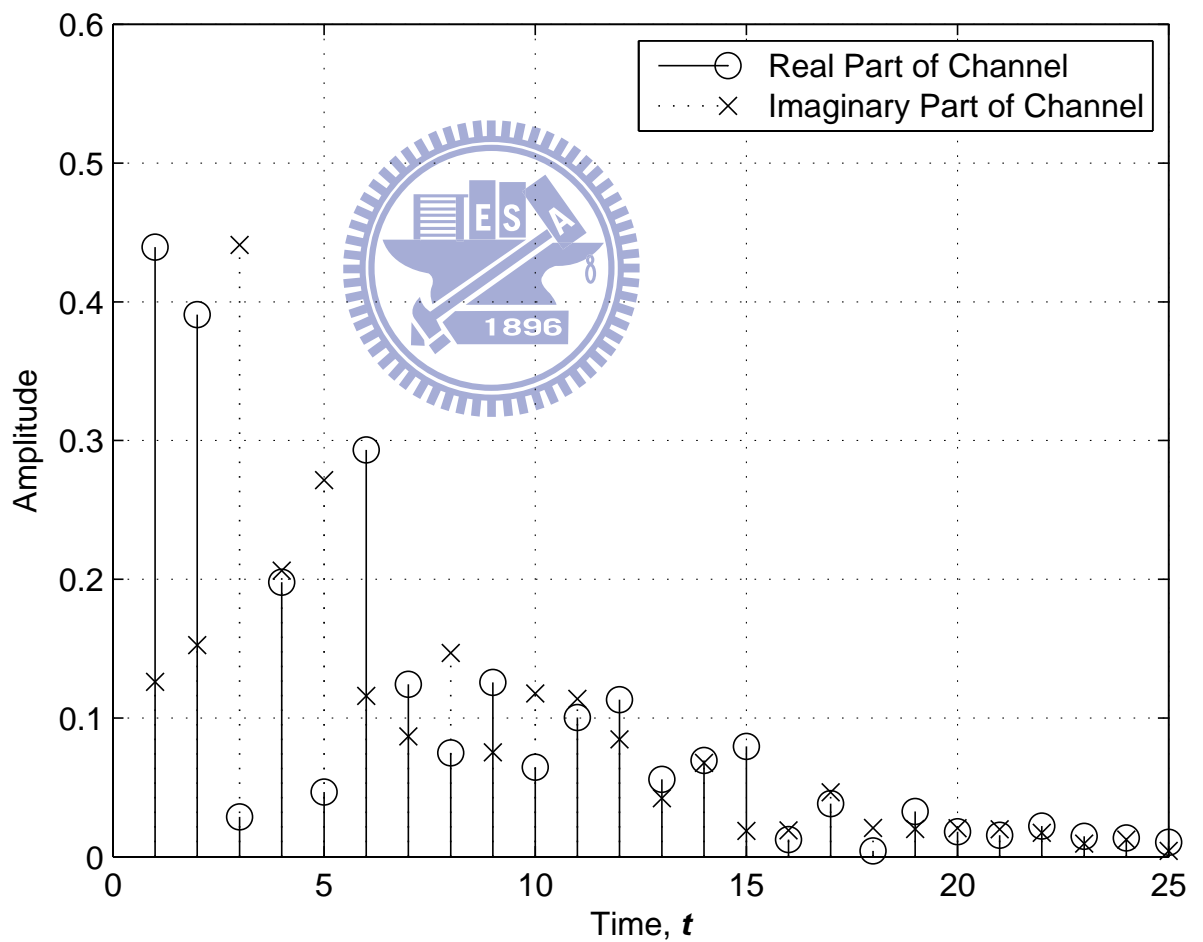


Figure 4.4: A typical wireless channel impulse response

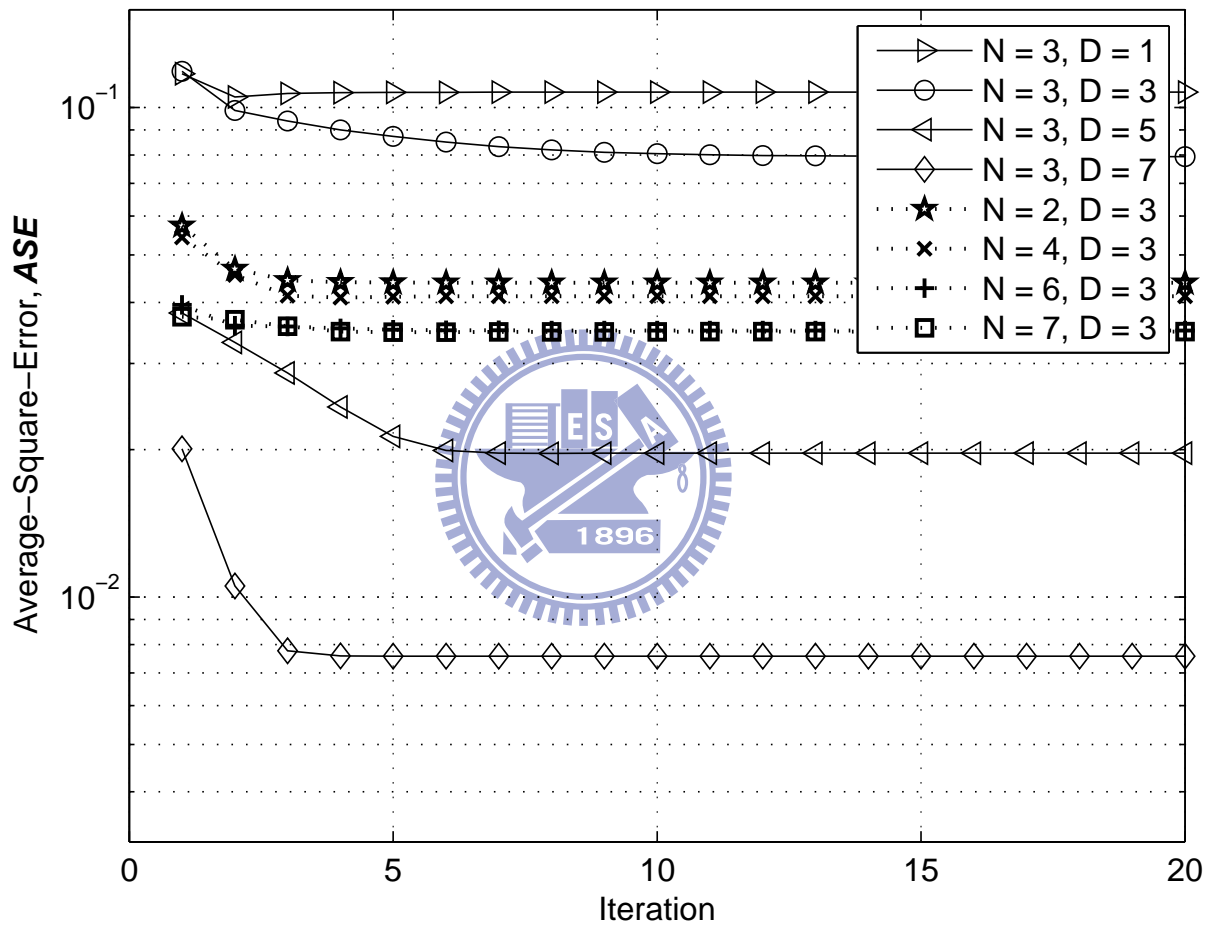


Figure 4.5: Average-squared-error of IIR TEQ fitted with SMM (for various pole/zero order)

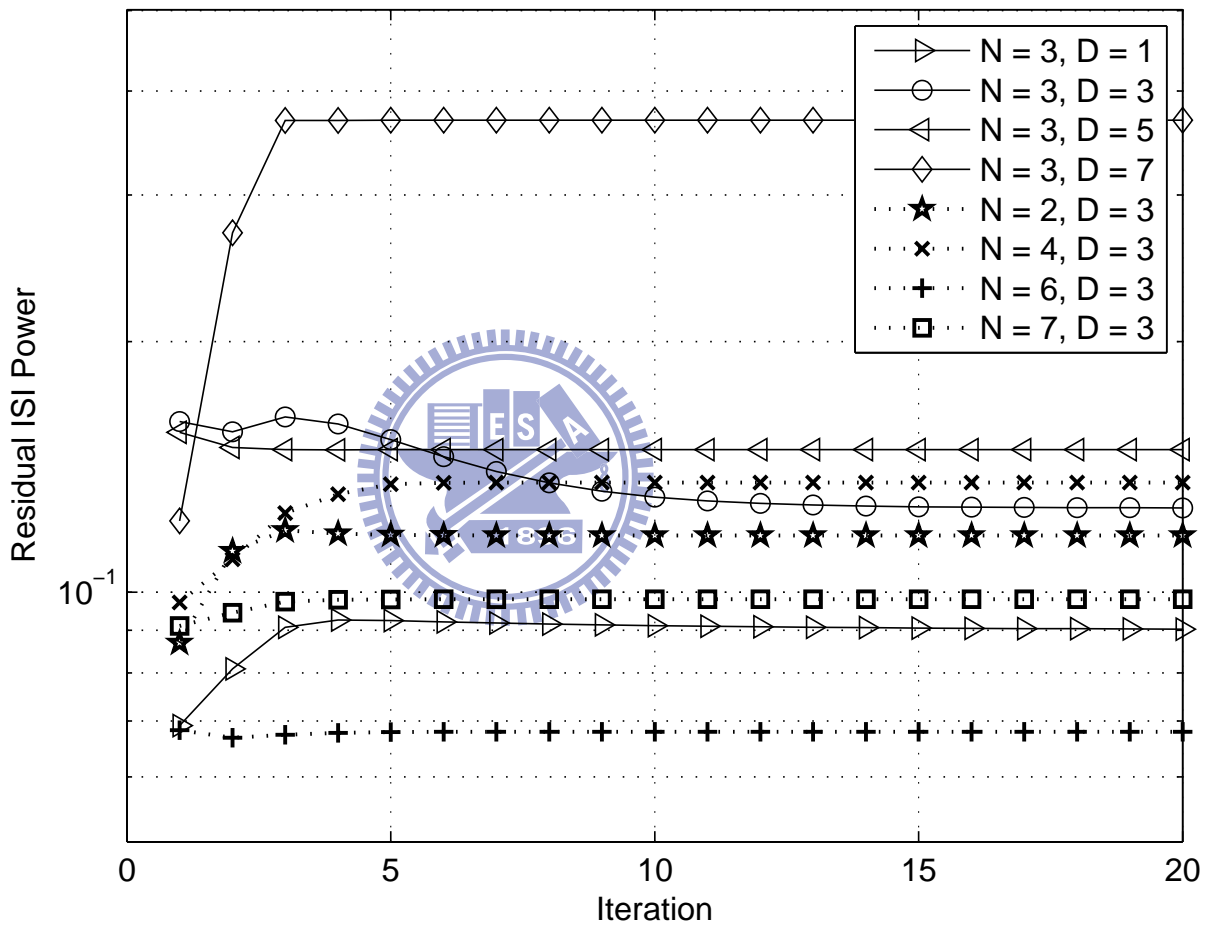


Figure 4.6: Residual ISI power of IIR TEQ fitted with SMM (for various pole/zero order)

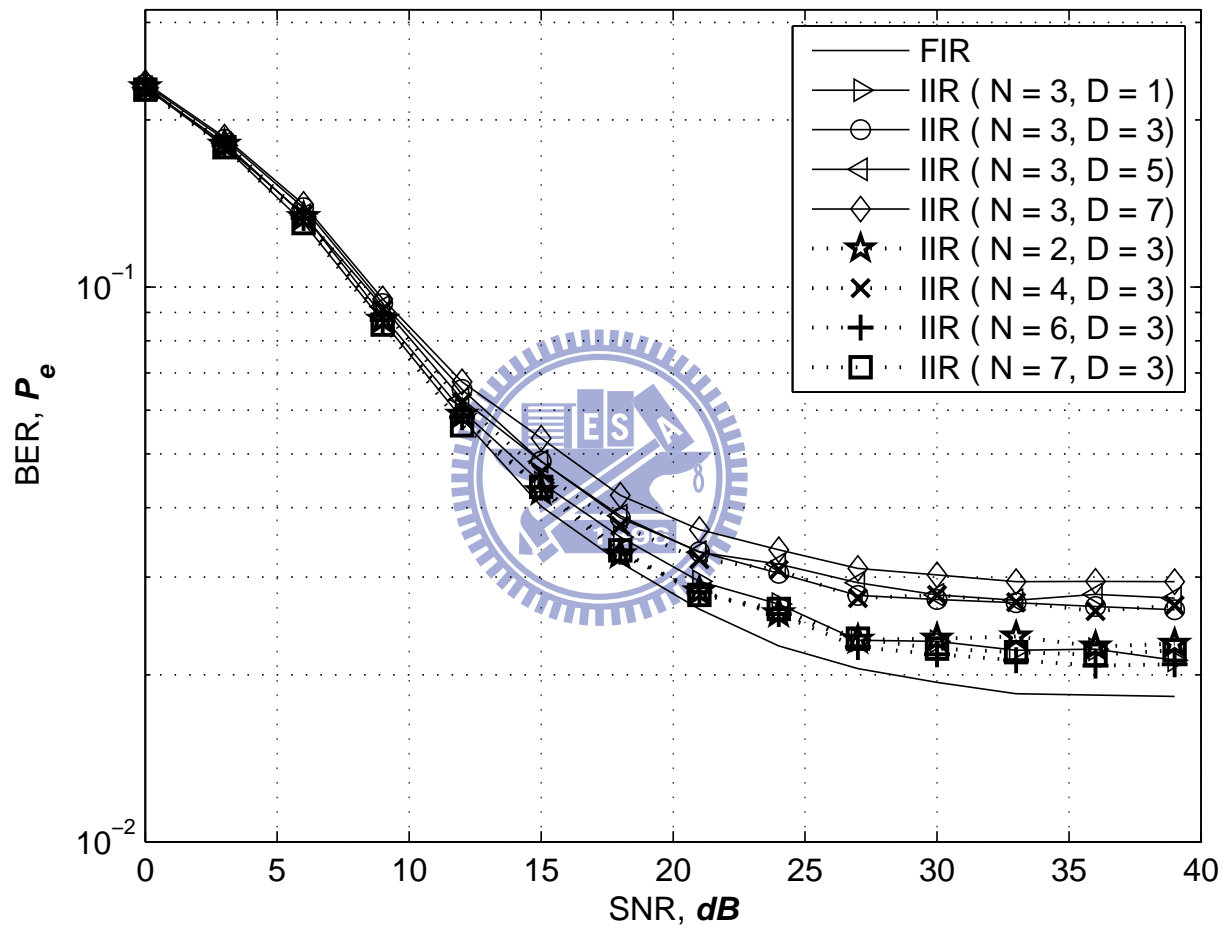


Figure 4.7: SER Performance of IIR TEQ fitted with SMM (for various pole/zero order)

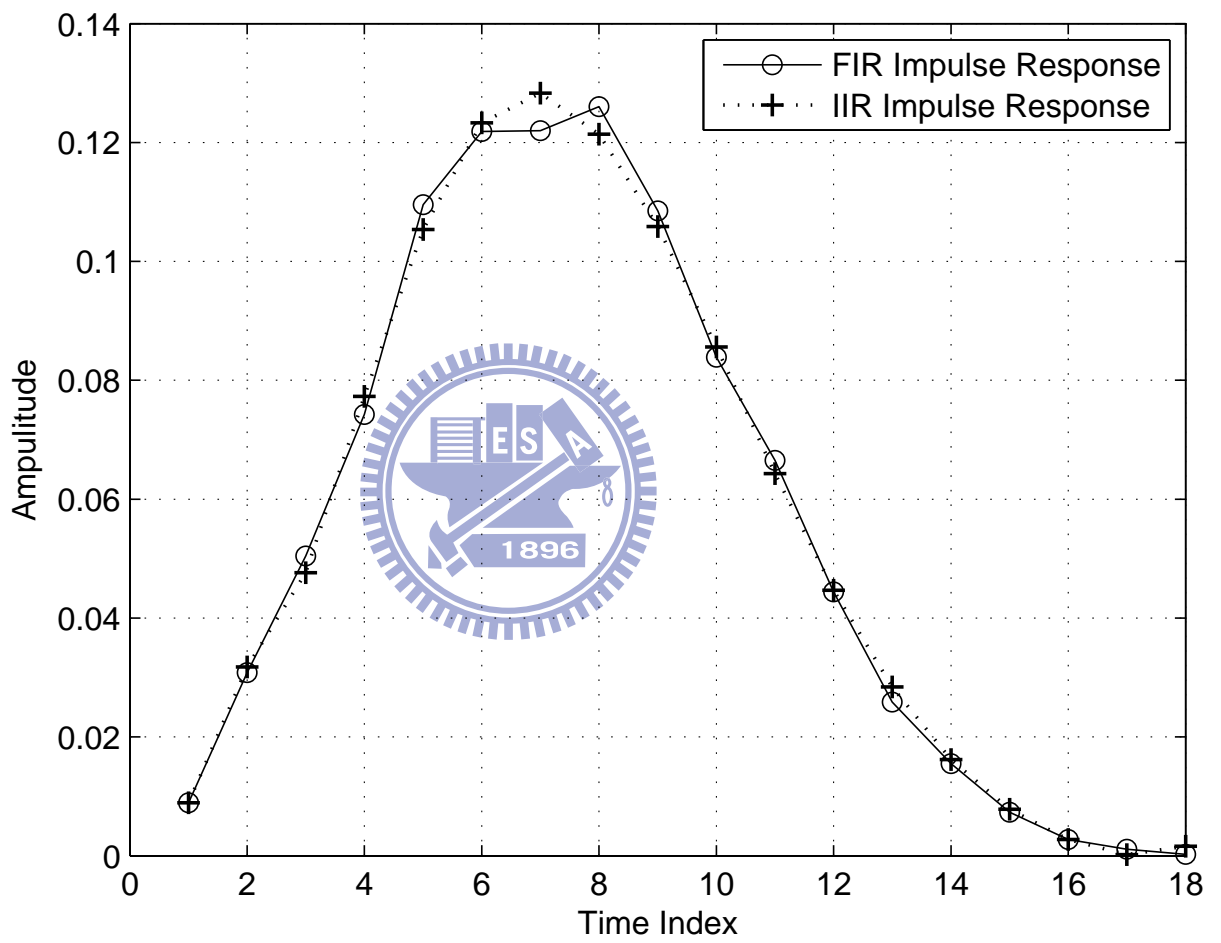


Figure 4.8: Impulse response of an FIR TEQ and its fitted IIR TEQ

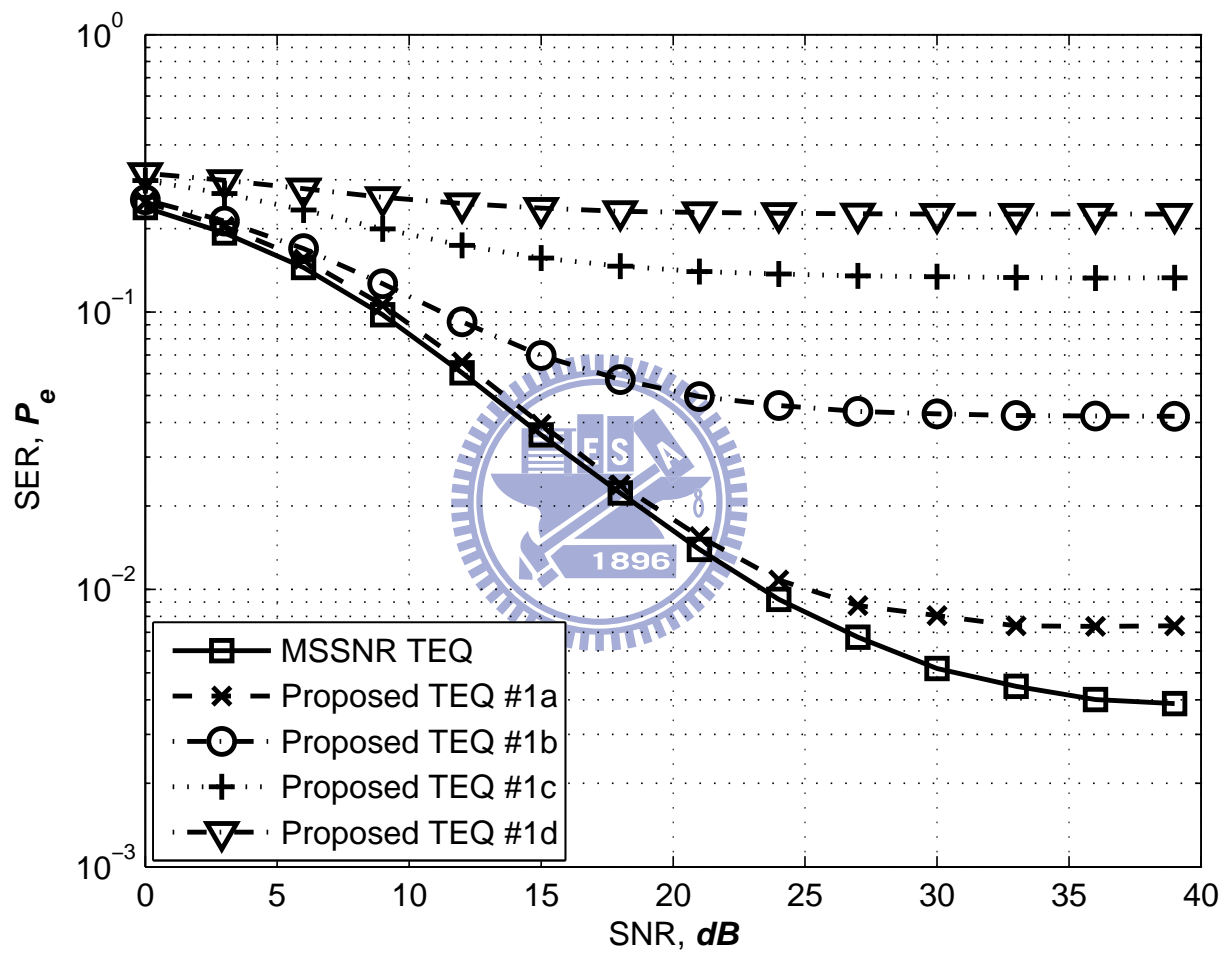


Figure 4.9: SER performance of Experiment #1 (for various stage number)

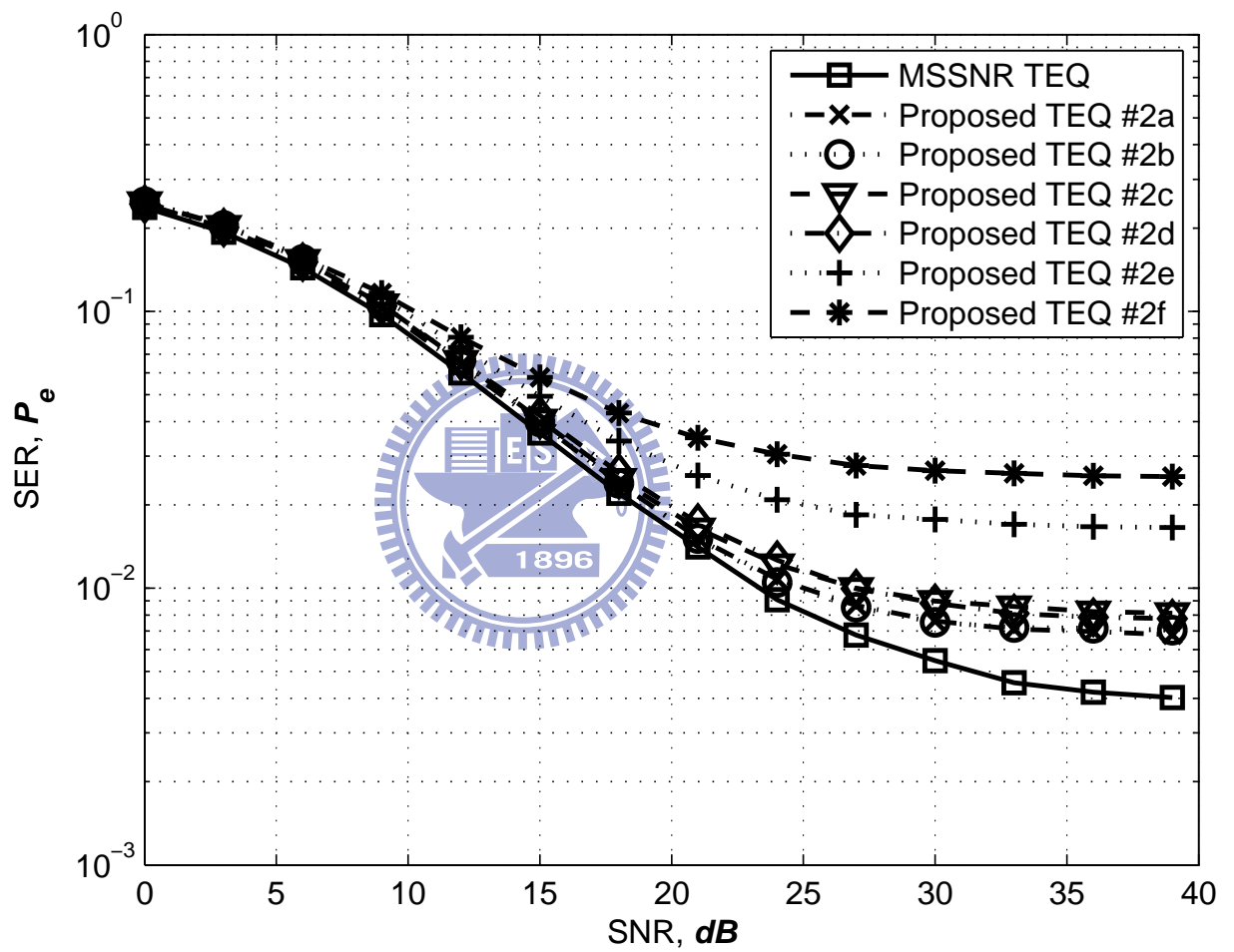


Figure 4.10: SER performance of Experiment #2 (for various TEQ order in the first stage)

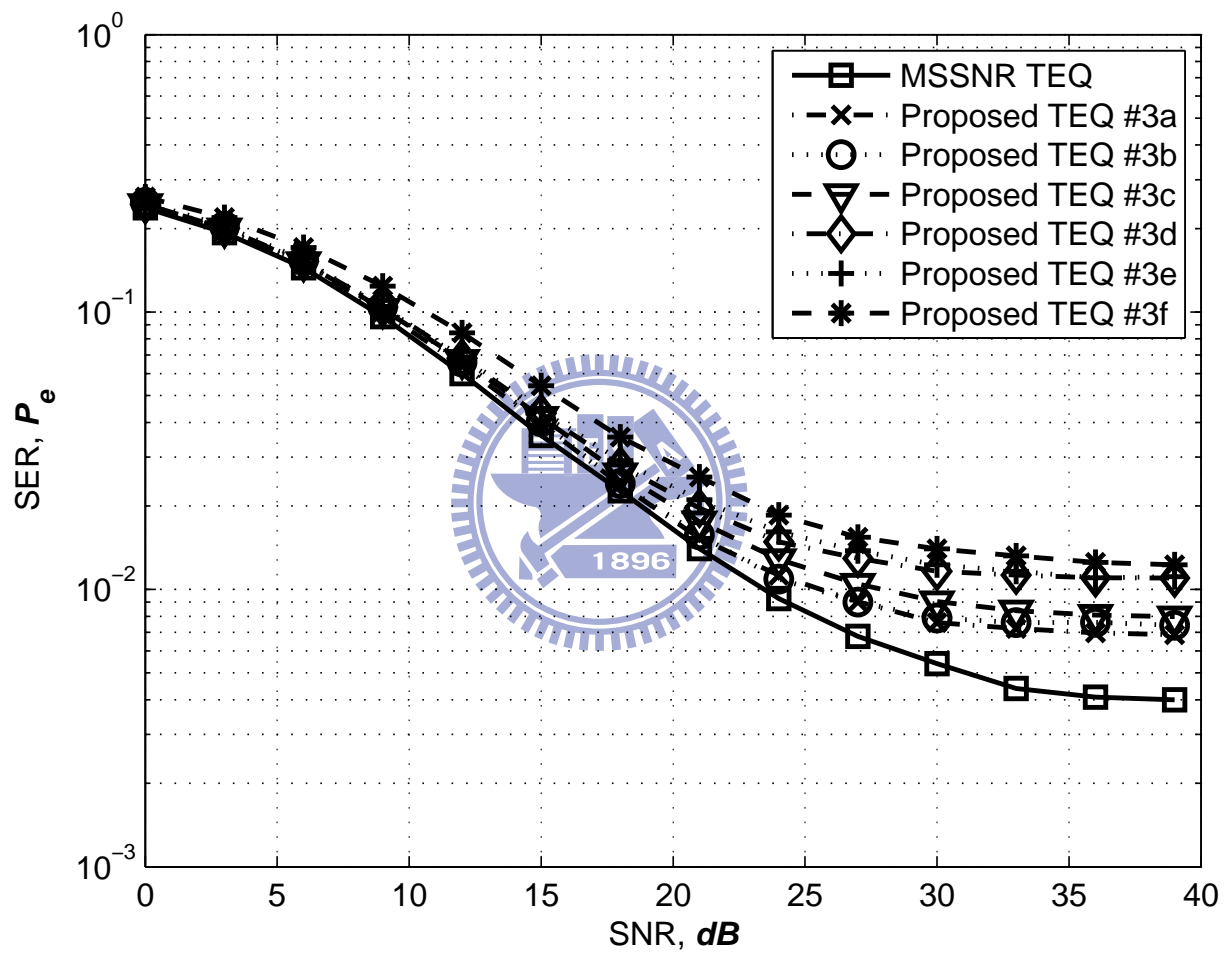


Figure 4.11: SER performance of Experiment #3 (for various TEQ order in the second stage)

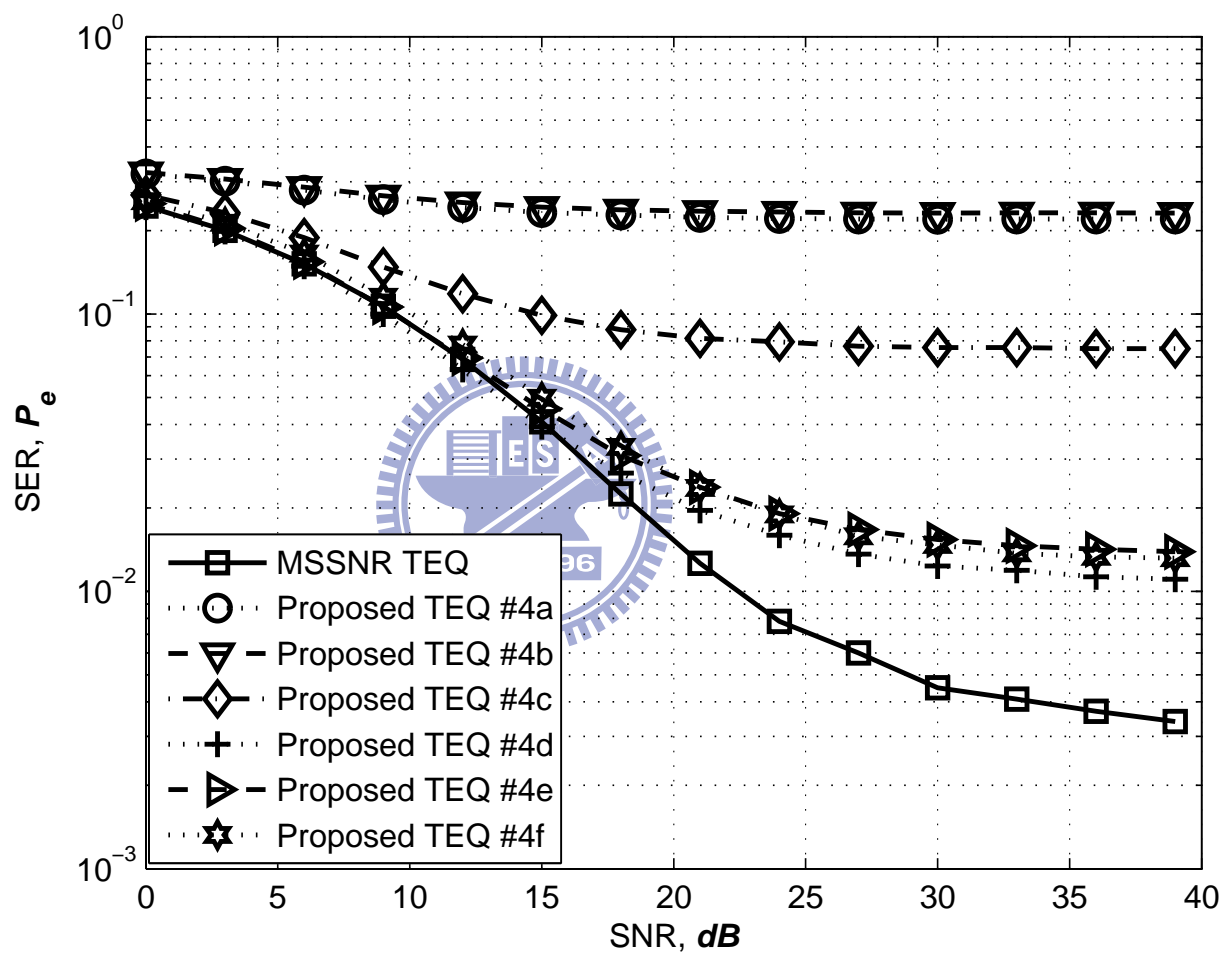


Figure 4.12: SER performance of Experiment #4 (for various TLS per Stage)

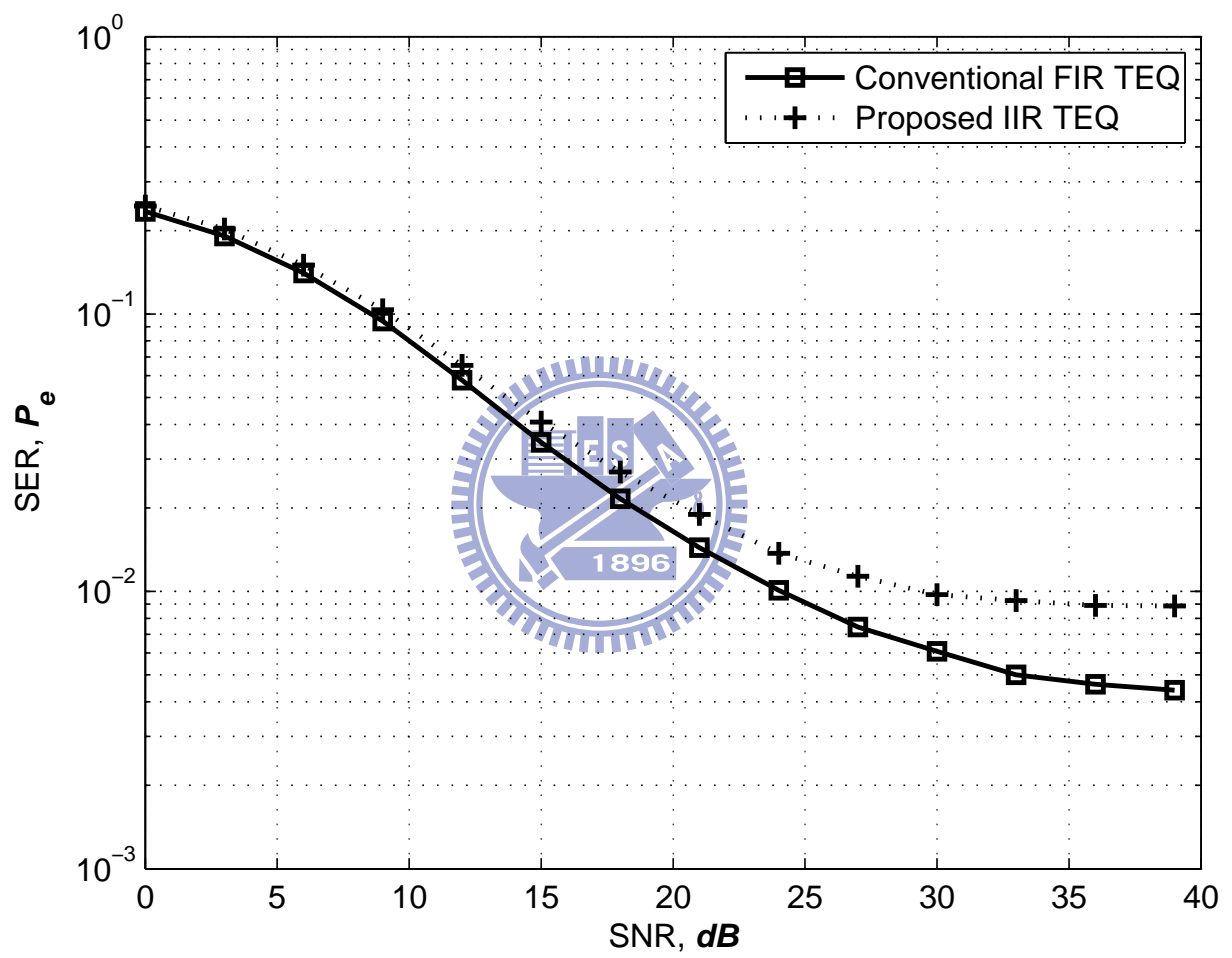


Figure 4.13: SER comparison of conventional FIR TEQ and proposed IIR TEQ

Table 4.1: Plot definitions of simulation scenario A (for various IIR order)

Figure #	TEQ #	Multistage Order	TEQ order per stage	TLS per stage
Figure 4.9	TEQ #1a	2	[8, 9]	[4, 5]
	TEQ #1b	3	[6, 6, 6]	[3, 3, 3]
	TEQ #1c	4	[5, 5, 5, 4]	[3, 2, 2, 2]
	TEQ #1d	5	[4, 4, 4, 4, 4]	[2, 2, 2, 2, 1]

Table 4.2: Plot definitions of simulation scenario B (for various pole/zero order per stage)


Figure #	TEQ #	Multistage Order	TEQ order per stage	TLS per stage
Figure 4.10	TEQ #2a	2	[16, 16]	[4, 5]
	TEQ #2b	2	[13, 16]	[4, 5]
	TEQ #2c	2	[11, 16]	[4, 5]
	TEQ #2d	2	[8, 16]	[4, 5]
	TEQ #2e	2	[6, 16]	[4, 5]
	TEQ #2f	2	[4, 16]	[4, 5]
Figure 4.11	TEQ #3a	2	[16, 16]	[4, 5]
	TEQ #3b	2	[16, 13]	[4, 5]
	TEQ #3c	2	[16, 11]	[4, 5]
	TEQ #3d	2	[16, 9]	[4, 5]
	TEQ #3e	2	[16, 6]	[4, 5]
	TEQ #3f	2	[16, 4]	[4, 5]

Table 4.3: Plot definitions of simulation scenario C (for various TLS per stage)

Figure #	TEQ #	Multistage Order	TEQ order per stage	TLS per stage
Figure 4.12	TEQ #4a	2	[16, 16]	[7, 2]
	TEQ #4b	2	[16, 16]	[6, 3]
	TEQ #4c	2	[16, 16]	[5, 4]
	TEQ #4d	2	[16, 16]	[4, 5]
	TEQ #4e	2	[16, 16]	[3, 6]
	TEQ #4f	2	[16, 16]	[2, 7]

Chapter 5

Time Domain Equalization for OFDM Systems with Unitary Precoding



In this chapter, we propose an OFDM system with unitary precoding. In conventional OFDM systems, the diversity of each subcarrier's channel is one. With precoding, the diversity can be greatly enhanced. Precoding in OFDM systems also provides another advantage facilitating the TEQ design. We propose a design method based on the MSINR criterion. It turns out that the method is simple and effective. Due to precoding, the transmit and the receive signal vectors can be formulated as the input and the output of a MIMO system. As a result, MIMO detection has to be conducted in the receiver. Various MIMO detection algorithms are well known, e.g., successive interference cancellation (SIC) and sphere decoding (SD). The SIC method is simple but the performance is not optimal. On the contrary, the SD method requires higher computational complexity but can achieve near-optimum performance. To solve the problem, we propose a hybrid detection algorithm, called SDSIC. The SDSIC method can achieve near-optimum performance but the computational complexity is low. Simulation results show that precoded OFDM systems with the proposed SMSINR TEQ and the proposed SDSIC detection method significantly outperform unprecoded OFDM systems with conventional TEQs.

This chapter is organized as follows. In Section 5.1, we give the motivation of the proposed

precoded OFDM systems. In Section 5.2, we describe the precoding method for OFDM systems and the SDSIC detection scheme. In Section 5.3, we show simulation results demonstrating the performance of the proposed system.

§ 5.1 Motivation

Consider an equivalent OFDM channel model shown in Figure 5.1(a). In the figure, the OFDM signal passes through a wireless channel with the CIR denoted as \mathbf{h} . We first consider a special case that $M = I$ and $L = I - 1$. In this case, no ISI occurs and the CP overhead approaches 100%. Consider a specific OFDM symbol and let the input and output signal vector in Figure 5.1(a) be $\tilde{\mathbf{x}}$ and $\tilde{\mathbf{y}}$, respectively. We then have

$$\begin{aligned}\tilde{\mathbf{y}} &= \mathbf{F}\mathbf{H}_F\mathbf{F}^H\tilde{\mathbf{x}} + \tilde{\mathbf{v}} \\ &= \mathbf{\Lambda}_h\tilde{\mathbf{x}} + \tilde{\mathbf{v}}\end{aligned}\quad (5.1)$$

where

$$\mathbf{H}_F = \begin{bmatrix} h(0) & h(I-1) & \dots & h(2) & h(1) \\ h(1) & h(0) & \dots & h(3) & h(2) \\ \vdots & \vdots & \ddots & \vdots & \vdots \\ h(I-1) & h(I-2) & \dots & h(1) & h(0) \end{bmatrix}_{M \times M}, \quad (5.2)$$

$\mathbf{\Lambda}_h$ is a diagonal matrix, and $\tilde{\mathbf{v}}$ is AWGN vector in frequency domain. Let $\tilde{\mathbf{h}}_I = [\tilde{h}_0, \dots, \tilde{h}_{I-1}]^T$, where \tilde{h}_l is the channel response of the $(l + 1)$ th subcarrier. Note that in the case of $M = I$, we have $\tilde{\mathbf{h}}_M = \tilde{\mathbf{h}}_I$. Then, we have $\mathbf{\Lambda}_h = \text{diag}[\tilde{h}_0, \dots, \tilde{h}_{I-1}]$. From the definition, \tilde{h}_l can be derived as

$$\tilde{h}_l = \sum_{n=0}^{I-1} \alpha^{ln} h(n), \quad (5.3)$$

where α is defined in (2.1). If $h(n)$ is a tap with Rayleigh fading, $h(n)$ can be seen as a complex Gaussian random variable. From (5.3), we see that \tilde{h}_l is a complex Gaussian random variable. Hence, \tilde{h}_l also experiences Rayleigh fading. It is apparent that the diversity gain

for each subcarrier is only one. Thus, the conventional OFDM system does not exploit the frequency diversity gain provided by the channel and there is a plenty of room for performance improvement.

Now, we consider an OFDM system with a precoding structure shown in Figure 5.1(b). For simplicity, we let the precoding is linear and the precoding matrix is unitary. In the receiver, unitary decoding is conducted to recovery the signal. The matrix for precoding is denoted by \mathbf{U} and that for decoding by \mathbf{U}^H . The input and output signal vectors can then be expressed by

$$\tilde{\mathbf{y}} = \mathbf{U}^H \mathbf{F} \mathbf{H}_F \mathbf{F}^H \mathbf{U} \tilde{\mathbf{x}} + \tilde{\mathbf{v}}.$$

Then, the equivalent channel matrix can be expressed as

$$\tilde{\mathbf{H}} = \mathbf{U}^H \mathbf{F} \mathbf{H}_F \mathbf{F}^H \mathbf{U} = \mathbf{U}^H \Lambda_h \mathbf{U}. \quad (5.4)$$

As we can see from (5.4), the channel matrix is not diagonal anymore (except for the AWGN channel). To facilitate later derivation, we let $h(n)$'s be independent and identically-distributed (i.i.d.). With this assumption, we then have

$$\mathbb{E} \left\{ \tilde{\mathbf{h}}_l \tilde{\mathbf{h}}_l^H \right\} = \mathbb{E} \left\{ \mathbf{F} \mathbf{h} \mathbf{h}^H \mathbf{F}^H \right\} = \sigma_h^2 \mathbf{I}, \quad (5.5)$$

where $\sigma_h^2 = \mathbb{E}\{h_l^2\}$ for every l . In other words, \tilde{h}_l 's are also i.i.d. In the following, we will show that the diversity gain of the precoded OFDM system is I .

Consider two transmit signal vectors $\tilde{\mathbf{x}}_a$ and $\tilde{\mathbf{x}}_b$. We want to find the pairwise error probability (PEP) that the receive signal vector is erroneously detected as $\tilde{\mathbf{x}}_b$ when $\tilde{\mathbf{x}}_a$ is transmitted. The PEP is given by [44]

$$\mathbb{P}(\tilde{\mathbf{x}}_a \rightarrow \tilde{\mathbf{x}}_b) = \mathbb{E} \left\{ \mathcal{Q} \left(\frac{\| \tilde{\mathbf{H}}(\tilde{\mathbf{x}}_a - \tilde{\mathbf{x}}_b) \|}{2\sqrt{N_o/2}} \right) \right\}, \quad (5.6)$$

where

$$\mathcal{Q}(m) \triangleq \frac{1}{\sqrt{2\pi}} \int_m^\infty \exp\left(-\frac{x^2}{2}\right) dx, \quad (5.7)$$

and $\exp(\cdot)$ an exponential function. We first calculate the term $\| \tilde{\mathbf{H}}(\tilde{\mathbf{x}}_a - \tilde{\mathbf{x}}_b) \|$ in the \mathcal{Q} function:

$$\begin{aligned}
\| \tilde{\mathbf{H}}(\tilde{\mathbf{x}}_a - \tilde{\mathbf{x}}_b) \| &= \sqrt{(\tilde{\mathbf{x}}_a - \tilde{\mathbf{x}}_b)^H \tilde{\mathbf{H}}^H \tilde{\mathbf{H}} (\tilde{\mathbf{x}}_a - \tilde{\mathbf{x}}_b)} \\
&= \sqrt{[\mathbf{U}(\tilde{\mathbf{x}}_a - \tilde{\mathbf{x}}_b)]^H |\mathbf{\Lambda}_h|^2 [\mathbf{U}(\tilde{\mathbf{x}}_a - \tilde{\mathbf{x}}_b)]} \\
&= \sqrt{\sum_{l=1}^I |\tilde{h}_l|^2 \| \mathbf{u}_l^T (\tilde{\mathbf{x}}_a - \tilde{\mathbf{x}}_b) \|^2}, \tag{5.8}
\end{aligned}$$

where \mathbf{u}_l is the l th column of \mathbf{U} . Denote the averaged SNR as SNR_a where $\text{SNR}_a = E\{|\tilde{h}_l|^2\}/N_0$, and the normalized \tilde{h}_l as \tilde{h}'_l where $\tilde{h}'_l = \tilde{h}_l/E\{|\tilde{h}_l|^2\}$. Also, let $c_l = \| \mathbf{u}_l^T (\tilde{\mathbf{x}}_a - \tilde{\mathbf{x}}_b) \|^2$. Substituting (5.8) into (5.6), we can rewrite the PEP as

$$\begin{aligned}
\mathbb{P}(\tilde{\mathbf{x}}_a \rightarrow \tilde{\mathbf{x}}_b) &= \mathbb{E} \left\{ \mathcal{Q} \left(\sqrt{\frac{\text{SNR}_a \sum_{l=1}^I |\tilde{h}'_l|^2 \| \mathbf{u}_l^T (\tilde{\mathbf{x}}_a - \tilde{\mathbf{x}}_b) \|^2}{2}} \right) \right\} \\
&= \mathbb{E} \left\{ \mathcal{Q} \left(\sqrt{\frac{\text{SNR}_a \sum_{l=1}^I |\tilde{h}'_l|^2 c_l}{2}} \right) \right\} \\
&\leq \prod_{l=1}^I \frac{1}{1 + \frac{c_l}{4} \text{SNR}_a} \\
&\leq \frac{4^I}{\text{SNR}_a^I \prod_{l=1}^I c_l}, \tag{5.9}
\end{aligned}$$

From (5.9), we can see that the diversity gain is I , compared to one for conventional OFDM systems [44].

In practice, the DFT size, M , is generally much greater than the channel length, I . Without loss of generality, we let $M = N_p I$ where N_p is an integer. It is simple to see that $\tilde{\mathbf{h}}$ is not a white vector anymore. However, if we down-sample $\tilde{\mathbf{h}}$ by a factor of N_p , the resultant vector will be white. This property can be derived as follows. Let $\tilde{\mathbf{h}}_l = [\tilde{h}_l, \tilde{h}_{N_p+l}, \dots, \tilde{h}_{(I-1)N_p+l}]^T$, where l is an offset number ranging from $[0, N_p - 1]$. The corresponding DFT matrix to obtain

$\tilde{\mathbf{h}}_l$ is given by

$$\mathbf{F}_l = \frac{1}{\sqrt{I}} \begin{bmatrix} 1 & \alpha^l & \alpha^{2l} & \dots & \alpha^{(I-1)l} \\ 1 & \alpha^{N_p+l} & \alpha^{2(N_p+l)} & \dots & \alpha^{(N_p+l)(I-1)l} \\ \vdots & \vdots & \vdots & \ddots & \vdots \\ 1 & \alpha^{(I-1)N_p+l} & \alpha^{2((I-1)N_p+l)} & \dots & \alpha^{(I-1)((I-1)N_p+l)} \end{bmatrix}_{I \times I}. \quad (5.10)$$

It is simple to check that \mathbf{F}_l is a unitary matrix, that is, $\mathbf{F}_l \mathbf{F}_l^H = \mathbf{I}_{I \times I}$. Then,

$$\mathbb{E} \left\{ \tilde{\mathbf{h}}_l \tilde{\mathbf{h}}_l^H \right\} = \mathbb{E} \left\{ \mathbf{F}_l \mathbf{h} \mathbf{h}^H \mathbf{F}_l^H \right\} = \sigma_h^2 \mathbf{I}. \quad (5.11)$$

In other words, the elements of $\tilde{\mathbf{h}}_l$ are i.i.d. This suggests that we can use a precoding block with the size of I and the subcarriers in the block are evenly drawn from the frequency domain. From the above discussion, we know that precoding in OFDM systems can enhance the frequency diversity, and the maximum diversity gain is I . Based on this property, we propose a new precoded OFDM system shown in Figure 5.2. In the system, the OFDM symbol is divided into p_M subsymbols where each subsymbol has p subcarriers and $p \leq I$. Precoding is then conducted for each subsymbol.

Precoding in OFDM systems was also proposed in [49] and [50]. The precoding structure in [49] is somewhat different from ours. In [49], redundancy is added in precoding and its purpose is to replace channel coding. In the proposed system, no extra redundancy is added and the purpose is to enhance diversity gain. Channel coding is still used in the proposed system to obtain coding gain. In [50], the size of the precoding block is M and the linear receivers such as the MMSE and ZF are used. As discussed, the frequency diversity for a precoded OFDM system is I . Using a coding block larger than I results in little performance improvement. However, the required computational complexity for signal detection may become much higher. The block size for precoding in the proposed algorithm can be varied. Generally, it is less than I . Also, the receivers we use are nonlinear.

§ 5.2 Proposed Method

In Section 5.2.1, we first describe the proposed precoded OFDM system. In Section 5.2.2, we then propose a TEQ design method called MSINR for the precoded system in which the channel delay spread exceeds the CP range. In Section 5.2.3, we then review various MIMO detection methods and propose a new detection algorithm. Finally, in Section 5.2.4, we analyze the computational complexity of the proposed detection scheme.

§ 5.2.1 System Model

Figure 5.2 shows the proposed precoded OFDM system. As we can see, the main operations in the transmitter (for the transmit signal vector $\tilde{\mathbf{d}}_i$) include precoding, permutation, and IDFT. Precoding is conducted by the multiplication of $\tilde{\mathbf{d}}_i$ with a $M \times M$ matrix \mathbf{U} . The matrix includes p_M unitary submatrices given by:

$$\mathbf{U} = \begin{bmatrix} \mathbf{U}_p & \mathbf{0}_{p \times p} & \cdots & \mathbf{0}_{p \times p} \\ \mathbf{0}_{p \times p} & \mathbf{U}_p & \cdots & \mathbf{0}_{p \times p} \\ \vdots & \vdots & \ddots & \vdots \\ \mathbf{0}_{p \times p} & \mathbf{0}_{p \times p} & \cdots & \mathbf{U}_p \end{bmatrix} \quad (5.12)$$

where $p = 2^m$, $m \in [1, \log_2 M]$, is the block size for precoding and \mathbf{U}_p a $p \times p$ unitary matrix. For computational efficiency, we will use the Walsh-Hadamard matrix for \mathbf{U}_p . The permutation matrix \mathbf{P} is used to conduct the downsampling operation such that the symbols involved in a precoding block are approximately uncorrelated. Let \mathbf{p}_k be the $(k + 1)$ th column vector of \mathbf{P} and \mathbf{i}_k the $(k + 1)$ th column vector of the identity matrix \mathbf{I}_M . Then, $\mathbf{p}_{mp_M+n} = \mathbf{i}_{np_M+m}$, $0 \leq m, n \leq p - 1$. After the IDFT operation, the corresponding time domain signal vector, denoted by \mathbf{d}_i , can be expressed as

$$\mathbf{d}_i = \mathbf{F}^H \mathbf{P} \mathbf{U} \tilde{\mathbf{d}}_i = \mathbf{F}_U^H \tilde{\mathbf{d}}_i, \quad (5.13)$$

where $\mathbf{F}_U^H = \mathbf{F}^H \mathbf{P} \mathbf{U}$ is defined as the precoded IDFT matrix. At the receiver side, the i th received symbol at the TEQ output can be expressed as

$$\begin{aligned} \mathbf{r}_i &= \mathbf{y}_i + \mathbf{v}_i = \mathbf{G} \mathbf{F}_U^H \tilde{\mathbf{d}}_i + \mathbf{v}_i \\ &= \mathbf{G}_S \mathbf{F}_U^H \tilde{\mathbf{d}}_i + \mathbf{G}_I \mathbf{F}_U^H \tilde{\mathbf{d}}_i + \mathbf{v}_i, \end{aligned} \quad (5.14)$$

where the first two terms are the signal part and residual ISI part of the received signal, respectively, and the last term the AWGN.

After the processing of the TEQ, the signal is then passed through the DFT (\mathbf{F}), the inverse permutation \mathbf{P}^H , and the unitary decoding (\mathbf{U}^H) modules, sequentially. At the decoder output, we then have

$$\tilde{\mathbf{r}}_i = \tilde{\mathbf{G}}_S \tilde{\mathbf{d}}_i + \tilde{\mathbf{G}}_I \tilde{\mathbf{d}}_i + \tilde{\mathbf{v}}_i, \quad (5.15)$$

where

$$\begin{aligned} \tilde{\mathbf{G}}_S &= \mathbf{F}_U \mathbf{G}_S \mathbf{F}_U^H, \\ \tilde{\mathbf{G}}_I &= \mathbf{F}_U \mathbf{G}_I \mathbf{F}_U^H, \text{ and} \\ \tilde{\mathbf{v}}_i &= \mathbf{F}_U \mathbf{v}_i, \end{aligned} \quad (5.16)$$

respectively. From (5.15), we can have the signal term, denoted by $\tilde{\mathbf{y}}_{S,i}$, as

$$\tilde{\mathbf{y}}_{S,i} = \tilde{\mathbf{G}}_S \tilde{\mathbf{d}}_i = \mathbf{F}_U \mathbf{G}_S \mathbf{F}_U^H \tilde{\mathbf{d}}_i, \quad (5.17)$$

and the noise-plus-interference term, denoted by $\tilde{\mathbf{e}}_i$, as

$$\tilde{\mathbf{e}}_i = \tilde{\mathbf{G}}_I \tilde{\mathbf{d}}_i + \tilde{\mathbf{v}}_i = \tilde{\mathbf{y}}_{I,i} + \tilde{\mathbf{v}}_i = \mathbf{F}_U \mathbf{G}_I \mathbf{F}_U^H \tilde{\mathbf{d}}_i + \tilde{\mathbf{v}}_i, \quad (5.18)$$

where $\tilde{\mathbf{y}}_{I,i}$ is the received signal contributed by the residual ISI. Note that from (5.13) and (5.16), we can also express $\tilde{\mathbf{G}}_S$ as

$$\tilde{\mathbf{G}}_S = \mathbf{U}^H \mathbf{P}^H \mathbf{F} \mathbf{G}_S \mathbf{F}^H \mathbf{P} \mathbf{U} = \mathbf{U}^H \hat{\mathbf{G}}_S \mathbf{U}, \quad (5.19)$$

where $\hat{\mathbf{G}}_S = \mathbf{P}^H \mathbf{F} \mathbf{G}_S \mathbf{F}^H \mathbf{P}$ and $\hat{\mathbf{G}}_S$ is a diagonal matrix. Finally, $\tilde{\mathbf{r}}_i$ is used as the input to a MIMO detection algorithm. Some existing and proposed algorithms are described in Section 5.2.3.

§ 5.2.2 TEQ Design with MSINR Method

At the decoder output, we have $\tilde{\mathbf{r}}_i = \tilde{\mathbf{y}}_{S,i} + \tilde{\mathbf{e}}_i$. Now, we can partition $\tilde{\mathbf{r}}_i$ into p_M subvectors. Each subvector, having p data symbols, corresponds to a coded signal block. We call a subvector as a received OFDM sub-symbol. Denoting the j th OFDM sub-symbol as $\tilde{\mathbf{r}}_{i,j}$, we then have $\tilde{\mathbf{r}}_i = [\tilde{\mathbf{r}}_{i,0}^T, \dots, \tilde{\mathbf{r}}_{i,p_M-1}^T]^T$. Using the similar partition, we can also have $\tilde{\mathbf{y}}_{S,i} = [\tilde{\mathbf{y}}_{S,i,0}^T, \dots, \tilde{\mathbf{y}}_{S,i,p_M-1}^T]^T$ and $\tilde{\mathbf{e}}_i = [\tilde{\mathbf{e}}_{i,0}^T, \dots, \tilde{\mathbf{e}}_{i,p_M-1}^T]^T$. From (5.15), we see that

$$\tilde{\mathbf{r}}_i = \tilde{\mathbf{y}}_{S,i} + \tilde{\mathbf{y}}_{I,i} + \tilde{\mathbf{v}}_i. \quad (5.20)$$

Thus, we can have the following relationships,

$$\begin{aligned} \tilde{\mathbf{r}}_{i,k} &= \tilde{\mathbf{y}}_{S,i,k} + \tilde{\mathbf{e}}_{i,k}, \text{ and} \\ \tilde{\mathbf{e}}_{i,k} &= \tilde{\mathbf{y}}_{I,i,k} + \tilde{\mathbf{v}}_{i,k}, \end{aligned} \quad (5.21)$$

where $\tilde{\mathbf{v}}_i = [\tilde{\mathbf{v}}_{i,0}^T, \dots, \tilde{\mathbf{v}}_{i,p_M-1}^T]^T$. Let the precoding submatrix, \mathbf{U}_p , be

$$\mathbf{U}_p = \begin{bmatrix} u_{1,1} & u_{1,2} & \cdots & u_{1,p} \\ u_{2,1} & u_{2,2} & \cdots & u_{2,p} \\ \vdots & \vdots & \ddots & \vdots \\ u_{p,1} & u_{p,2} & \cdots & u_{p,p} \end{bmatrix}. \quad (5.22)$$

and $\tilde{y}_{S,i}(k)$, $\tilde{y}_{I,i}(k)$, $\tilde{v}_i(k)$, and $\tilde{e}_i(k)$ be the $(k+1)$ th subcarrier components of $\tilde{\mathbf{y}}_{S,i}$, $\tilde{\mathbf{y}}_{I,i}$, $\tilde{\mathbf{v}}_i$, and $\tilde{\mathbf{e}}_i$, respectively. Since $\tilde{y}_{S,i}(k) = \tilde{g}_S(k)\tilde{d}_i(k)$, and $\tilde{y}_{I,i}(k) = \tilde{g}_I(k)\tilde{d}_i(k)$, we have

$$\begin{aligned} |\tilde{y}_{S,i}(mp+k)|^2 &= \frac{1}{p} \sum_{j=0}^{p-1} \left| u_{k,j}^H \tilde{g}_S(jp_M+m) \tilde{d}_i(jp_M+m) \right|^2, \text{ and} \\ |\tilde{e}_i(mp+k)|^2 &= \frac{1}{p} \sum_{j=0}^{p-1} \left| u_{k,j}^H \tilde{g}_I(jp_M+m) \tilde{d}_i(jp_M+m) \right|^2 + \\ &\quad \frac{1}{p} \sum_{j=0}^{p-1} \left| u_{k,j}^H \tilde{v}_i(jp_M+m) \right|^2, \end{aligned} \quad (5.23)$$

where $0 \leq m \leq p_M - 1$, $0 \leq k \leq p - 1$.

Recall that $s_d(k)$ and $s_\eta(k)$ are the signal power and the noise power in the $(k + 1)$ th sub-channel defined in (2.40) and (2.41), respectively. In general, $s_d(k) = s_d$ where s_d is a constant, and $s_\eta(k) = s_\eta$ where s_η is also a constant. The SINR of the $(mp + k)$ th subchannel at the decoder output is then

$$\begin{aligned}
\text{SINR}_m^p(k) &= \frac{s_d \sum_{j=0}^{p-1} |\mathbf{u}_{k,j}^H \mathbf{f}^T(jp_M + m) \mathbf{T}_G \mathbf{D}_S \mathbf{H} \mathbf{w}|^2}{s_d \sum_{j=0}^{p-1} |\mathbf{u}_{k,j}^H \mathbf{f}^T(jp_M + m) \mathbf{T}_G \mathbf{D}_I \mathbf{H} \mathbf{w}|^2 + s_\eta \sum_{j=0}^{p-1} |\mathbf{u}_{k,j}^H \mathbf{f}^T(jp_M + m) \mathbf{T}_W \mathbf{w}|^2} \\
&= \frac{\sum_{j=0}^{p-1} \mathbf{w}^H \mathbf{A}_{j,m} \mathbf{w}}{\sum_{j=0}^{p-1} \mathbf{w}^H \mathbf{B}_{j,m} \mathbf{w}} \\
&= \frac{\mathbf{w}^H \sum_{j=0}^{p-1} \mathbf{A}_{j,m} \mathbf{w}}{\mathbf{w}^H \sum_{j=0}^{p-1} \mathbf{B}_{j,m} \mathbf{w}}, \tag{5.24}
\end{aligned}$$

where m is the OFDM sub-symbol index, $0 \leq m \leq p_M - 1$, k the data symbol index in the m th OFDM sub-symbol, $0 \leq k \leq p - 1$,

$$\begin{aligned}
\mathbf{A}_{j,m} &= |u_{k,j}|^2 \mathbf{H}^H \mathbf{D}_S^H \mathbf{T}_G^H \mathbf{f}^*(jp_M + m) \mathbf{f}^T(jp_M + m) \mathbf{T}_G \mathbf{D}_S \mathbf{H}, \text{ and} \\
\mathbf{B}_{j,m} &= |u_{k,j}|^2 \mathbf{H}^H \mathbf{D}_I^H \mathbf{T}_G^H \mathbf{f}^*(jp_M + m) \mathbf{f}^T(jp_M + m) \mathbf{T}_G \mathbf{D}_I \mathbf{H} + \\
&\quad \frac{s_\eta}{s_d} |u_{k,j}|^2 \mathbf{T}_W^H \mathbf{f}^*(jp_M + m) \mathbf{f}^T(jp_M + m) \mathbf{T}_W. \tag{5.25}
\end{aligned}$$

Let

$$\mathbb{A}_m = \sum_{j=0}^{p-1} \mathbf{A}_{j,m}, \text{ and } \mathbb{B}_m = \sum_{j=0}^{p-1} \mathbf{B}_{j,m}. \tag{5.26}$$

Then

$$\text{SINR}_m^p(k) = \frac{\mathbf{w}^H \mathbb{A}_m \mathbf{w}}{\mathbf{w}^H \mathbb{B}_m \mathbf{w}}. \tag{5.27}$$

As mentioned, the unitary matrix we consider is the Hadamard matrix. For the matrix, $|u_{k,j}|^2 =$

1. Then,

$$\begin{aligned}
\mathbb{A}_m &= \mathbf{H}^H \mathbf{D}_S^H \mathbf{T}_G^H \sum_{j=0}^{p-1} \mathbf{f}^*(jp_M + m) \mathbf{f}^T(jp_M + m) \mathbf{T}_G \mathbf{D}_S \mathbf{H}, \text{ and} \\
\mathbb{B}_m &= \mathbf{H}^H \mathbf{D}_I^H \mathbf{T}_G^H \sum_{j=0}^{p-1} \mathbf{f}^*(jp_M + m) \mathbf{f}^T(jp_M + m) \mathbf{T}_G \mathbf{D}_I \mathbf{H} + \\
&\quad \frac{s_\eta}{s_d} \mathbf{T}_W^H \sum_{j=0}^{p-1} \mathbf{f}^*(jp_M + m) \mathbf{f}^T(jp_M + m) \mathbf{T}_W. \tag{5.28}
\end{aligned}$$

It is important to see that the SINR of each subcarrier in an OFDM sub-symbol is the same. To minimize the error rate performance of sub-symbol m , we then have to maximize $\text{SINR}_m^p(k)$. However, the TEQ may not be able to maximize the SINRs of all OFDM sub-symbols. An compromised scheme is to maximize the average SINR, i.e.,

$$\max_{\mathbf{w}} \sum_{m=0}^{pM-1} \frac{\mathbf{w}^H \mathbb{A}_m \mathbf{w}}{\mathbf{w}^H \mathbb{B}_m \mathbf{w}}. \quad (5.29)$$

We call the method as the MSINR method. For a special case that $p = 1$, we have

$$\begin{aligned} & \max_{\mathbf{w}} \sum_{m=0}^{M-1} \frac{\mathbf{w}^H \mathbb{A}_m \mathbf{w}}{\mathbf{w}^H \mathbb{B}_m \mathbf{w}} \\ &= \max_{\mathbf{w}} \sum_{m=0}^{M-1} \frac{\mathbf{w}^H \mathbf{H}^H \mathbf{D}_S^H \mathbf{T}_G^H \mathbf{f}^*(m) \mathbf{f}^T(m) \mathbf{T}_G \mathbf{D}_S \mathbf{H} \mathbf{w}}{\mathbf{w}^H \mathbf{H}^H \mathbf{D}_I^H \mathbf{T}_G^H \mathbf{f}^*(m) \mathbf{f}^T(m) \mathbf{T}_G \mathbf{D}_I \mathbf{H} + \frac{s_\eta}{s_d} \mathbf{T}_W^H \sum_{j=0}^{p-1} \mathbf{f}^*(m) \mathbf{f}^T(m) \mathbf{T}_W \mathbf{w}} \end{aligned} \quad (5.30)$$

As we can see, the MSINR method is equivalent to the MBR method in [18]. For this case, the subcarrier SINR will have largest variation since no diversity can be exploited. For another special case that $p = M$, we have

$$\begin{aligned} \mathbb{A}_m &= \mathbf{H}^H \mathbf{D}_S^H \mathbf{T}_G^H \sum_{j=0}^{M-1} \mathbf{f}^*(j) \mathbf{f}^T(j) \mathbf{T}_G \mathbf{D}_S \mathbf{H}, \text{ and} \\ &= \mathbf{H}^H \mathbf{D}_S^H \mathbf{T}_G^H \mathbf{T}_G \mathbf{D}_S \mathbf{H}, \text{ and} \\ \mathbb{B}_m &= \mathbf{H}^H \mathbf{D}_I^H \mathbf{T}_G^H \sum_{j=0}^{M-1} \mathbf{f}^*(j) \mathbf{f}^T(j) \mathbf{T}_G \mathbf{D}_I \mathbf{H} + \frac{s_\eta}{s_d} \mathbf{T}_W^H \sum_{j=0}^{M-1} \mathbf{f}^*(j) \mathbf{f}^T(j) \mathbf{T}_W \\ &= \mathbf{H}^H \mathbf{D}_I^H \mathbf{T}_G^H \mathbf{T}_G \mathbf{D}_I \mathbf{H} + \frac{s_\eta}{s_d} \mathbf{T}_W^H \mathbf{T}_W. \end{aligned} \quad (5.31)$$

Hence,

$$\max_{\mathbf{w}} \frac{\mathbf{w}^H \mathbb{A}_m \mathbf{w}}{\mathbf{w}^H \mathbb{B}_m \mathbf{w}} = \max_{\mathbf{w}} \frac{\mathbf{w}^H \mathbf{H}^H \mathbf{D}_S^H \mathbf{T}_G^H \mathbf{T}_G \mathbf{D}_S \mathbf{H} \mathbf{w}}{\mathbf{w}^H \mathbf{H}^H \mathbf{D}_I^H \mathbf{T}_G^H \mathbf{T}_G \mathbf{D}_I \mathbf{H} + \frac{s_\eta}{s_d} \mathbf{T}_W^H \mathbf{T}_W \mathbf{w}}. \quad (5.32)$$

Since only one precoding block is used, the SINRs of all subcarriers are equal. Then, maximization of averaged SNR is identical to maximization of the SNR of each subcarrier. Thus, the MSINR becomes optimal. However, the computational complexity for precoding and signal detection is also the highest. Also note that in this case the MSINR method is exactly the same

as that of the min-ISI method. In other words, the TEQ derived will be the same as that of the min-ISI method. As we can see, the min-ISI method is not optimal while the MSINR method is optimal. The difference lies in that precoding is conducted when the MSINR method is applied.

As mentioned, the diversity gain provided by the channel is I . Note that the CP size is L . To maintain the circular convolution property, the CIR length I must be shortened to the CP size L . That is, the diversity gain provided by the system is L . To fully explore the diversity, a precoding size of L (i.e., $p = L$) will be sufficient. We now show that a precoding size of L is also sufficient (optimal) for the MSINR method. Let the channel taps be i.i.d. and $p = L$. From (5.11), we know that the elements in the downsampled vector $\tilde{\mathbf{h}}_l$ are i.i.d. Let \mathbf{U}_L be an $L \times L$ unitary matrix, and $\mathbf{U}_L \mathbf{U}_L^H = \mathbf{I}_{L \times L}$. The l th precoded OFDM sub-symbol is then $\mathbf{U}_L^H \tilde{\mathbf{h}}_l$. Thus,

$$\mathbf{E} \left\{ \mathbf{U}_L^H \tilde{\mathbf{h}}_l \tilde{\mathbf{h}}_l^H \mathbf{U}_L \right\} = \mathbf{E} \left\{ \mathbf{U}_L^H \mathbf{F}_l \mathbf{h} \mathbf{h}^H \mathbf{F}_l^H \mathbf{U}_L \right\} = \sigma_h^2 \mathbf{I}_{L \times L}. \quad (5.33)$$

In other words, the signal power of each subcarrier after precoding is the same. Thus, maximizing the averaged SINR is equivalent to maximizing the SINR of each subcarrier. The MSINR method is then optimal. Note that the optimality is based on the assumption that the channel taps are i.i.d. In practice, this assumption may not be held. As a result, the signal power in each coding block is not the same. For simplicity, we can simplify the cost function in (5.29) as

$$\max_{\mathbf{w}} \frac{\mathbf{w}^H \sum_{m=0}^{P_M-1} \mathbf{A}_m \mathbf{w}}{\mathbf{w}^H \sum_{m=0}^{P_M-1} \mathbf{B}_m \mathbf{w}}. \quad (5.34)$$

And we call the TEQ design using the cost function in (5.34) as the simplified MSINR (SM-SINR) method. If the size of the coding block is properly chosen, the variation of the signal power in each coding block will be small and the TEQ obtained with (5.34) is nearly optimal.

§ 5.2.3 Detection Methods

Precoding in OFDM systems exploits the frequency diversity the channel provides. However, the precoding also results in a MIMO system for the subcarriers in the same coding block. One of the advantage of OFDM systems is that the equalization can be conducted by a single-tap

FEQ. As we will see, the single-tap FEQ cannot be used in precoded systems since the diversity gain will be reduced back to one [44]. To explore the diversity the precoded system has, we then have to use more sophisticated detection methods such as the SIC and ML methods. The SIC is a simple MIMO detection method. Due to its lower computational complexity, it is frequently considered in real-world implementation. The ML method is the optimum detection method; however, its computational complexity grows exponentially along with the QAM size and the system dimension. In many cases, the computational complexity becomes prohibitively high. To solve the problem, many near-optimum detectors have been proposed. Among these detectors, SD is considered as one of the most efficient ML algorithms. It has been proved that for an $L \times L$ MIMO system, the diversity gain with the ML detector is L [44]. Thus, to obtain the full diversity gain for precoded OFDM systems, we then have to use the ML detector. In many real-world applications, the channel length (i.e., L) is generally large. Even with the SD algorithm, the computational complexity is still too high. In this section, we propose a new method to solve the problem. The proposed method, combining the merits of SIC and SD, can have a similar performance as that of SD. However, the required computational complexity can be significantly reduced.

Zero Forcing FEQ (ZF-FEQ)

When detecting a signal component, the ZF-FEQ completely removes the interference from other components. Let the receive signal vector $\tilde{\mathbf{r}}_i$ in (5.15) be multiplied by a ZF-FEQ matrix, denoted as \mathbf{S} . The output signal, denoted as $\tilde{\mathbf{u}}'_i$, is then passed through a hard-decision device and a decided signal vector, denoted as $\tilde{\mathbf{u}}_i$, is obtained. The equalized signal vector can be expressed as

$$\begin{aligned}
 \tilde{\mathbf{u}}'_i &= \mathbf{S}\tilde{\mathbf{r}}_i \\
 &= \mathbf{S}\tilde{\mathbf{y}}_{S,i} + \mathbf{S}\tilde{\mathbf{y}}_{I,i} + \mathbf{S}\tilde{\mathbf{v}}_i \\
 &= \mathbf{S}\tilde{\mathbf{G}}_S\tilde{\mathbf{d}}_i + \mathbf{S}\tilde{\mathbf{G}}_I\tilde{\mathbf{d}}_i + \mathbf{S}\tilde{\mathbf{v}}_i,
 \end{aligned} \tag{5.35}$$

where $\tilde{\mathbf{y}}_{S,i}$, $\tilde{\mathbf{y}}_{I,i}$, and $\tilde{\mathbf{v}}_i$ are those defined in (5.17) and (5.18). To have a ZF-FEQ result, we have \mathbf{S} as

$$\mathbf{S} = \tilde{\mathbf{G}}_S^{-1}. \quad (5.36)$$

As a result, we have $\tilde{\mathbf{u}}'_i$ as

$$\tilde{\mathbf{u}}'_i = \tilde{\mathbf{d}}_i + \tilde{\mathbf{G}}_S^{-1} \tilde{\mathbf{G}}_I \tilde{\mathbf{d}}_i + \tilde{\mathbf{G}}_S^{-1} \tilde{\mathbf{v}}_i. \quad (5.37)$$

From (5.19), we can see that

$$\tilde{\mathbf{G}}_S^{-1} = \mathbf{U}^H \hat{\mathbf{G}}_S^{-1} \mathbf{U} \quad (5.38)$$

Note that $\hat{\mathbf{G}}_S^{-1}$ is just the single-tap FEQ used in conventional OFDM systems. The ZF-FEQ in the precoded OFDM system is exactly the same as that in the uncoded system. Thus, the required computational complexity is low. However, as mentioned, the diversity gain for the ZF detection in MIMO systems is one [44]. As a result, no performance improvement can be obtained with precoding.

Successive Interference Cancelation (SIC)

The SIC is a nonlinear detection method. The main idea is to estimate and detect each signal component of the transmitted symbol sequentially. Each detected component is then removed from the received signal before the estimation of the next component [63]. To apply the SIC method, we first partition the receive OFDM symbol, $\tilde{\mathbf{r}}_i$ in (5.15), into p_M sub-symbols with size $p = M/p_M$. Also, $\tilde{\mathbf{v}}_i$ in (5.16) and $\tilde{\mathbf{u}}_i$ are also partitioned accordingly. Let

$$\begin{aligned} \tilde{\mathbf{r}}_i &= [\tilde{\mathbf{r}}_{i,0}^T, \tilde{\mathbf{r}}_{i,1}^T, \dots, \tilde{\mathbf{r}}_{i,p_M-1}^T]^T, \\ \tilde{\mathbf{v}}_i &= [\tilde{\mathbf{v}}_{i,0}^T, \tilde{\mathbf{v}}_{i,1}^T, \dots, \tilde{\mathbf{v}}_{i,p_M-1}^T]^T, \text{ and} \\ \tilde{\mathbf{u}}_i &= [\tilde{\mathbf{u}}_{i,0}^T, \tilde{\mathbf{u}}_{i,1}^T, \dots, \tilde{\mathbf{u}}_{i,p_M-1}^T]^T, \end{aligned} \quad (5.39)$$

where

$$\begin{aligned}\tilde{\mathbf{r}}_{i,k} &= [\tilde{r}_i(pk), \tilde{r}_i(pk+1), \dots, \tilde{r}_i(pk+p-1)]^T, \\ \tilde{\mathbf{u}}_{i,k} &= [\tilde{u}_i(pk), \tilde{u}_i(pk+1), \dots, \tilde{u}_i(pk+p-1)]^T, \text{ and} \\ \tilde{\mathbf{v}}_{i,k} &= [\tilde{v}_i(pk), \tilde{v}_i(pk+1), \dots, \tilde{v}_i(pk+p-1)]^T, \text{ for } 0 \leq k \leq p_M - 1.\end{aligned}\quad (5.40)$$

$$\hat{\mathbf{G}}_S = \begin{bmatrix} \hat{\mathbf{G}}_{S,0} & \mathbf{0}_{p \times p} & \cdots & \mathbf{0}_{p \times p} \\ \mathbf{0}_{p \times p} & \hat{\mathbf{G}}_{S,1} & \cdots & \mathbf{0}_{p \times p} \\ \vdots & \vdots & \ddots & \vdots \\ \mathbf{0}_{p \times p} & \mathbf{0}_{p \times p} & \cdots & \hat{\mathbf{G}}_{S,p_M-1} \end{bmatrix}, \quad (5.41)$$

where $\hat{\mathbf{G}}_{S,k}$ is a $p \times p$ diagonal matrix. Then, with the property of the permutation matrix, $\tilde{\mathbf{G}}_S$ can be also represented as

$$\tilde{\mathbf{G}}_S = \begin{bmatrix} \tilde{\mathbf{G}}_{S,0} & \mathbf{0}_{p \times p} & \cdots & \mathbf{0}_{p \times p} \\ \mathbf{0}_{p \times p} & \tilde{\mathbf{G}}_{S,1} & \cdots & \mathbf{0}_{p \times p} \\ \vdots & \vdots & \ddots & \vdots \\ \mathbf{0}_{p \times p} & \mathbf{0}_{p \times p} & \cdots & \tilde{\mathbf{G}}_{S,p_M-1} \end{bmatrix} \quad (5.42)$$

where the k th component is given by

$$\tilde{\mathbf{G}}_{S,k} = \mathbf{U}_p^H \hat{\mathbf{G}}_{S,k} \mathbf{U}_p, \text{ for } k = 0, \dots, p_M - 1. \quad (5.43)$$

As we can see, all $\tilde{\mathbf{G}}_{S,k}$, \mathbf{P}_k , \mathbf{U}_p , and $\hat{\mathbf{G}}_{S,k}$ are $p \times p$ matrices. The corresponding k th component of ISI matrix can be represented as

$$\tilde{\mathbf{G}}_{I,k} = \mathbf{U}_p^H \hat{\mathbf{G}}_{I,k} \mathbf{U}_p, \text{ for } k = 0, \dots, p_M - 1. \quad (5.44)$$

As a result, we have the receive k th sub-symbol as

$$\tilde{\mathbf{r}}_{i,k} = \tilde{\mathbf{G}}_{S,k} \tilde{\mathbf{d}}_{i,k} + \tilde{\mathbf{G}}_{I,k} \tilde{\mathbf{d}}_{i,k} + \tilde{\mathbf{v}}_{i,k}, \text{ for } k = 0, \dots, p_M - 1, \quad (5.45)$$

$\tilde{\mathbf{u}}_{i,k}$, $\tilde{\mathbf{r}}_{i,k}$ and $\tilde{\mathbf{v}}_{i,k}$ are those defined in (5.39), and $\tilde{\mathbf{G}}_{S,k}$, $\tilde{\mathbf{G}}_{I,k}$ in (5.43) and (5.44), respectively. As we can see, (5.45) is a MIMO system representation.

From [42], we see that the probability density function of the receive signal conditioned on the transmit signal is defined as the likelihood function. For our problem, the likelihood function is then $p\{\tilde{\mathbf{r}}_{i,k}|\tilde{\mathbf{d}}_{i,k}\}$. The criterion to choose $\tilde{\mathbf{d}}_{i,k}$ that maximizes $p\{\tilde{\mathbf{r}}_{i,k}|\tilde{\mathbf{d}}_{i,k}\}$ is called the ML criterion. It is simple to prove that the decision rule can be reduced to find the $\tilde{\mathbf{d}}_i$ that is closest in distance to the received signal vector $\tilde{\mathbf{r}}_{i,k}$. Therefore, the ML detection criterion for our precoded OFDM systems can be reduced to

$$\tilde{\mathbf{u}}_{i,k} = \arg \min_{\tilde{\mathbf{d}}_{i,k} \in \Psi_p} \|\tilde{\mathbf{r}}_{i,k} - \tilde{\mathbf{G}}_{S,k} \tilde{\mathbf{d}}_{i,k}\|^2, \quad (5.46)$$

where Ψ_p is a set including all possible $\tilde{\mathbf{d}}_i$. Using the QR decomposition, we can decompose $\tilde{\mathbf{G}}_{S,k}$ into $\tilde{\mathbf{G}}_{S,k} = \tilde{\mathbf{Q}}_k \tilde{\mathbf{R}}_k$, where $\tilde{\mathbf{R}}_k$ is an upper-triangular matrix given by

$$\tilde{\mathbf{R}}_k = \begin{bmatrix} \tilde{r}_k(0,0) & \tilde{r}_k(0,1) & \tilde{r}_k(0,2) & \cdots & \tilde{r}_k(0,p-1) \\ 0 & \tilde{r}_k(1,1) & \tilde{r}_k(1,2) & \cdots & \tilde{r}_{2p}(1,p-1) \\ 0 & 0 & \tilde{r}_k(2,2) & \cdots & \tilde{r}_k(2,p-1) \\ \vdots & \vdots & \vdots & \ddots & \vdots \\ 0 & 0 & 0 & \cdots & \tilde{r}_k(p-1,p-1) \end{bmatrix}, \quad (5.47)$$

and $\tilde{\mathbf{Q}}_k$ is a unitary matrix. Then, we have the ML detection as

$$\begin{aligned} \tilde{\mathbf{u}}_{i,k} &= \arg \min_{\tilde{\mathbf{d}}_{i,k} \in \Psi_p} \|\tilde{\mathbf{r}}_{i,k} - \tilde{\mathbf{Q}}_k \tilde{\mathbf{R}}_k \tilde{\mathbf{d}}_{i,k}\|^2 \\ &= \arg \min_{\tilde{\mathbf{d}}_{i,k} \in \Psi_p} \|\tilde{\mathbf{r}}'_{i,k} - \tilde{\mathbf{R}}_k \tilde{\mathbf{d}}_{i,k}\|^2, \end{aligned} \quad (5.48)$$

where $\tilde{\mathbf{r}}'_{i,k} = \tilde{\mathbf{Q}}_k^H \tilde{\mathbf{r}}_{i,k}$. The SIC tries to implement the ML detection and conducts signal detection starting from the last data symbol. From (5.48), we see that the last symbol can be detected by

$$\hat{u}_{i,k}(p-1) = \arg \min_{\tilde{d}_{i,k}(p-1) \in \Psi_d} \left| \tilde{r}'_{i,k}(p-1) - \tilde{r}_k(p-1,p-1) \tilde{d}_{i,k}(p-1) \right|^2, \quad (5.49)$$

where Ψ_d is the set for all possible transmit $\tilde{d}_{i,k}(p-1)$. Now, if the detection is correct, i.e., $\hat{u}_{i,k}(p-1) = \tilde{d}_{i,k}(p-1)$, we can subtract its interference from the received signal and this will

enhance the probability of correct detection of $\tilde{d}_{i,k}(p-2)$. This process can be repeated until all the symbols are detected. For $(m+1)$ th symbol, we then have the detection as

$$\hat{u}_{i,k}(m) = \arg \min_{\tilde{d}_{i,k}(m) \in \Psi_d} \left(\left| \tilde{r}'_{i,k}(m) - \sum_{j=m}^{p-1} \tilde{\mathbf{r}}_k(m,j) \tilde{d}_{i,k}(j) \right|^2 \right), \quad (5.50)$$

where $\tilde{d}_{i,k}(n) = \hat{u}_{i,k}(n)$ for $(m+1) \leq n \leq (p-1)$, and $0 \leq m \leq p-1$. Note that the SIC method cannot achieve the ML performance since detection errors can occur in any stage. Also, an detection error in a certain stage will increase the probability of detection error in later stages. This is called error propagation.

Maximum Likelihood Sequential Estimation

The ML detector is an optimal detector and it needs an exhaustive search over the entire set of Ψ_p [54]. If the QAM constellation size is R and the size of the OFDM sub-symbol $\tilde{\mathbf{d}}_{i,k}$ is p , the computational complexity for the ML detector is $\mathcal{O}(R^p)$. The complexity of the ML detection can become extremely high for a high constellation modulation size R and large symbol size p . Many suboptimum methods have been developed to reduce the required computational complexity. These methods can have near-ML performance but the required computational complexity is much lower. Among them, the most well known is the SD method. In this dissertation, we use the SD-based method for the implementation of the ML detector.

Sphere Decoding (SD)

From (5.48), we see that the ML detection can be conducted as

$$\begin{aligned} \tilde{\mathbf{u}}_{i,k} &= \arg \min_{\tilde{\mathbf{d}}_{i,k} \in \Psi_p} \left\| \tilde{\mathbf{Q}}_k^H \tilde{\mathbf{r}}_{i,k} - \tilde{\mathbf{R}}_k \tilde{\mathbf{d}}_{i,k} \right\|^2 \\ &= \arg \min_{\tilde{\mathbf{d}}_{i,k} \in \Psi_p} \left\| \tilde{\mathbf{r}}'_{i,k} - \tilde{\mathbf{R}}_k \tilde{\mathbf{d}}_{i,k} \right\|^2. \end{aligned} \quad (5.51)$$

Note that $\tilde{\mathbf{R}}_k$ is an upper-triangular matrix. The main idea of the SD method is to search a subset of Ψ_p such that

$$\left\| \tilde{\mathbf{r}}'_{i,k} - \tilde{\mathbf{R}}_k \tilde{\mathbf{d}}_{i,k} \right\|^2 < r_{SD}^2, \quad (5.52)$$

where r_{SD} is the radius of the searching sphere [54]. The search starts with the last symbol of $\tilde{\mathbf{r}}'_{i,k}$ and forms a tree structure excluding unlikely candidates located out of the sphere. Considering the p th component $\tilde{\mathbf{r}}'_{i,k}$, we have

$$|\tilde{r}'_{i,k}(p-1) - \tilde{r}_k(p-1, p-1)\tilde{d}_{i,k}(p-1)|^2 < r_{\text{SD}}^2. \quad (5.53)$$

We then choose all possible $\tilde{d}_{i,k}(p-1)$'s such that $|\tilde{r}'_{i,k}(p-1) - \tilde{r}_k(p-1, p-1)\tilde{d}_{i,k}(p-1)|^2 < r_{\text{SD}}^2$ as the candidates for the p th component of $\tilde{\mathbf{r}}_{i,k}$. Now, consider the $(p-1)$ th and p th components of $\tilde{\mathbf{r}}'_{i,k}$ in (5.52). For each candidate of $\tilde{d}_{i,k}(p-1)$, we then choose all $\tilde{d}_{i,k}(p-2)$'s such that

$$\left\| \begin{bmatrix} \tilde{u}_{i,k}(p-2)' \\ \tilde{u}_{i,k}(p-1)' \end{bmatrix} - \begin{bmatrix} \tilde{r}_k(p-2, p-2) & \tilde{r}_k(p-2, p-1) \\ 0 & \tilde{r}_k(p-1, p-1) \end{bmatrix} \begin{bmatrix} \tilde{d}_{i,k}(p-2) \\ \tilde{d}_{i,k}(p-1) \end{bmatrix} \right\|^2 < r_{\text{SD}}^2 \quad (5.54)$$

as the candidates. The remaining components, $[\hat{d}_{i,k}(p-3), \dots, \hat{d}_{i,k}(0)]^T$, can be determined in a similar manner. For a general expanding form of (5.52), we have

$$\tilde{\mathbf{u}}_{i,k} = \min_{\tilde{\mathbf{d}}_{i,k} \in \Psi_p} \left| \sum_{n=0}^{p-1} \tilde{r}'_{i,k}(n) - \sum_{m=n}^{p-1} \tilde{r}_k(n, m)\tilde{d}_{i,k}(m) \right|^2 < r_{\text{SD}}^2 \quad (5.55)$$

where $\tilde{\mathbf{r}}'_{i,k} = [\tilde{r}'_{i,k}(0), \dots, \tilde{r}'_{i,k}(p-1)]^T$, $\tilde{\mathbf{d}}_{i,k} = [\tilde{d}_{i,k}(0), \dots, \tilde{d}_{i,k}(p-1)]^T$. The search from $\tilde{d}_{i,k}(p-1)$ to $\tilde{d}_{i,k}(0)$ then forms a tree structure. A complete path in the tree give a solution candidate ($\tilde{\mathbf{d}}_{i,k}$). Since the tree has many paths satisfying (5.55), we then have a list of candidates. Finally, we can find the one minimizing (5.51) as the detection output.

The efficiency of the SD method greatly depends on the choice of the radius r_{SD} . The complexity will be high if r_{SD} is large. This is because more candidates will be included in the sphere of (5.55). If r_{SD} is small, the optimum solution may not be included in the sphere. In [55], a proper radius is suggested as:

$$r_{\text{SD}}^2 = \mathcal{C} |\det(\tilde{\mathbf{G}}_{S,k})|^{\frac{1}{p}} \quad (5.56)$$

where \mathcal{C} is a constant, and $\det(\tilde{\mathbf{G}}_{S,k})$ the determinant of $\tilde{\mathbf{G}}_{S,k}$. The matrix $\tilde{\mathbf{G}}_{S,k}$ is defined in (5.46). It has been shown that the choice can have a good compromise between performance and computational complexity [56].

Ordering for SIC and SD

For the SIC method, detection is conducted in a backward fashion. As mentioned, the SIC method described in (5.50) has an error propagation problem. The diagonal element of $\tilde{\mathbf{R}}_k$, i.e., $\tilde{r}_k(m, m)$, $0 \leq m \leq p - 1$, determines the SINR of the m th signal component. If $\tilde{r}_{i,k}$ can be ordered before the QR decomposition such that $\tilde{r}_k(m, m)$ (after QR decomposition) has an ascending order, the error propagation effect can be reduced. However, the optimum ordering resulting an ascending order of $\tilde{r}_k(m, m)$ has not been found yet. Some suboptimum ordering methods have been proposed in the literature [56], [64], [61], [62]. For the SD method, a proper ordering also gives better result. This is because for the determination of the candidates of the m th $\tilde{\mathbf{d}}_{i,k}$, the number of components involved in (5.55) is $m - 1$. When the tree is expanded in early stages, m is small. The distance calculation in (5.55) is not reliable. If an proper ordering is conducted, the SINR can be enlarged and the radius of the sphere can be reduced. As a result, the number of candidates can be reduced too. As we see in (5.56), the computational complexity of the SD method is related to the number of candidates. A proper ordering can then reduce the computational complexity of the SD method.

From (5.48), we see that the equivalent MIMO system obtained from the precoded OFDM system has a special structure. The existing ordering algorithms may not be proper for this application. For example, the scheme in [56] uses the column norms of the channel matrix for ordering. However, from (5.19), we see that the column norms are all the same and the method in [56] cannot be applied. Here, we propose an simple ordering scheme for the precoded OFDM system.

Recall that the ML detection for precoded OFDM systems can be expressed as

$$\tilde{\mathbf{u}}_{i,k} = \arg \min_{\tilde{\mathbf{d}}_{i,k} \in \Psi_p} \|\tilde{\mathbf{r}}_{i,k} - \tilde{\mathbf{G}}_{S,k} \tilde{\mathbf{d}}_{i,k}\|^2 \quad (5.57)$$

where

$$\tilde{\mathbf{r}}_{i,k} = \tilde{\mathbf{G}}_{S,k} \tilde{\mathbf{d}}_{i,k} + \tilde{\mathbf{G}}_{I,k} \tilde{\mathbf{d}}_{i,k} + \tilde{\mathbf{v}}_{i,k}, \text{ for } k = 0, \dots, p_M - 1. \quad (5.58)$$

Here, $\tilde{\mathbf{u}}_{i,k}$, $\tilde{\mathbf{r}}_{i,k}$ and $\tilde{\mathbf{v}}_{i,k}$ are those defined in (5.39), and $\tilde{\mathbf{G}}_{S,k}$, $\tilde{\mathbf{G}}_{I,k}$ in (5.43) and (5.44), re-

spectively. As defined, $\hat{\mathbf{G}}_{S,k}$ in (5.41) is a diagonal matrix. We propose ordering the diagonal elements of $\hat{\mathbf{G}}_{S,k}$ such that the elements have an ascending order. That is

$$\tilde{\mathbf{g}}_{S,k} = [\tilde{g}_{S,k}(0), \dots, \tilde{g}_{S,k}(p-1)]^T = \mathbf{O}_k \text{diag} [\hat{\mathbf{G}}_{S,k}] \quad (5.59)$$

where $\tilde{g}_{S,k}(0) \leq \dots \leq \tilde{g}_{S,k}(p-1)$, and \mathbf{O}_k is a permutation matrix ($\mathbf{O}_k^T \mathbf{O}_k = \mathbf{I}_p$). Therefore, we can have ordered $\hat{\mathbf{G}}_{S,k}$, denoted by $\hat{\mathbf{G}}_{S,k}^o$, as

$$\hat{\mathbf{G}}_{S,k}^o = \text{diag} [\tilde{\mathbf{g}}_{S,k}] = \mathbf{O}_k \hat{\mathbf{G}}_{S,k} \mathbf{O}_k^T. \quad (5.60)$$

From (5.43), we know that $\tilde{\mathbf{G}}_{S,k} = \mathbf{U}_p^H \hat{\mathbf{G}}_{S,k} \mathbf{U}_p$, for $k = 0, \dots, p_M - 1$. From (5.57), we can rewrite the detection problem as

$$\begin{aligned} \tilde{\mathbf{u}}_{i,k} &= \arg \min_{\tilde{\mathbf{d}}_{i,k} \in \Psi_p} \left\| \mathbf{O}_k^T (\mathbf{O}_k \tilde{\mathbf{r}}_{i,k} - \mathbf{O}_k \tilde{\mathbf{G}}_{S,k} \tilde{\mathbf{d}}_{i,k}) \right\|^2 \\ &= \arg \min_{\tilde{\mathbf{d}}_{i,k} \in \Psi_p} \left\| \mathbf{O}_k^T (\tilde{\mathbf{r}}_{i,k}^o - \mathbf{O}_k \mathbf{U}_p^H \hat{\mathbf{G}}_{S,k} \mathbf{U}_p \tilde{\mathbf{d}}_{i,k}) \right\|^2 \\ &= \arg \min_{\tilde{\mathbf{d}}_{i,k} \in \Psi_p} \left\| \mathbf{O}_k^T (\tilde{\mathbf{r}}_{i,k}^o - \mathbf{O}_k \mathbf{U}_p^H \mathbf{O}_k^T \mathbf{O}_k \hat{\mathbf{G}}_{S,k} \mathbf{O}_k^T \mathbf{O}_k \mathbf{U}_p \mathbf{O}_k^T \mathbf{O}_k \tilde{\mathbf{d}}_{i,k}) \right\|^2 \\ &= \arg \min_{\tilde{\mathbf{d}}_{i,k} \in \Psi_p} \left\| \mathbf{O}_k^T (\tilde{\mathbf{r}}_{i,k}^o - (\mathbf{U}_p^o)^H \hat{\mathbf{G}}_{S,k}^o \mathbf{U}_p^o \tilde{\mathbf{d}}_{i,k}^o) \right\|^2 \\ &= \arg \min_{\tilde{\mathbf{d}}_{i,k} \in \Psi_p} \left\| \tilde{\mathbf{r}}_{i,k}^o - \mathbf{G}_{S,k}^o \tilde{\mathbf{d}}_{i,k}^o \right\|^2 \end{aligned} \quad (5.61)$$

where $\mathbf{U}_p^o = \mathbf{O}_k \mathbf{U}_p \mathbf{O}_k^T$, $\tilde{\mathbf{d}}_{i,k}^o = \mathbf{O}_k \tilde{\mathbf{d}}_{i,k}$, and $\mathbf{G}_{S,k}^o = (\mathbf{U}_p^o)^H \hat{\mathbf{G}}_{S,k}^o \mathbf{U}_p^o$. Note that \mathbf{U}_p^o is still a unitary matrix because that $(\mathbf{U}_p^o)^H \mathbf{U}_p^o = (\mathbf{O}_k \mathbf{U}_p^H \mathbf{O}_k^T) \mathbf{O}_k \mathbf{U}_p \mathbf{O}_k^T = \mathbf{I}_p$.

We now can conduct SIC or SD with (5.61). Let \mathbf{Q}_k and \mathbf{R}_k be the matrix pair of QR-decomposition of $\mathbf{G}_{S,k}^o$, where $\mathbf{Q}_k = [\mathbf{q}_k^0, \dots, \mathbf{q}_k^{p-1}]$ is a unitary matrix and \mathbf{R}_k is an upper-triangular matrix with the form

$$\mathbf{R}_k = \begin{bmatrix} r_k(0,0) & r_k(0,1) & \cdots & r_k(0,p-1) \\ 0 & r_k(1,1) & \cdots & r_k(1,p-1) \\ \vdots & \vdots & \ddots & \vdots \\ 0 & 0 & \cdots & r_k(p-1,p-1) \end{bmatrix}. \quad (5.62)$$

The operations are the same as those in (5.48), (5.51) except that \mathbf{Q}_k and \mathbf{R}_k are used to replace $\tilde{\mathbf{Q}}_k$ and $\tilde{\mathbf{R}}_k$, respectively.

$$\begin{aligned}\tilde{\mathbf{u}}_{i,k}^o &= \arg \min_{\tilde{\mathbf{d}}_{i,k}^o \in \Psi_p} \|\mathbf{Q}_k^H \tilde{\mathbf{r}}_{i,k}^o - \mathbf{R}_k \tilde{\mathbf{d}}_{i,k}^o\|^2 \\ &= \arg \min_{\tilde{\mathbf{d}}_{i,k}^o \in \Psi_p} \|\tilde{\mathbf{r}}_{i,k}^{\prime o} - \mathbf{R}_k \tilde{\mathbf{d}}_{i,k}^o\|^2,\end{aligned}\quad (5.63)$$

where $\tilde{\mathbf{r}}_{i,k}^{\prime o} = \mathbf{Q}_k^H \tilde{\mathbf{r}}_{i,k}^o$. Note that $\tilde{\mathbf{u}}_{i,k}^o$, $\tilde{\mathbf{r}}_{i,k}^o$, $\tilde{\mathbf{d}}_{i,k}^o$, $\tilde{\mathbf{r}}_{i,k}^{\prime o}$ are the ordered version of $\tilde{\mathbf{u}}_{i,k}$, $\tilde{\mathbf{r}}_{i,k}$, $\tilde{\mathbf{d}}_{i,k}$, $\tilde{\mathbf{r}}_{i,k}^{\prime}$. From (5.60), we know that $\hat{\mathbf{G}}_{S,k}^o$ is a matrix whose diagonal elements are in an ascending order of those of $\hat{\mathbf{G}}_{S,k}$. From simulations, we found that the $r_k(m, m)$ tends to be equal or larger than $\tilde{r}_k(m, m)$ when m is close to q . The result is similar to the method in [56]. However, the theoretical proof will be difficult.

Hybrid SD-SIC (SDSIC)

As described, the SD method can efficiently implement the ML detector. However, when the dimension of the MIMO system is high, the computational complexity is still high. The computational complexity of the SIC is much lower, but it suffers from the error propagation effect. For our precoded OFDM system, the equivalent MIMO system is of dimension $L \times L$ where L is the length of the time-domain channel response. For OFDM systems, the CP size indicates the maximum channel length. For wideband systems, the delay spread of the channel is usually large. For example, the CP size for the OFDM symbol defined in IEEE802.11a/g systems is 16. Thus, the equivalent MIMO system in precoded OFDM systems will be of dimension 16×16 . The computational complexity of the SD algorithm for such system will be very high.

We now propose a new detection method to solve the problem. The proposed method combines the merits of SD and SIC methods and its performance can approach to that of the SD method. We call it the SDSIC method. The main idea comes from the fact that for SIC, the decision errors at its early stages is more damaging. In other words, if the detection is erroneous in early stages, it is likely to be erroneous in later stages. To solve the problem, we can use the SD method to obtain decisions in early stages. The proposed SDSIC method can be described

as follows. Let $\tilde{\mathbf{u}}_{i,k}$ be divided into two parts, $\tilde{\mathbf{u}}_{D,i,k}$ and $\tilde{\mathbf{u}}_{C,i,k}$, where

$$\tilde{\mathbf{u}}_{i,k} = [\tilde{\mathbf{u}}_{C,i,k}^T, \tilde{\mathbf{u}}_{D,i,k}^T]^T, \quad (5.64)$$

$\tilde{\mathbf{u}}_{D,i,k} = [\tilde{u}_{i,k}(p-p_k), \dots, \tilde{u}_{i,k}(p-1)]^T$ is the vector to be detected by the SD method, and $\tilde{\mathbf{u}}_{C,i,k} = [\tilde{u}_{i,k}(0), \dots, \tilde{u}_{i,k}(p-p_k-1)]^T$ the remaining vector to be detected by the SIC method. Note that the parameter p_k determines the dimension of the MIMO system that the SD will work on. The larger the p_k , the higher the computational complexity the SD will require. To find the decision for $\tilde{\mathbf{u}}_{D,i,k}$, we modify the SD method in (5.55) as

$$\tilde{\mathbf{u}}_{D,i,k} = \sum_{n=p-p_k}^{p-1} \left| \tilde{r}'_{i,k}(n) - \sum_{m=n}^{p-1} r_k(n,m) \tilde{d}_{i,k}(m) \right|^2 < r_{SD}^2 \quad (5.65)$$

where $\tilde{r}'_{i,k}(n)$, $r_k(n,m)$, and $\tilde{d}_{i,k}(m)$ are those defined in (5.55). Starting a tree-search from $\tilde{d}_{i,k}(p_k-1)$ to $\tilde{d}_{i,k}(0)$, we can determine a list of $\tilde{\mathbf{d}}_{i,k}$ within the sphere as candidates, and find the one minimizing (5.65) as the detection result.

With the detected $\tilde{\mathbf{u}}_{D,i,k}$, we can subtract its interference to the system and then use the SIC method to detect the remaining vector, $\tilde{\mathbf{u}}_{C,i,k}$. The SIC method can be described as

$$\hat{u}_{i,k}(m) = \arg \min_{\tilde{d}_{i,k}(m) \in \Psi_d} \left(\left| \tilde{r}'_{i,k}(m) - \sum_{j=m}^{p-1} r_k(m,j) \tilde{d}_{i,k}(j) \right|^2 \right), \quad (5.66)$$

where $\tilde{d}_{i,k}(n) = \hat{u}_{i,k}(n)$ for $(m+1) \leq n \leq (p-1)$, and $0 \leq m \leq (p-p_k-1)$.

§ 5.2.4 Computational Complexity Analysis

In this section, we analyze the computational complexity of the ZF, SIC, SD, and SDSIC methods. The ZF receiver multiplies the received signal vector with the matrix $\tilde{\mathbf{G}}_S^{-1}$ and feeds the output to a slicer. Due to its special structure, the computational complexity for the matrix inverse $\tilde{\mathbf{G}}_S^{-1}$ is $\mathcal{O}(M^2)$. The QR decomposition is required for the SIC and SD methods. The computational complexity of the QR decomposition is $\mathcal{O}(M^3)$. In SIC, the upper triangular matrix \mathbf{R}_k is used for successive detection and interference cancellation. When detecting the

m th data symbol, the signal estimates from all previous detected data symbols are weighted and subtracted from the received signal. The overall detection complexity per vector symbol is hence roughly in the order of $\mathcal{O}(M^3)$. Therefore, the computational complexity for the ZF receiver is lower than that of the SIC receiver.

The detection complexity of SD is known to be higher than that of linear and SIC receivers [59]. The computational complexity of the proposed SDSIC method will be higher than that of the SIC method, but lower than the SD method. The complexity of the SD method is data-dependent, and in general it is difficult to determine its complexity order. In [57] and [58], a closed-form expression for the mean complexity is derived. It is shown that the computational complexity is a function of the SNR, the detection radius, the constellation size, and the symbol size. Here, we give the computational complexity for a 16-QAM scheme as a reference:

$$\mathcal{C}(m, \rho, d^2) = \sum_{k=1}^m F_p(k) \sum_q \frac{1}{2^{2k}} \sum_{l=0}^{2k} \binom{2k}{l} g_{kl}(q) \gamma \left(\frac{\alpha n}{1 + \frac{2\rho q}{5m}}, n - m + k \right), \quad (5.67)$$

where $g_{kl}(q)$ is the coefficient of x^q in the polynomial $(1 + x + x^4 + x^9)^l (1 + 2x + x^4)^{2k-l}$, $F_p(k) = 8k + 36$, ρ is SNR, d is the given search radius, m is the dimension of the sphere, α is chosen such that $\gamma(\frac{\alpha n}{2}, \frac{n}{2}) = 1 - e^{-i}$, m is the dimension size [58]. We now use an example to evaluate the mean complexity of the SD and SDSIC methods. The radius r_{SD} we used is as that in (5.56) and p is set to be 8. Figure 5.3 shows the complexity comparison for SIC, SD, and SDSIC while Table 5.1 gives the numerical figures. As we can see, the complexity of SDSIC is significantly lower than that of SD for low to medium SNR regions. For example, when the SNR is 20 dB, the complexity of SDSIC method is only about 15% of that of the SD method. Figure 5.4 shows the complexity comparison when p is varied. Here, the modulation is 16-QAM, the SNR is 10dB, and the radius r_{SD} is equal to (5.56). Table 5.2 illustrates the numerical figures for the comparison. Again, the complexity of SDSIC is significantly lower than that of SD. For example, when $p = 8$, the complexity of the SDSIC method is only about 3% of that of the SD method. As p becomes larger, the difference between these two methods becomes larger. We then conclude that the SDSIC method can reach a near-SD performance

and its computational complexity is much lower than that of the SD method.

§ 5.3 Simulations

In this section, we report simulation results evaluating the performance of the proposed algorithm. The simulation setup is described as follows. The OFDM system we use has a symbol size of 64. The wireless channel is generated using an exponential-decay power profile and the CIR length is assumed to be 25. The channel is quasi-static and its response changes for every OFDM packet. A single OFDM packet contains 1600 OFDM symbols. In our simulations, we assume that the CIR is known. The channel noise is modeled as the AWGN, and added at the channel output. We first consider the case with no ISI which means the CP size is larger than the channel length. For this case, the CP size is set to be 32. Figure 5.5 to Figure 5.11 show the simulation results. Then, we consider the case with ISI in which the CP size is set to be 16. Figure 5.12 to Figure 5.13 show the simulation results. All simulations are obtained with 200 independent runs.

We first compare the performance of various precoding matrices that may be used in the OFDM systems. Figure 5.5 shows results for the QPSK/16-QAM modulation schemes. In this figure, the legends indicate the modulation scheme, the detection scheme, and the precoding type, respectively. Here, CHT denotes complex HT. From the figure, we can see that the performance of the three precoders (HT/CHT/DFT) are almost the same, and the performance of the DFT precoding is slightly better than the other two precodings (HT/CHT). The result verifies the property reported in [50]. The optimum precoding matrix is the DFT matrix. In this case, the OFDM system becomes a single carrier system. Note that the computational complexity of DFT is higher than that of HT. Also, the performance difference is marginal. Thus, the HT matrix is a good choice for the precoding. In the later simulations, we only consider the precoding with the HT matrix.

Then, we evaluate the influence of the block size used for precoding. Figure 5.6 to Figure 5.9

show the simulation results for the QPSK and 16-QAM scheme with the SD and SIC detectors. In these figures, the legends indicate the detection scheme, the precoding type, and the block size for coding. We can see that as the block size increases, the performance becomes better and better in high SNR regions. Using our analysis, we can see that the diversity gain of the OFDM system is 25 and the largest coding block we need to use should be around 25. From the figures, we can clearly verify the result; the performance of precoding with size of 32 is close to that with 16. It is simple to see that the larger the block size, the higher the computational complexity the detector will require. To compromise, we will use the block size of 8 in the following simulations.

To see how much improvement we can obtain, we then compare the performance of the system with and without precoding. Figure 5.10 and Figure 5.11 show the simulation results for the QPSK and 16-QAM schemes. In the figures, the legends indicate the detection method (FEQ/SIC/SD/SDSIC) and if precoding is used or not (HT/no HT). From the figures, we can see that the performance of conventional OFDM systems without precoding has the worst performance in high SNR regions. With precoding, the performance can be significantly enhanced. We can clearly see that only the SD method can fully explore the diversity the channel provides. Precoding with the SIC detection method only performs slightly better than that without precoding. Also note that the performance of the SDSIC method is almost as good as that of the SD method. However, the computational complexity of the SDSIC method is much lower. The other advantage of SDSIC is that it improve the performance of SD in low SNR regions. Therefore, we can conclude that the proposed SDSIC method has a good compromise between the performance and computational complexity.

Finally, we evaluate the performance of precoded OFDM systems in ISI environments. In this case, the CP size is smaller than channel length and the ISI occurs. We let the TEQ size be 16 and employ an SMSINR TEQ for the channel shortening. The performance comparison for various detection methods is shown in Figure 5.12 and Figure 5.13 for the QPSK and 16-QAM schemes, respectively. In the Figures, the legend indicates if the TEQ is used or not (No

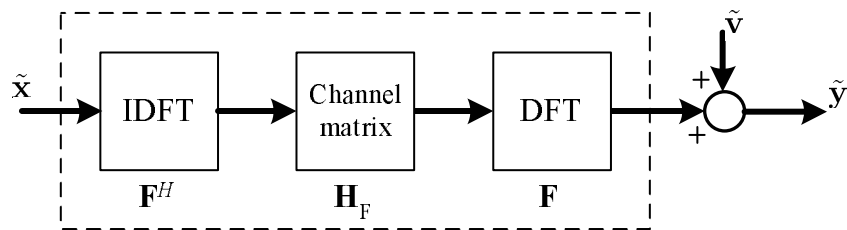
Table 5.1: Complexity comparison for various detection methods (SNR_a is varied)

SNR (dB)	12	16	20	24	28
SIC vs. SD	284.6	127.8	57.62	26.80	13.23
SDSIC vs. SD	7.60%	12.36%	19.56%	29.72%	42.68%
SDSIC vs. SIC	21.62	15.78	11.27	7.96	5.64

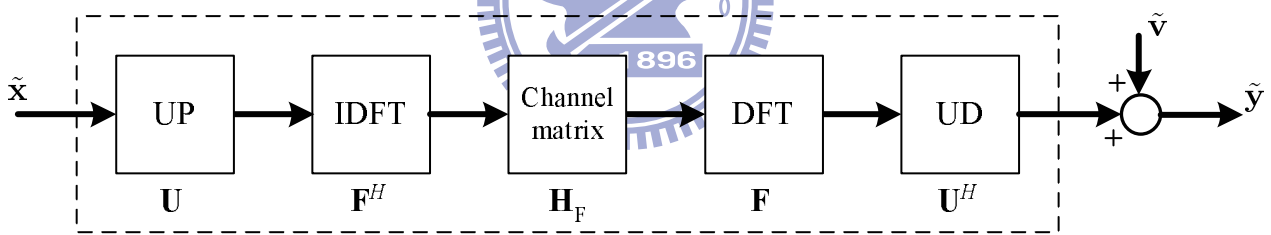
Table 5.2: Complexity comparison for various detection methods (p is varied)

p	2	4	8	16	32
SIC vs. SD	69.70	95.23	422	9844	10^5
SDSIC vs. SD	18.01%	9.15%	2.82%	0.54%	0.12%
SDSIC vs. SIC	12.55	8.71	11.90	52.78	1230

TEQ/TEQ), what detection methods is used, (FEQ/SIC/SD/SDSIC), and if precoding is used or not (HT/no HT). As shown in these figures, the MSINR TEQ can effectively improve the BER performance as compared to the case without TEQ. The behavior of all detectors is similar to that of the previous cases. Precoding with the SD detector has the best performance since it can fully explore the diversity gain the channel provides. It is much better than the system without precoding (even a TEQ is applied). We can also see that without a TEQ, the performance of the OFDM system is very poor. Still, the performance of the proposed SDSIC detector is close to that of the SD detector. Again, we conform that the proposed SDSIC detector is a good detection method for precoded OFDM systems with ISI.



(a).



(b).

Figure 5.1: (a). A conventional OFDM system, (b). An OFDM system with unitary precoding (UP) and unitary decoding (UD).

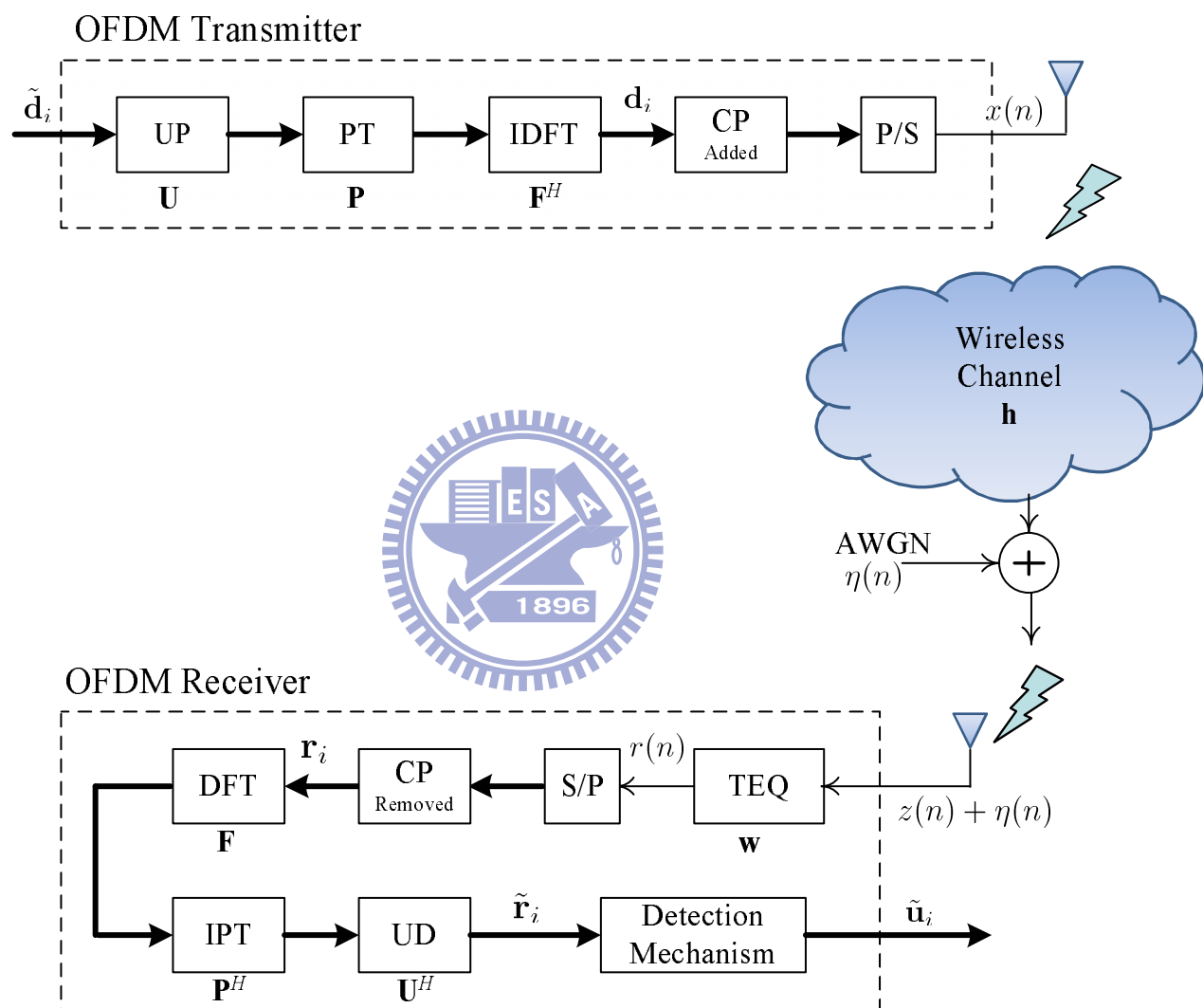


Figure 5.2: Proposed model for OFDM systems with a TEQ

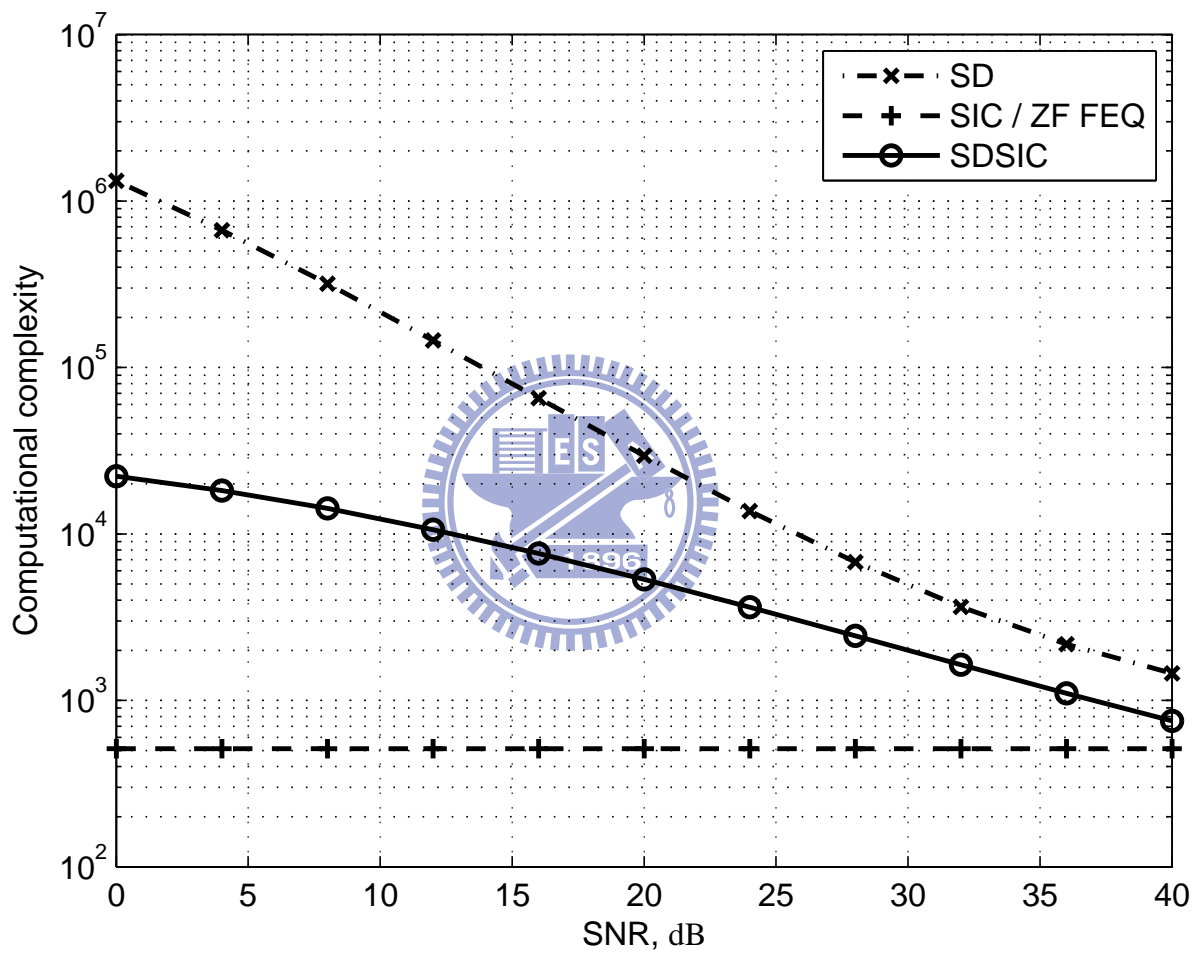


Figure 5.3: Complexity comparison for various detection methods

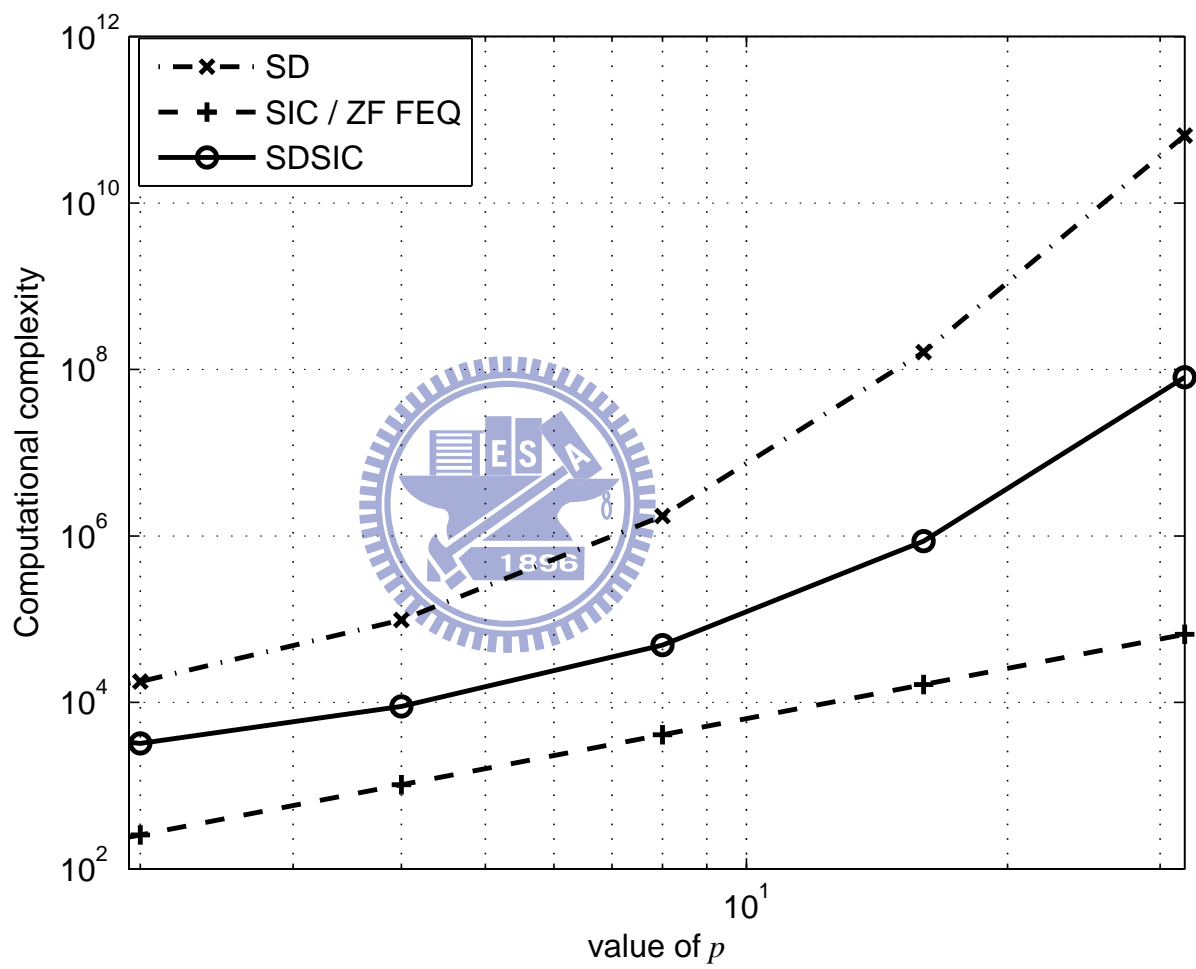


Figure 5.4: Complexity comparison for various detection methods

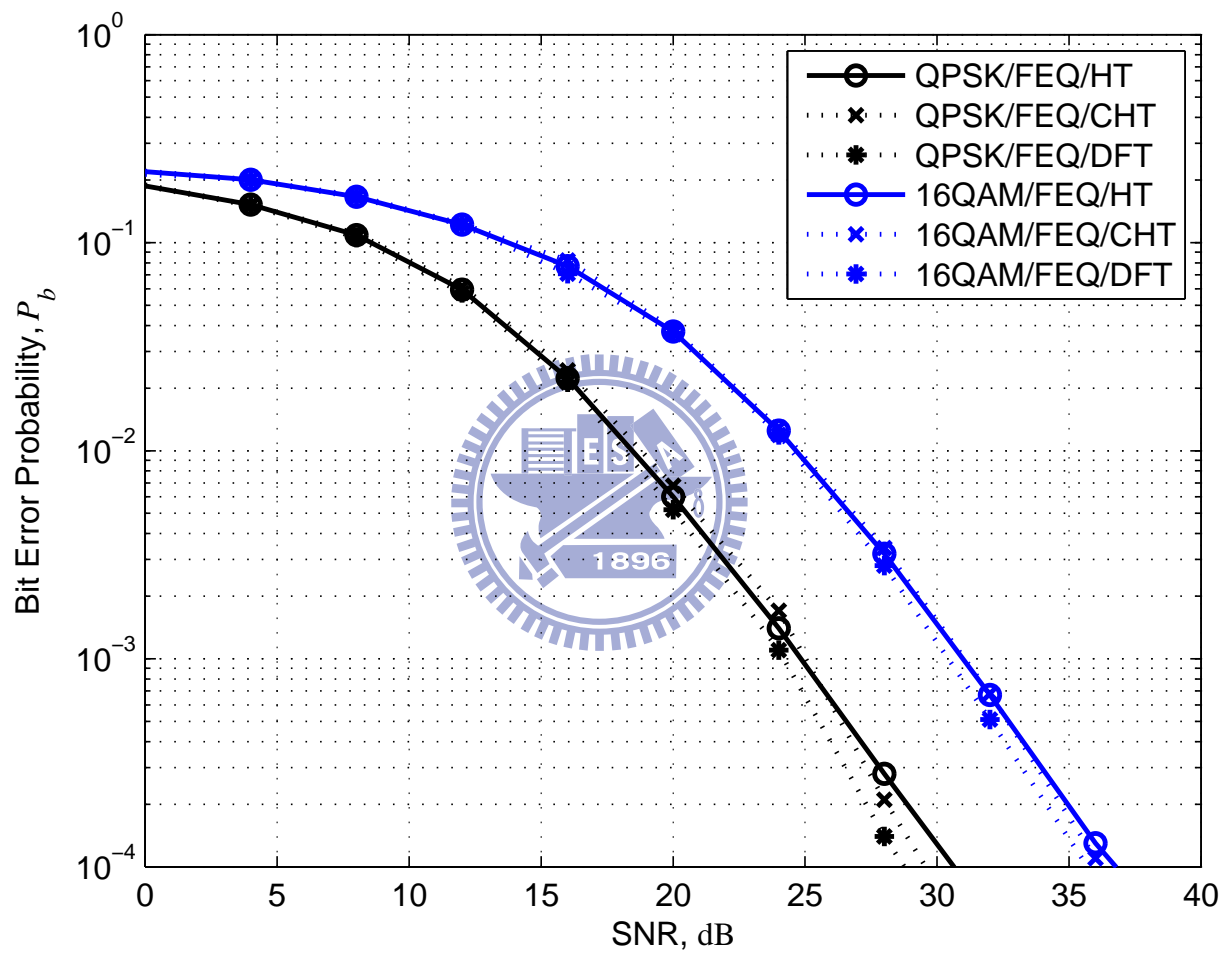


Figure 5.5: BER performance comparison for OFDM systems with various unitary precoders

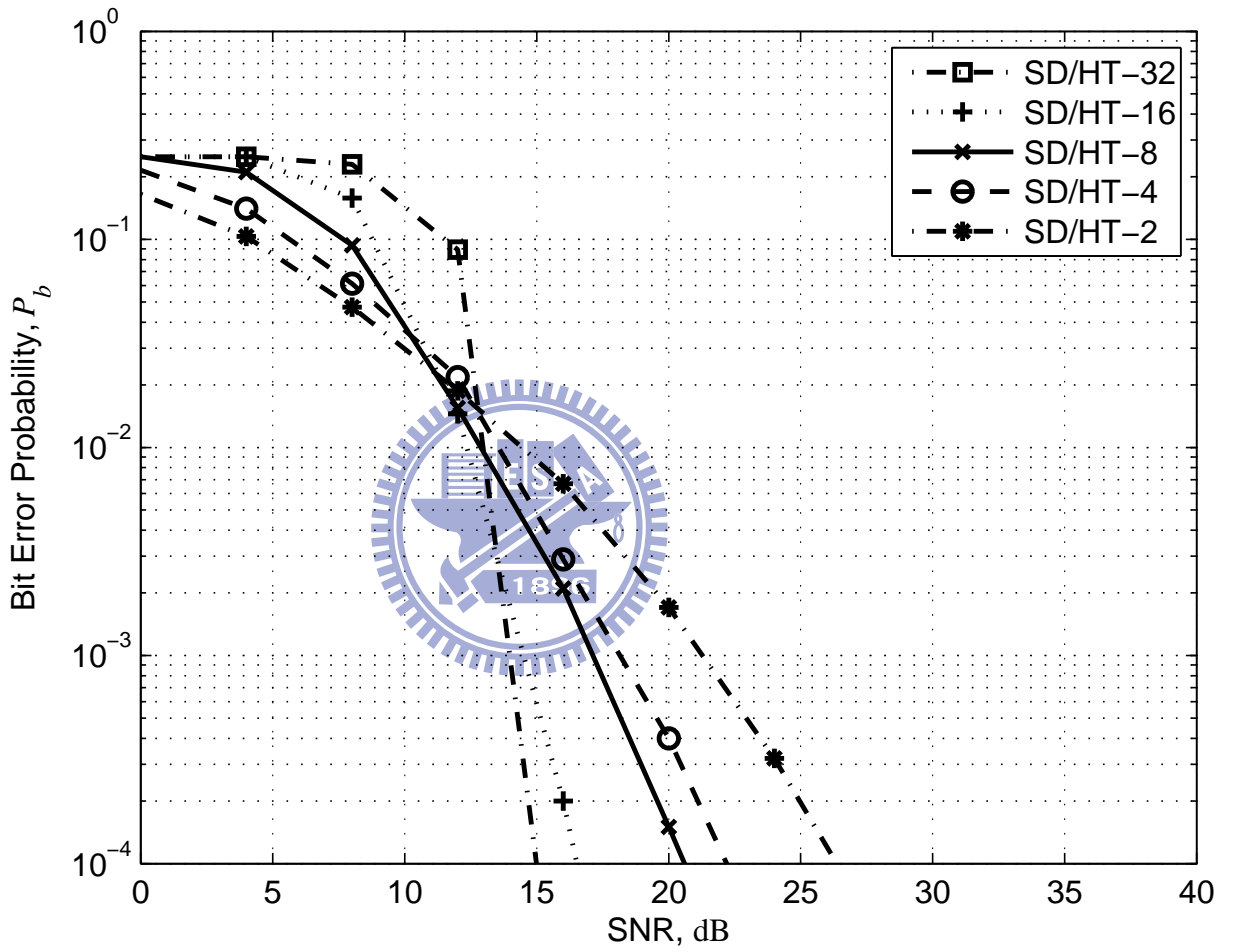


Figure 5.6: BER performance comparison for precoded OFDM systems with SD detector (QPSK scheme)

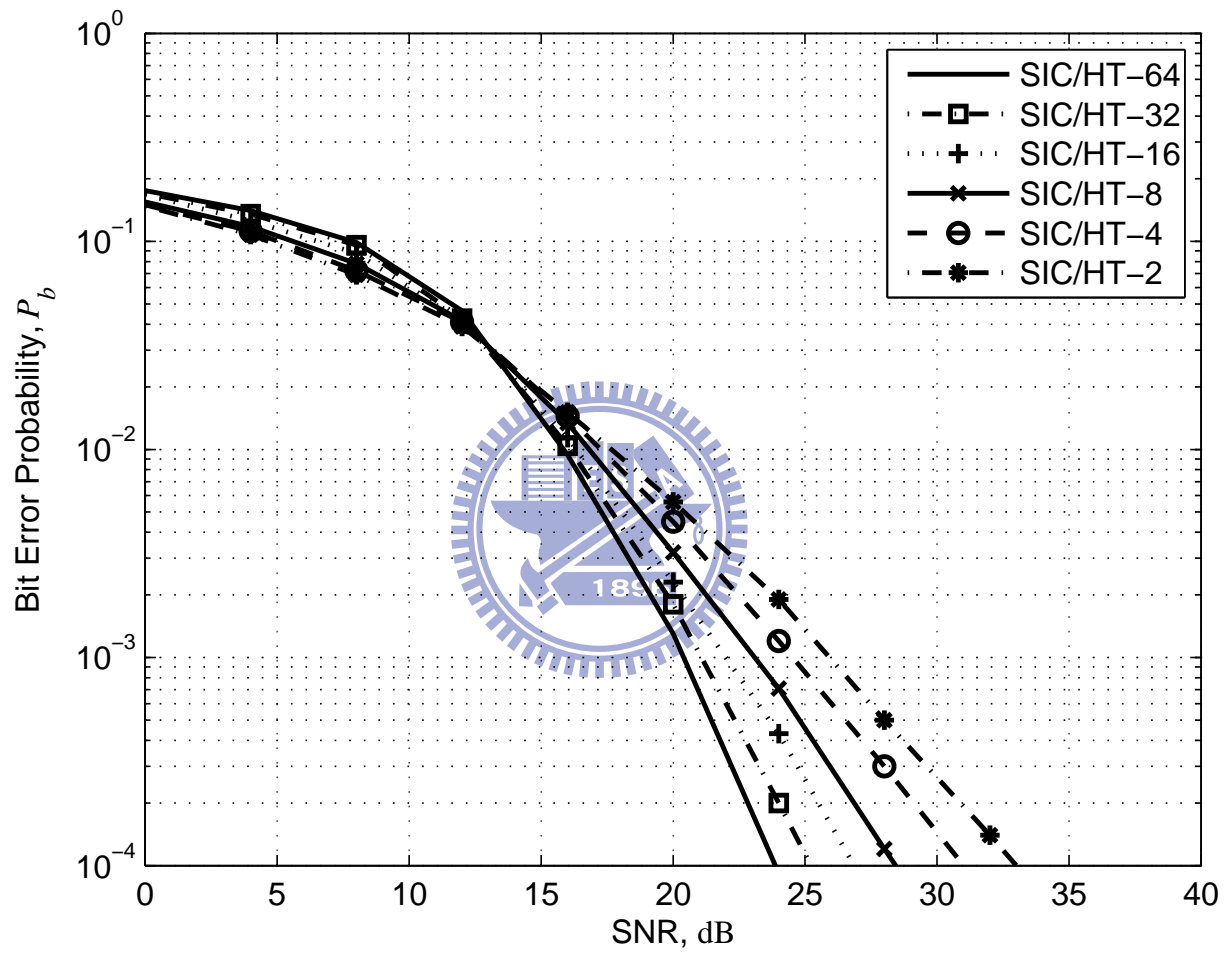


Figure 5.7: BER performance comparison for precoded OFDM systems with SIC detector (QPSK scheme)

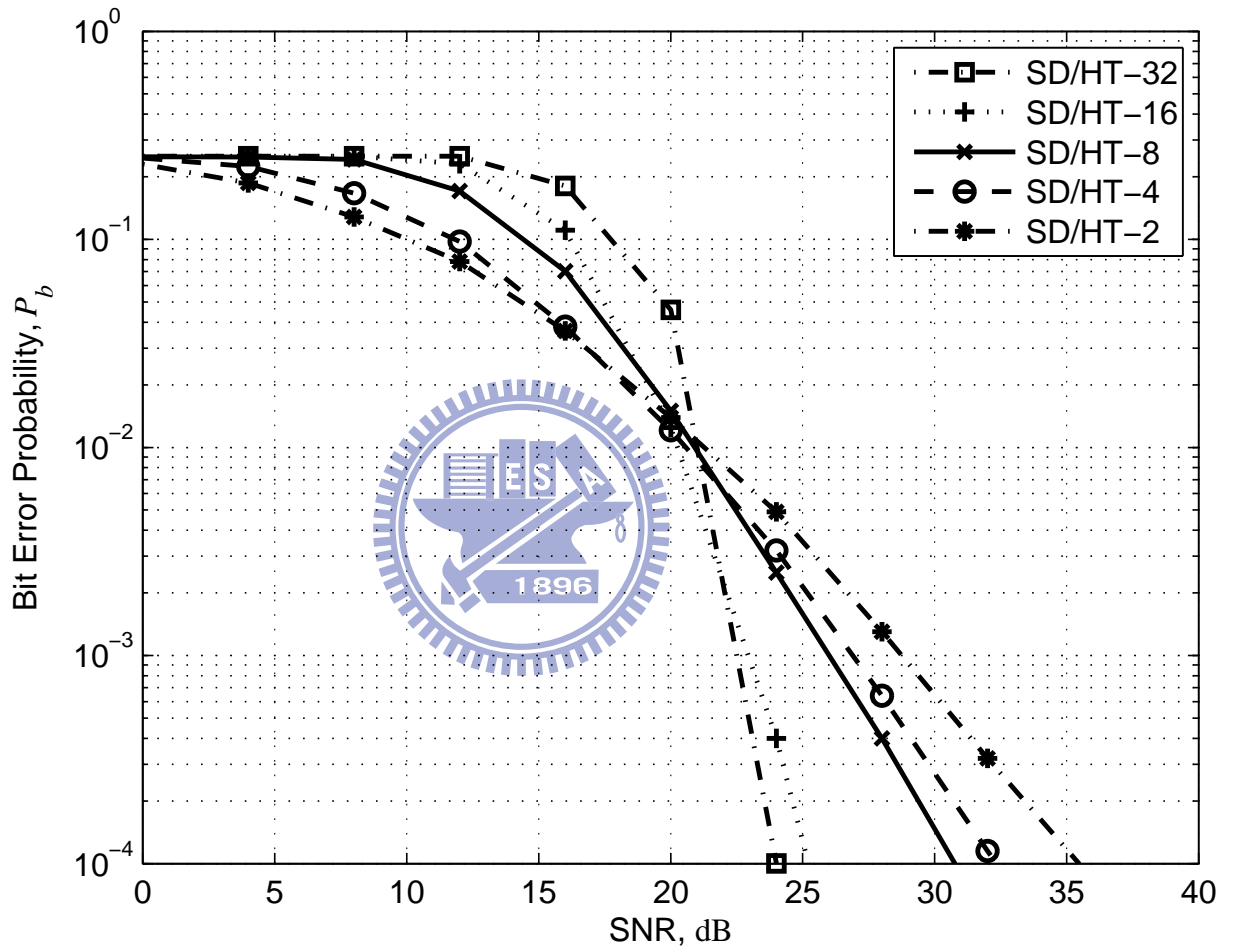


Figure 5.8: BER performance comparison for precoded OFDM systems with SD detector (16-QAM scheme)

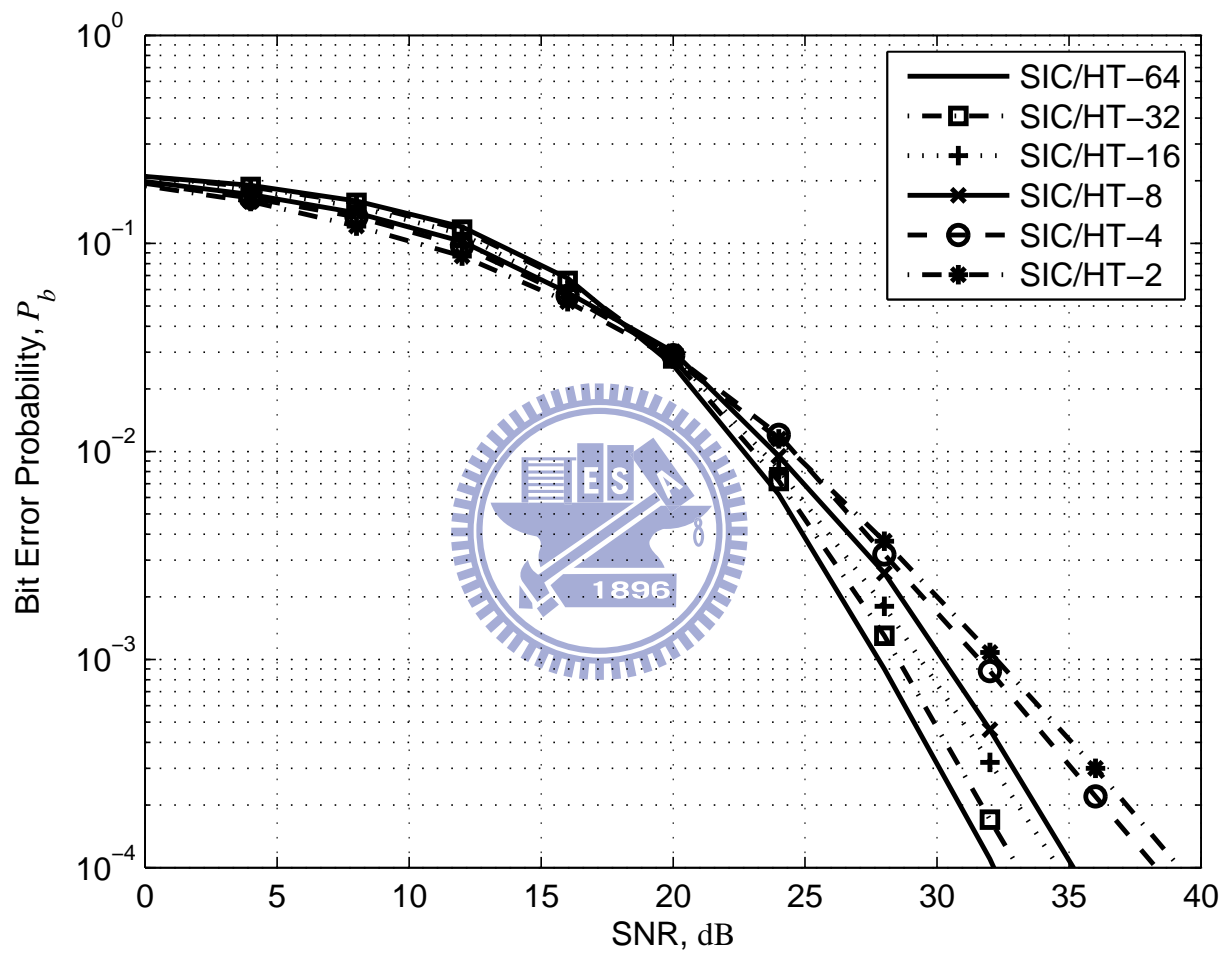


Figure 5.9: BER performance comparison for precoded OFDM systems with SIC detector (16-QAM scheme)

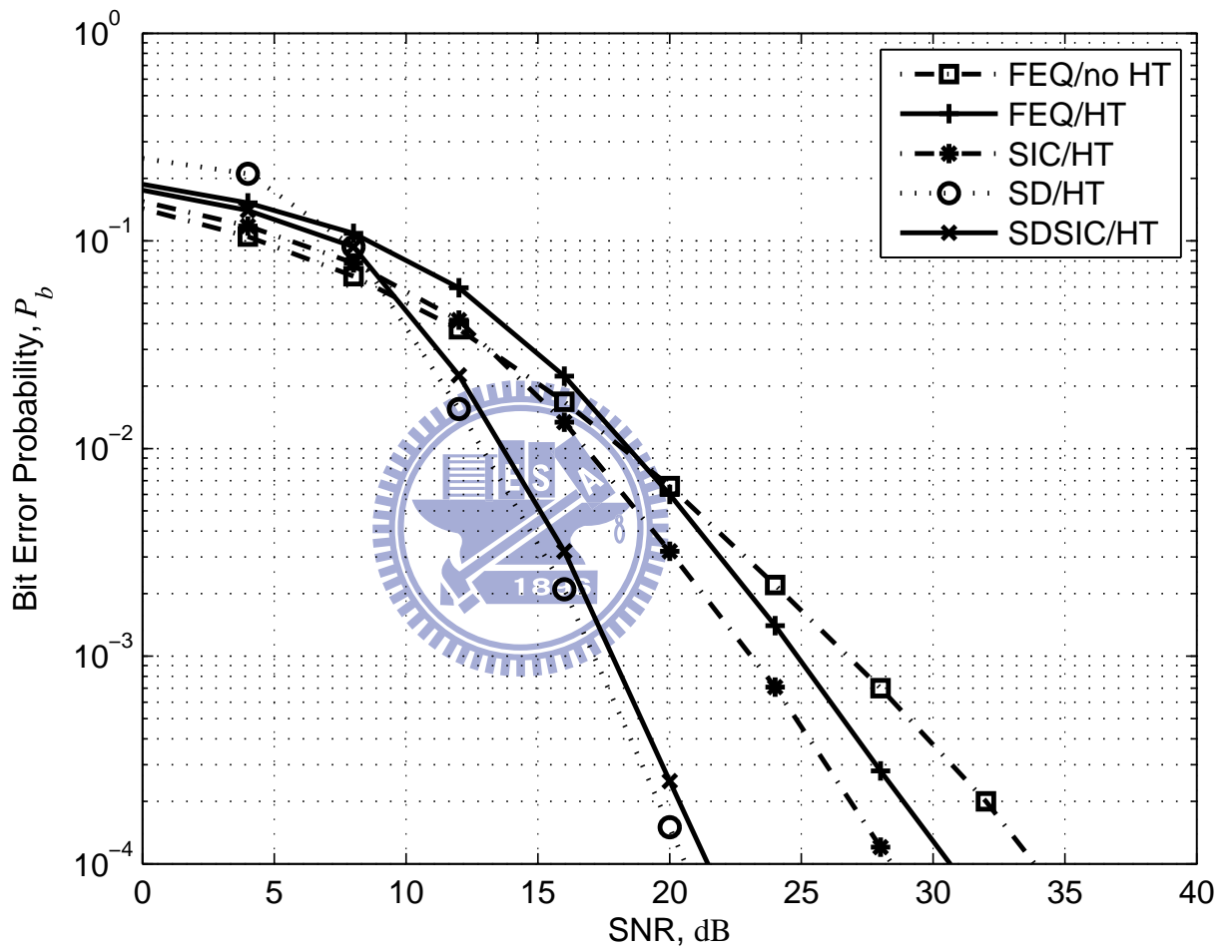


Figure 5.10: BER performance comparison for precoded systems with various detection methods (QPSK scheme)

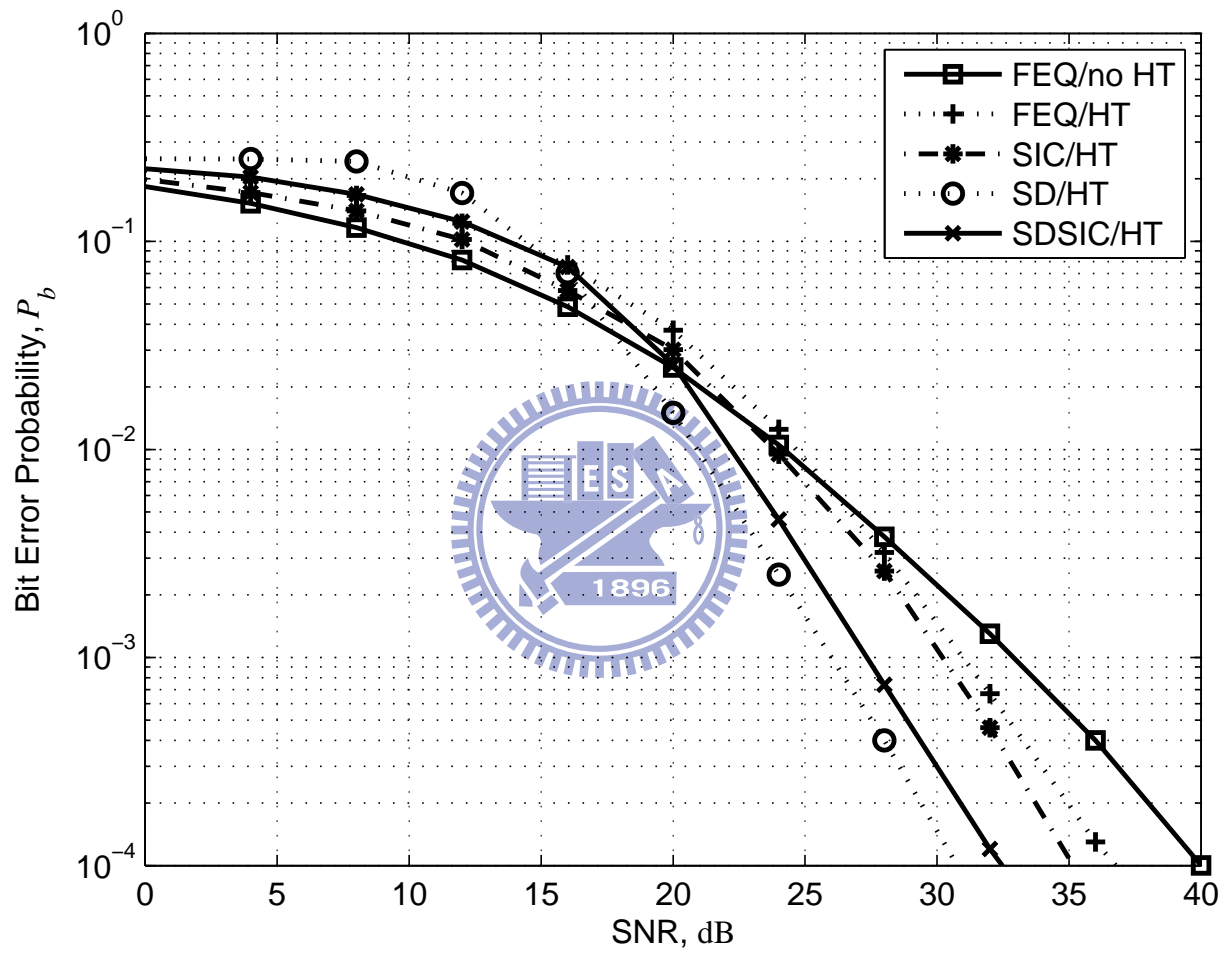


Figure 5.11: BER performance comparison for precoded OFDM systems with various detection methods (16-QAM scheme)

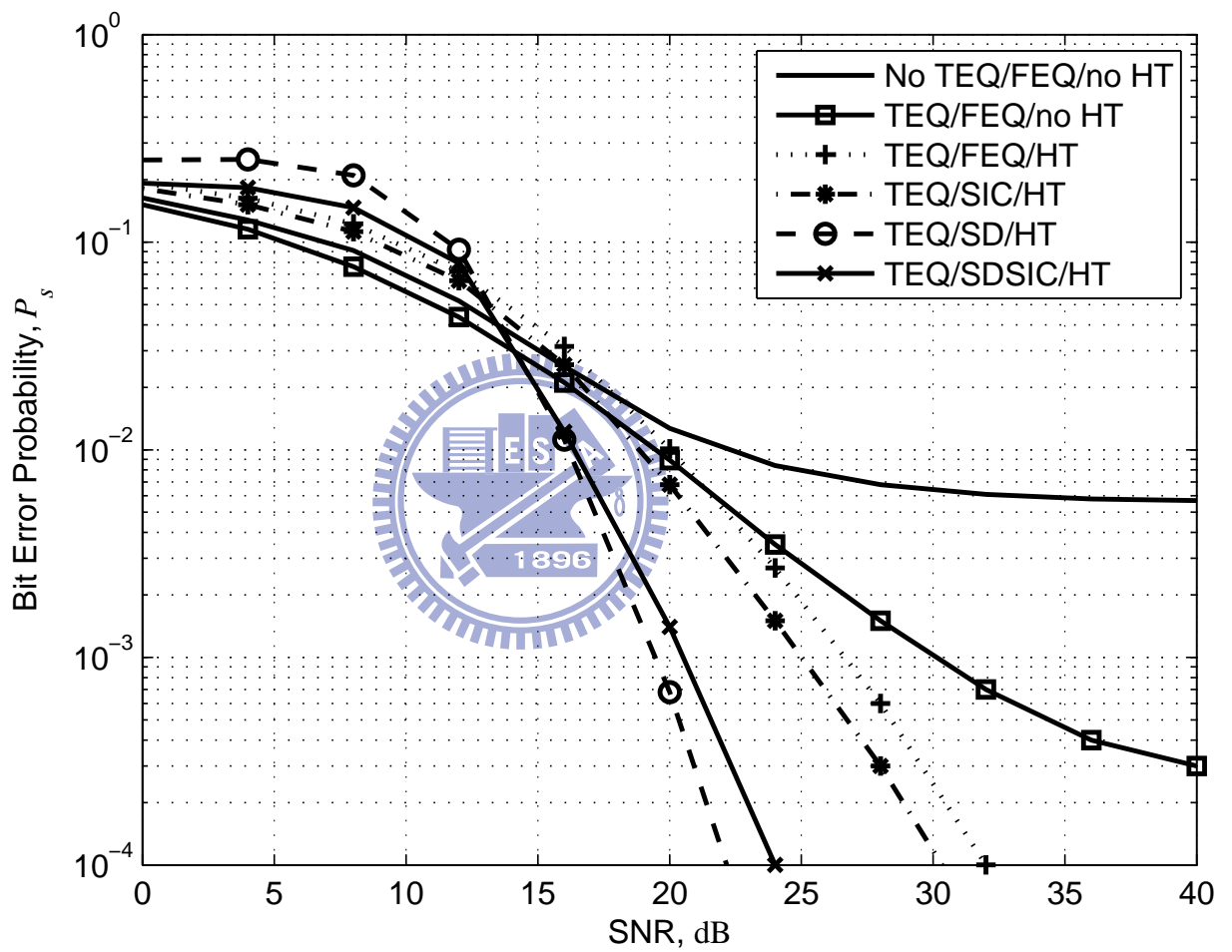


Figure 5.12: BER performance comparison for OFDM systems with ISI (QPSK scheme)

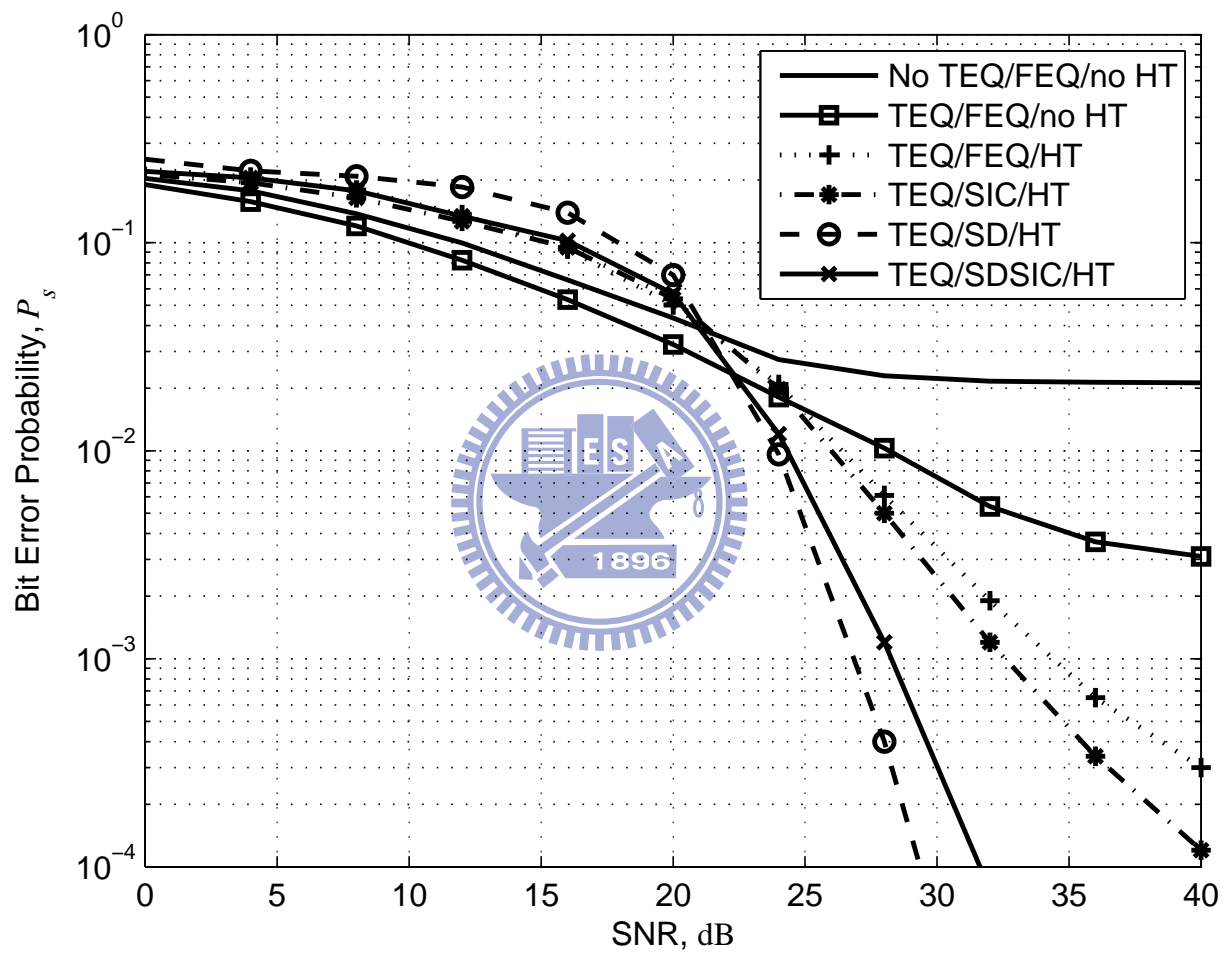


Figure 5.13: BER performance comparison for OFDM system with ISI (16-QAM)

Chapter 6

Conclusions

The TEQ is a device used in DMT systems to combat the ISI problem. Many methods have been proposed to obtain optimum TEQs. However, we have found that these optimum TEQs are actually not optimal. This is because the noise, observed in a DMT symbol, does not have a CP, and the circular convolution for the noise and the TEQ cannot be conducted. Conventional methods ignored these phenomena, and erroneously calculate the noise and residual ISI power of subcarriers. We have derived the correct formula for the calculation of noise and residual ISI powers. It turns out that these powers are larger than those calculated by the conventional methods. Using the capacity maximization criterion, we then propose a new optimal TEQ design method, called the EMBR method. The EMBR method requires solving a constrained nonlinear optimization problem and hence is not cost-effective. To reduce the computational complexity, we then derive a simplified EMBR method, i.e., the SEMBR method. Simulations based on various ADSL standard test loops show that the proposed SEMBR method outperforms the well-known min-ISI method. Furthermore, the throughput yielded by the proposed SEMBR method closely approaches the theoretical upper bound.

Since the TEQ in OFDM systems tends to have an IIR characteristic, the computational complexity of the conventional FIR TEQ may be high. To facilitate the application of the TEQ in OFDM systems, we then propose using the IIR TEQ for channel shortening. However, we

found that the direct derivation of the IIR TEQ is difficult. We then use a simpler two-step approach. In the first step, we use a multistage structure to obtain the FIR TEQ. In the second step, we use the SMM to convert the FIR TEQ into an equivalent IIR one. It is shown that the order of the IIR TEQ can be much lower than that of the FIR TEQ. Also, the TEQ derivation with the MS structure can be much more efficient than the conventional SS structure. We then obtain a low-complexity TEQ, both in the derivation and the shortening phase. Simulations show that while the proposed method can reduce the computational complexity significantly, its performance is almost as good as that of the existing methods.

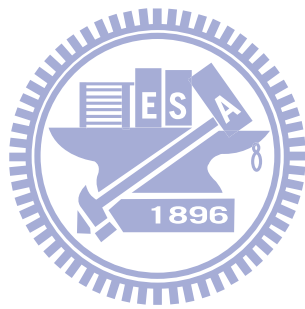
To further improve the performance, we finally propose an OFDM system with unitary precoding. Due to the precoding operation, the OFDM can exploit the frequency diversity the channel provides. Based on this structure, we propose a TEQ design method, called MSINR. It is shown that the MSINR method can maximize the SINR of all subcarriers, simultaneously. This results in a true optimum TEQ which cannot be obtained by the existing methods. To fully explore the diversity, however, we have to use the ML detector in the receiver. The SD, being an efficient ML detector, still requires high computational complexity when used in the proposed precoded OFDM systems. To solve the problem, we propose a detection method, called the SDSIC method, which has near-SD performance and a complexity much lower than that of the SD. Simulations show the precoded OFDM system with the proposed MSINR TEQ with the SDSIC detector significantly outperforms the unprecoded OFDM system with conventional TEQs.

In concluding the dissertation, we suggest some possible topics for future research.

1. In MIMO-OFDM systems, the TEQ design becomes more complicated and challenging. However, the fundamental problems encountered in MIMO-OFDM systems are the same as those in SISO-OFDM systems. With some modifications, the proposed EMBR/SEMBR method can be extended to MIMO-OFDM systems.
2. Similarly, the IIR TEQ designed method proposed in this dissertation can be also extended to MIMO-OFDM systems. How to convert a MIMO FIR filter into a MIMO IIR filter is

the key problem. Also, the stability is an important issue that has to be considered.

3. In this dissertation, all TEQs are designed based on the assumption that perfect channel information is available. In practical systems, however, this may not be always possible since the channel estimation will introduce errors. How to design a robust TEQ overcoming the channel uncertainty problem deserves further studies.
4. In this dissertation, we only consider the channel-independent precoder which can explore the receiver frequency diversity. The transmitter diversity, however, is not considered. A more involved problem is to design a channel-dependent precoder. In this case, channel feedback will be required and the optimization problem will become much more complicated.
5. The proposed precoded method can be extended to MIMO-OFDM systems easily. With the precoding, the diversity gain can be further increased and the performance of MIMO-OFDM systems can also be improved. In addition, the MSINR TEQ design method for channel shortening can also be extended to MIMO-OFDM systems.
6. In conventional OFDM systems, channel coding is usually invoked to provide the coding and diversity gains. Channel coding, however, has to include redundancy. The proposed precoding scheme can also be generalized to include redundancy. How to combine channel coding and precoding in OFDM systems in an efficient way also deserves further studies.



Bibliography

- [1] M.R. Nakhai, "Multicarrier transmission," *IET Signal Processing*, Vol.2, No.1, pp.1-14, Mar. 2008.
- [2] S. Hara, M. Okada, and N. Morinaga, "Multicarrier modulation technique for wireless local area networks," in *Fourth European Conference on Radio Relay Systems, IEE*, pp.33-38 Oct. 1993.
- [3] P.S. Chow, J.M. Cioffi, and J.A.C. Bingham, "DMT-based ADSL: concept, architecture, and performance," *IEE Colloquium on High speed Access Technology and Services*, pp.3/1-3/6, Oct. 1994.
- [4] F. Moulin, M. Ouzzif, A. Zeddou, and F. Gauthier, "Discrete-multitone-based ADSL and VDSL systems performance analysis in an impulse noise environment," *Science, Measurement and Technology, IEE Proceedings*, - Vol.150, Issue 6, pp.273-278, Nov. 2003.
- [5] ITU-T Recommendation G.992.1: *Asymmetrical Digital Subscriber Line (ADSL) Transceivers*, Mar. 1999.
- [6] ANSI standard T1.424: *Very-high bit-rate Digital Subscriber Lines (VDSL) Metallic Interface, Part 3: Multicarrier Modulation (MCM) Specification*, 2003
- [7] ITU-T Recommendation G.996.1: *Test procedures for digital subscriber line (DSL) transceivers*, Feb. 2001.

- [8] ETS 300 401, *Radio broadcast systems; digital audio broadcasting (DAB) to mobile, portable and fixed receivers*, 1994. European Telecommunications Standards Institute (ETSI).
- [9] ETS 300 744, *Digital broadcasting systems for television, sound and data services; framing structure, channel coding and modulation for digital terrestrial television*, 1997. European Telecommunications Standards Institute (ETSI).
- [10] IEEE Std. 802.11, *Wireless LAN Medium Access Control (MAC) and Physical Layer (PHY) Specification*, 1999.
- [11] IEEE Std. 802.11g, *Further Higher-Speed Physical Layer Extension in the 2.4 GHz Band*, 2003.
- [12] J. Chow, and J.M. Cioffi, "A cost effective maximum likelihood receiver for multicarrier systems," in *Int Conf Commun.*, Chicago, pp.948-952, Jun., 1992.
- [13] B.F. Boroujeny and M. Ding, "Design methods for time-domain equalizers in DMT transceivers," *IEEE Trans. on Comm.*, Vol.49, No.3, pp.554-562, Mar., 2001.
- [14] P.J. Melsa, R.C. Younce, and C.E. Rohrs, "Impulse response shortening for discrete multitone transceiver," *IEEE Trans. On Commun.*, Vol.44, No.12, pp.1662-1672, Dec., 1996.
- [15] N. Al-Dhahir, and J.M. Cioffi, "Optimum finite-length equalization for multicarrier transceivers," *IEEE Trans. On Commun.*, Vol.44, No.1, pp.56-64, Jan. 1996.
- [16] N. Al-Dhahir and J.M. Cioffi, "Efficiently computed reduced-parameter input-aided MMSE equalizers for ML detection: A unified approach," *IEEE Trans. on Info. Theory*, Vol.42, pp.903-915, May 1996.
- [17] W. Henkel, G. Taubock, P. Odling, P. O. Borjesson, and N. Petersson, "The cyclic prefix of OFDM/DMT - an analysis," in *Int'l Zurich Seminar Broadband Commun., Access, Transm., Networking*, Vol.2, pp.1-3, Feb. 2002.

- [18] G. Arslan, B.L. Evans, and S. Kiaei, "Equalization for discrete multitone transceivers to maximize bit rate," *IEEE Trans. On Signal Processing*, Vol.49, No.12, pp.3123-3135, Dec., 2001.
- [19] M. Milosevic, *Maximizing data rate of discrete multitone systems using time domain equalization design*, PhD thesis, University of Texas at Austin, May 2003.
- [20] R. Shur and J. Speidel, "An efficient equalization method to minimize delay spread in OFDM / DMT systems," in *Proc. IEEE Int. Conf. On Commun*, Helsinki, Finland, Vol.5, pp.1481-1485, Jun. 2001.
- [21] R. L'opez-Valcarce, "Minimum delay spread TEQ design in multicarrier systems," *IEEE Signal Processing Letters*, Vol.11, No.8, pp.682-685, Aug., 2004.
- [22] R.K. Martin, K. Vanbleu, M. Ding, G. Ysebaert, M. Milosevic, B.L. Evans, M. Moonen, and C.R. Johnson, Jr., "Unification and evaluation of equalization structures and design algorithms for discrete multitone modulation systems," *IEEE Trans. On Signal Processing*, Vol.53, No.10, pp.3880-3894, Oct. 2005.
- [23] K. Van Acker, G. Leus, M. Moonen, O. van de Wiel, and T. Pollet, "Per tone equalization for DMT-based systems," *IEEE Trans. On Commun.*, Vol.49, No.1, pp.109-119, Jan. 2001.
- [24] K. Vanbleu, G. Ysebaert, G. Cuypers, M. Moonen, and K. Van Acker, "Bitrate maximizing time-domain equalizer design for DMT-based systems," *IEEE Trans. on Comm.*, Vol.52, No.6, pp.871-876, June 2004.
- [25] J. Kim, and E.J. Powers, "Subsymbol equalization for discrete multitone systems," *IEEE Trans. On Commun.*, Vol.53, No.9, pp.1551-1560, Sep. 2005.
- [26] Y.F. Chen, *The optimal time-domain equalization of DMT transceivers*, Master thesis, Chiao Toung University, Taiwan, 2001.

- [27] W.R. Wu, and C.F. Lee, "Time domain equalization for DMT transceivers : A new result," in *Proc. Intelligent Signal Processing and Communication Systems*, Hong-Kong, pp.553-556, Dec. 2005.
- [28] G. Leus, and M. Moonen, "Per-tone equalization for MIMO OFDM systems," *IEEE Trans. On Signal Processing*, Vol.51, No.11, pp.2965 - 2975, Nov. 2003.
- [29] L. Yang, and C. G. Kang, "Design of novel time-domain equalizer for OFDM systems," *IEICE Trans. On Commun.*, Vol.E89-B, No.10, pp.2940-2944, Oct., 2006.
- [30] J.M. Zhang, and W. Ser, "New criterion for time-domain equalizer design in OFDM systems," *Acoustics, Speech, and Signal Processing, 2002. Proceedings. (ICASSP '02)*, Vol.3, pp.2561-2564, May, 2002.
- [31] W.R. Wu, and C.F. Lee, "An IIR time domain equalizer for OFDM systems," *AWPCS 2007*, Hsin-Chu, pp.1-5, Aug. 2007.
- [32] C.F. Lee, and W.R. Wu, "A multistage IIR time domain equalizer for OFDM systems," *TENCON 2007*, Taipei, pp.1-5, Oct. 2007.
- [33] D. Rawal, and C. Vijaykumar, "QR-RLS based adaptive channel TEQ for OFDM wireless LAN," in *Conference on Signal Processing, Communications and Networking*, Chennai, pp.46-51, Jan. 2008.
- [34] D. Rawal, C. Vijaykumar, and K.K. Arya, "QR-RLS based adaptive channel shortening IIR-TEQ for OFDM wireless LAN," in *Proc. Wireless Communication and Sensor Networks*, Havana, pp.21-26, Dec. 2007.
- [35] K. Steiglitz, and L.E. McBride, "A technique for the identification of linear system," *IEEE Trans. On Auto. Cont.*, Vol.AC-10, pp.461-464, Jul., 1965.

- [36] P.A. Regalia, M. Mboup, and M. Ashari, "On the existence of stationary points for the Steiglitz-McBride algorithm," *IEEE Trans. on Auto Contr.*, Vol.42, pp.1592-1596, Nov, 1997.
- [37] P. Stoica, and T. Söderström, "The Steiglitz-McBride identification algorithm revised - Convergence analysis and accuracy aspects," *IEEE Trans. On Auto. Cont.*, Vol.AC-26, pp.712-717, Jun., 1981.
- [38] S.L. Netto, P.S.R. Diniz, and P. Agathoklis, "Adaptive IIR filtering algorithms for system identification: A general framework," *IEEE Trans. On Educ.*, Vol.38, pp.54-66, Feb., 1995.
- [39] M.H., Cheng, and V.L. Stonick, "Convergence, convergence point and convergence rate for Steiglitz-McBride method; a unified approach" *ICASSP-94*, Vol.3, pp.477 - 480, Apr, 1994.
- [40] P. Crespo, and M. Honig, "Pole-zero decision feedback equalization with a rapidly converging adaptive IIR algorithm," *IEEE J. Select. Areas Commun.*, Vol.9, pp.817-829, Aug., 1991.
- [41] K.P. Chong, and S.H. Zak, *An Introduction to Optimization*, John Wiley & Sons, 2001.
- [42] J.G. Proakis, *Digital Communications*, McGraw-Hill, Inc., 4th ed., 2001.
- [43] S.M. Kay, *Fundamentals of Statistical Signal Processing: Estimation Theory*, Prentice Hall, 1993.
- [44] D. Tse, and P. Viswanath, *Fundamentals of wireless communication*, Cambridge, 2005.
- [45] A.K. Gupta, and D.K. Nagar, *Matrix Variate Distributions*, Boca Raton, FL. CRC, 2000.

- [46] S. Tamura, M. Fujii, M. Itami and K. Itoh, "Detection of precoded OFDM by recovering symbols on degraded carriers," Book chapter of *Multi-Carrier Spread-Spectrum*, pp.183-190, 2006.
- [47] A. Petropulu, R. Zhang, and R. Lin, "Blind OFDM channel estimation through simple linear precoding," *IEEE Trans. On Wireless Communs*, Vol.3, No.2, pp.647-655, Mar., 2004.
- [48] Y. Yu, R. Lin, and A.P. Petropulu, "Linearly precoded OFDM system with adaptive modulation," *ICASSP*, Vol.2, pp.417-420, May, 2004.
- [49] Z. Wang, and G.B. Giannakis, "Linearly precoded or coded OFDM against wireless channel fades?" *3rd IEEE Signal Processing Workshop on Signal Processing Advances in Wireless Communications*, pp.267-270, Taoyuan, Taiwan, Mar., 2001.
- [50] Y.P. Lin, and S.M. Phoong, "BER minimized OFDM systems with channel independent precoders," *IEEE Trans. On Signal Processing*, Vol.51, No.9, pp.2369-2380, Sep., 2003.
- [51] S. Zhou, Z. Wang, N. Bapat, and G.B. Giannakis, "Turbo decoding of error control coded and unitary precoded OFDM," *IEEE Vehicular Tech.*, Vol.3, pp.1237-1241, May, 2002,
- [52] Z. Wang, S. Zhou, and G.B. Giannakis, "Joint coded-precoded OFDM with low-complexity turbo-decoding," *IEEE Trans. On Wireless Communs.*, Vol.3, No.3, May 2004.
- [53] B. Schubert, "Analysis of sphere decoding in linear cooperative wireless relay networks," *PhD Thesis*, German, Jan., 2006.
- [54] J.Y. Wu, W.R. Wu, and N.C. Lien, "Low-complexity MIMO detection using a list projection technique," *2nd International Conference on Signal Processing and Communication Systems (ICSPCS 2008)*, Dec., 2008.
- [55] W. Zhao, and G.B. Giannakis, "Sphere decoding algorithms with improved radius search," *IEEE Trans. on Comm.*, Vol.53, No.7, pp.1104-1109, Jul., 2005.

- [56] W. Zhao, and G.B. Giannakis, "Reduced complexity closest point decoding algorithms for random lattices," *IEEE Trans. On Wireless Commun.*, Vol.5, No.1, pp.101-111, Jan., 2006.
- [57] B. Hassibi and H. Vikalo, "On the sphere decoding algorithm I. expected complexity," *IEEE Trans. on Signal Processing*, Vol.53, No.8, pp.2806-2818, Aug., 2005.
- [58] B. Hassibi and H. Vikalo, "On the sphere decoding algorithm II. generalizations, second-order statistics, and applications to communications," *IEEE Trans. on Signal Processing*, Vol.53, No.8, pp.2819-2834, Aug., 2005.
- [59] E. Zimmermann, W. Rave, and G. Fettweis, "On the complexity of sphere decoding," in *Proc. International Symp. on Wireless Pers. Multimedia Commun.*, Abano Terme, Italy, Sep., 2004.
- [60] M.O. Damen, H.E. Gamal, and G. Caire, "On maximum-likelihood detection and the search for the closest lattice point," *IEEE Trans. Inform. Theory*, Vol.49, No.10, pp.2389-2402, Oct. 2003.
- [61] D. Wübben, R. Böhnke, J. Rinas, V. Kühn, and K.D. Kammeyer, "Efficient algorithm for decoding layered space-time codes," *IEE Electronics Lett.*, Vol.37, No.22, pp.1348-1350, Nov., 2001.
- [62] J.K. Zhang, A. Kavčić and K.M. Wong, "Equal-diagonal QR decomposition and its application to precoder design for successive-cancellation detection," *IEEE Trans. on Info. Theo.*, Vol.51, No.1, pp.154-172, Jan., 2005.
- [63] L. Meilhac, A. Chiodini, C. Boudesocque, Chrislin Lele, and A. Gerçekci, "MIMO-OFDM modem for WLAN," White paper for NewLogic Technologies, France.
- [64] K. Puttegowda, G. Verma, S. Bali, and R.M. Buehrer, "On the effect of cancellation order in successive interference cancellation for CDMA systems," *Vehicular Technology Conference, VTC 2003-Fall* Vol.2, pp.1035-1039, Oct.,2003.